REMOTE SENSING AND GIS IN SUPPORT OF SUSTAINABLE AGRICULTURAL DEVELOPMENT

A Thesis Submitted to the College of

Graduate Studies and Research

in Partial Fulfillment of the Requirements

for the Degree of Doctor of Philosophy

in the School of Environment and Sustainability

University of Saskatchewan

Saskatoon

By

Dennis Correa Duro

PERMISSION TO USE

In presenting this thesis in partial fulfillment of the requirements for a Postgraduate degree from the University of Saskatchewan, I agree that the Libraries of this University may make it freely available for inspection. I further agree that permission for copying of this thesis in any manner, in whole or in part, for scholarly purposes may be granted by the professor or professors who supervised my thesis work or, in their absence, by the Head of the Department or the Dean of the College in which my thesis work was done. It is understood that any copying or publication or use of this thesis or parts thereof for financial gain shall not be allowed without the author's written permission. It is also understood that due recognition shall be given to me and to the University of Saskatchewan in any scholarly use which may be made of any material in my thesis.

Requests for permission to copy or to make other uses of materials in this thesis in whole or part should be addressed to:

Dean
College of Graduate Studies and Research
University of Saskatchewan
107 Administration Place
Saskatoon, Saskatchewan S7N 5A2
Canada

ABSTRACT

Over the coming decades it is expected that the vast amounts of area currently in agricultural production will face growing pressure to intensify as world populations continue to grow, and the demand for a more Western-based diet increases. Coupled with the potential consequences of climate change, and the increasing costs involved with current energy-intensive agricultural production methods, meeting goals of environmental and socioeconomic sustainability will become ever more challenging. At a minimum, meeting such goals will require a greater understanding of rates of change, both over time and space, to properly assess how present demand may affect the needs of future generations. As agriculture represents a fundamental component of modern society, and the most ubiquitous form of human induced landscape change on the planet, it follows that mapping and tracking changes in such environments represents a crucial first step towards meeting the goal of sustainability. In anticipation of the mounting need for consistent and timely information related to agricultural development, this thesis proposes several advances in the field of geomatics, with specific contributions in the areas of remote sensing and spatial analysis: First, the relative strengths of several supervised machine learning algorithms used to classify remotely sensed imagery were assessed using two image analysis approaches: pixel-based and object-based. Second, a feature selection process, based on a Random Forest classifier, was applied to a large data set to reduce the overall number of object-based predictor variables used by a classification model without sacrificing overall classification accuracy. Third, a hybrid object-based change detection method was introduced with the ability to handle disparate image sources, generate per-class change thresholds, and minimize map updating errors. Fourth, a spatial disaggregation procedure was performed on coarse scale agricultural census data to render an indicator of agricultural development in a spatially explicit manner across a 9,000 km^2 watershed in southwest Saskatchewan for three time periods spanning several decades. The combination of methodologies introduced represents an overall analytical framework suitable for supporting the sustainable development of agricultural environments.

ACKNOWLEDGEMENTS

Along the path to accomplishing any significant goal in life we often encounter barriers and even large setbacks that test our resolve. A Japanese proverb states “fall seven times and stand up eight”. Such perseverance is required to surmount the mountain that is one’s doctoral degree, but there is also much to say of those people who help us reach our goals, whose recognition is often underestimated, or worse, overlooked entirely. It is in this space that time is taken to acknowledge those who have contributed to my achievements.

Special thanks must be given to my supervisors who guided me along at various stages of my research: Dr. Monique Dubé for her initial supervision and contagious vision that inspired me to take on the challenge of pursuing my doctoral degree in the first place; and, Dr. Steven Franklin, without whose steadfast mentoring and tireless effort I would not have accomplished my goals. Members of my committee must also be acknowledged as they provided the necessary foundation for success: Drs. Xulin Guo and Paul Treitz for their guidance and insights into the finer aspects of remote sensing and geospatial analysis, Dr. Charles Maule for our thought provoking discussions on defining sustainability, and Dr. Geoff Cunfer who ensured that I remembered that people were underneath all those pixels.

A whole menagerie of people were also involved in getting my research off the ground: Elise Pietroniro, for her technical insights and encyclopedic knowledge of GIS datasets held by the University of Saskatchewan; Mike Andersen (SK MoE), Dave MacDonald (SWA), John Potter (SGIC), and Brent Bitter (SK MoE), who were all instrumental in providing data and insight into its use.

I’d also like to thank those fellow students whose support and shared moments of commiseration over copious amounts of coffee made the journey more bearable: Allison Squires, Jorgelina Muscatello, and Allison Henderson. A very special thanks goes to my good friend Steven Zdunich, who easily introduced me to the majority of Saskatoon’s colorful and

wonderful characters. While I am neglecting to mention many more people in this very short list, rest assured that your friendship and company made my time in Saskatchewan some of the most memorable that anyone could hope for. I'll always consider Saskatoon my home away from home because of you all.

While perhaps more in the distant past on my long journey to this point, I would also like to thank my two former supervisors at Environment Canada: Andrea Ryan and Beverly McNaughton. They opened up the world of water and science to me in a way that university never did.

Finally, I'd like to thank my parents for their unwavering support throughout the years.

TABLE OF CONTENTS

LIST OF TABLES

LIST OF FIGURES

INTRODUCTION

Human activities have resulted in significant environmental change globally with an estimated half of the earth's terrestrial surface directly transformed to varying degrees by human activities (Steffen et al. 2005). Agricultural lands occupy an estimated one-third of the planet's terrestrial surface (Ramankutty et al. 2006), utilize approximately two-thirds of all water withdrawn from rivers, lakes, and aquifers (Postel 2000), and represent society's largest consumptive use of water (Gleick et al. 2008). Modern agricultural practices are a primary driver of human induced change in water quality and quantity (Gordon et al. 2008), and have contributed to the pollution and degradation of freshwater and terrestrial ecosystems globally (Foley et al. 2005). It has been estimated that over half of the world's geographically accessible freshwater runoff has already been appropriated for human use (Postel et al. 1996). Of the total amount of freshwater consumed for human use, the vast majority (70-80%) is used for agricultural purposes (Gleick 2003; Gleick et al. 2008).

Over the last 40 years, cereal production has doubled from advances made during the Green Revolution (Conway 1997) and modern agriculture currently feeds approximately 6 billion people (Tilman et al. 2002). However, rising populations in developing countries and increasing demand for meat-rich diets in emerging markets signal a trend towards intensifying land use on existing arable lands, and an increase in the conversion of less suitable areas for agricultural purposes (OECD/FAO 2011). Demand for food is predicted to double by 2025 and, based on best available estimates, will require that the volume of irrigation more than triple from 1995 levels of 900 km^3 to 2950 km^3, along with an increase in the total share of water consumed by crops using irrigation from 28% to 46% (Postel 1998). Based on present trajectories, it is predicted that over the next 50 years 10^9 hectares of natural ecosystems will be converted to agriculture, accompanied by more than a doubling in anthropogenic eutrophication of terrestrial, freshwater, and near-shore marine ecosystems, along with a comparable increase in pesticide use, culminating in increased habitat destruction,

unprecedented ecosystem simplification, a loss of ecosystem services, and species extinctions (Tilman et al. 2001).

In Canada's western prairie provinces, researchers have warned that the cumulative environmental effects associated with increasing development activities, growing populations, and shifts in regional climate conditions may have disastrous consequences for freshwater ecosystems in the region (Schindler 2001; Schindler et al. 2006; Schindler & Donahue 2006). An analysis of trends in the annual minimum and mean daily flows of several major river systems in this region suggest that a significant decrease over the last 30 years has occurred (Yue et al. 2003). Tree-ring based estimates of mass-balance reveal a net reduction in the amount of ice covering the Peyto glacier between 1966 and 1995 (Watson & Luckman 2004), a trend which has been linked to alterations in water flow for river systems within the prairie provinces (Young 1996). During a similar period, historical land cover change related to agricultural development in the province of Saskatchewan's Boreal Plains revealed an annual deforestation rate of 0.87%, a rate almost three times the world average (Hobson et al. 2002). Expansion of bitumen production in the Athabasca watershed is forecast to triple by 2020, which is expected to result in more water withdrawals, declines in habitat for a variety of species, and an expansion of the already significant amounts of area used to store tailings from the production process (Griffiths et al. 2006).

Within the province of Saskatchewan, prospective management decisions concerning both agricultural development and water resources will require a greater understanding of how the former may influence the latter over various spatial and temporal scales. Accordingly, the management of water resources is shifting towards more integrated management approaches involving large, ecological relevant scales and boundaries such as those provided by drainage basins, which can span several jurisdictional boundaries and scales (Dubé 2003; Heathcote 2009; Seitz et al. 2011). In such integrated approaches, both the water resource itself and the condition of the surrounding landscape that may impinge upon its quality and quantity are assessed in combination (Verdonschot 2000; Snyder et al. 2005; Pinto et al. 2006). For example, the recent State of the Watershed report, conducted by the Saskatchewan Watershed Authority (SWA), reveals that nearly every watershed in the province is experiencing stressed or

impacted conditions overall, and that the intensity of fertilizer and pesticide applications in watersheds draining into the South Saskatchewan River range from moderate to high (Government of Saskatchewan 2010). Such integrated regional reporting frameworks utilize ecologically relevant boundaries (e.g., watersheds) and represent an improvement over traditional reporting methods; however, there remain some methodological shortcomings in the approach outlined in the SWA State of Watershed report and other reporting frameworks that utilize similar approaches.

Chief among these shortcomings are that the thresholds and reporting scheme used for various stressor-based indicators (e.g., manure and pesticide inputs) are completely dependent on the underlying dataset. In other words, the reported condition of various stressor-based variables is merely relative: either higher or lower than other watersheds. As such, an individual watershed can report "stressed" conditions simply because other watersheds have reported comparatively lower values for the same variable. Using such an approach, there is relatively little or no ecologically relevant evidence for stating that a watershed is actually experiencing stressed conditions as comparatively higher (or lower) values may be required for such a threshold to be met. While not all variables reported in the SWA State of the Watershed report utilize such relative thresholds, many of the stressor-based variables indicative of landscape developmental pressures do.

Another shortfall of such reporting frameworks is the lack of spatially explicit data used in their assessments. The source of information used for many of the stressor variables in the SWA State of the Watershed report are derived from agricultural census data that are reported in aggregated form over relatively large watershed areas. While such an approach is an improvement over using traditional non-ecologically relevant jurisdictional boundaries (e.g., census divisions), the relative size of the watersheds and aggregation of the underlying census data within them poses a problem for understanding how agricultural development activities, which occur at local landscape scales where human activity is primarily concentrated (Drigo 2004; Lesschen et al. 2005), are linked to changes in ecosystem condition and functioning within individual watersheds.

A more robust approach would be capable of representing the variability of land use and land cover within individual watersheds, as this would allow for spatially explicit analysis within watersheds to be conducted. Information derived from spatially explicit analysis can be used to better gauge how agricultural development at local scales is linked to changes in aquatic ecosystem condition or function. Such relationships would be based on empirical evidence and would therefore offer a more scientifically defensible threshold as compared to using relative data-driven thresholds.

At present, there exists an opportunity to develop a cohesive analytical framework suitable for assessing spatial and temporal trends in land cover and land use at local landscape scales in agricultural environments. The collection and analysis of such information represents a fundamental first step towards relating agricultural development, conducted at local landscape scales, with relevant environmental variables of interest (e.g., water quality). Such an analytical framework should be capable of acquiring consistent and timely information over large areas to enhance existing integrated regional environmental reporting frameworks (e.g., SWA's State of Watershed report). To accomplish this goal, several methods are introduced in this thesis that allow for processing of earth observation imagery and agricultural land use information in a cohesive manner suitable for informing regional environmental reporting frameworks.

OBJECTIVES

The objective of this thesis is to develop methods for determining spatial and temporal trends in agricultural land cover and land use at local scales, over large areas and relatively long time frames. In addition, these methods are applied to a relatively large watershed in southwest Saskatchewan for three time periods spanning over three decades. Such information represents a critical first step towards relating agricultural development with environmental variables of interest to ascertain thresholds that can be used for management decisions. In order for such relationships to be useful to management decisions that impact local-scale development, suitable information must be obtained that is spatially explicit, temporally dense, and cover relatively large areas. With these conditions in mind, several key methodological advances are proposed in the field of geomatics, with specific contributions made in the areas of remote sensing and spatial analysis. As part of a larger combined analytical framework driven by land cover information derived from remotely sensed imagery and land use information contained in agricultural census data, these methodological advances represent a cohesive analytical framework suitable for supporting the sustainable development of agricultural environments. Specific objectives towards achieving this goal are described below, which highlight both individual contributions and their place within the larger analytical framework for determining spatial and temporal trends in agricultural land cover and land use.

The first objective of this thesis was to compare the relative strengths and weaknesses of several supervised machine learning algorithms used to classify remotely sensed imagery. In addition, two image analysis approaches (pixel-based and object-based) are used to compare the output from the several classification algorithms examined. These classification algorithms, or classifiers, and the underlying image analysis approach, ultimately dictates how individual land cover types are depicted in the final output map. Therefore, it is essential to understand the relative strengths and weaknesses that each classifier provides in conjunction with a particular image analysis approach. Chapter 2 carries out this comparison while providing

recommendations in the context of operational settings that would be encountered in support of regional environmental reporting frameworks (e.g., Saskatchewan Watershed Authority's State of the Watershed report).

The second objective of this thesis was to assess a means of incorporating multiple sources of remotely sensed imagery, gathered at fundamentally different spatial and spectral resolutions. Such multi-scale information can provide a better depiction of land cover information than would be otherwise possible using just a single source of remotely sensed information. In addition, such multi-scale information can provide a richer understanding of relationships between land cover and response variables of interest (e.g., water quality) that might be assessed within a regional environmental reporting framework. Unfortunately, such fundamentally dense datasets are often too unwieldy and/or violate assumptions of traditional statistical approaches. As such, Chapter 3 introduces the use of a feature selection process, based on a Random Forest classifier. This feature selection procedure is applied to a data set in order to reduce the large number of object-based predictor variables used by a classification model without sacrificing overall classification accuracy. In addition, a feature importance measure generated by the Random Forest classifier is used to assess the relative significance of individual predictor variables used in the classification model. This methodological contribution allows for multi-scale remotely sensed information to be utilized in a manner that provides enhanced interpretability and efficiency.

The first two objectives focused on contributions to the classification and interpretation of information derived from remotely sensed imagery. Fundamental to the overall stated objective is the ability to assess landscape changes over time. As such, the third objective of this thesis was to introduce a change detection method suitable for such an application. As previously stated, operational land cover mapping efforts must be flexible enough to utilize disparate sources of imagery. This quality is especially relevant when conducting mapping exercises over long time periods as new remote sensing platforms are launched and/or eventually malfunction. As such, maintaining consistency in mapping products derived from disparate sources of imagery becomes an important quality for any analytical framework that will eventually be placed into an operational environment. In Chapter 4, a hybrid object-based

change detection method was introduced with the ability to handle disparate image sources. While the introduced change detection methodology performed slightly less well than similar methods, it provides a more consistent and flexible map updating strategy that provides per-class change thresholds. In addition, the introduced change detection method minimizes mapping errors due to "sliver" polygons as existing land cover boundaries and individual change objects are handled explicitly within the map updating strategy.

Using the above methods, the fourth objective of this thesis was to consistently map land cover information over a relatively large 9,000 km^2 watershed in southwest Saskatchewan spanning several decades in southwest Saskatchewan for three time periods (c. 1970, c. 1990, and c. 2000). This land cover information was then used to spatially disaggregate agricultural census data over a large watershed area. While such agricultural land use information is useful, it is unsuited to conducting spatially explicit analysis within such large watersheds. Such analysis requires an understanding of the spatial variability in both land cover and land use at local scales, as the relative composition and spatial configuration of land cover and land use at such scales will provide a greater understanding of how agricultural development affects water resources and associated ecosystem services. In Chapter 5, a spatial disaggregation procedure was performed on coarse scale agricultural census data in order to render an indicator of agricultural development in a spatially explicit manner.

The combination of methodologies introduced represents an overall analytical framework suitable for mapping and tracking changes in agricultural land cover across large areas over relatively long time periods in a spatially explicit manner. The information generated using the introduced methods in image analysis and change detection are subsequently used to spatially disaggregate coarse scale agricultural land use information. Such an analytical framework, and the spatially explicit information generated by such an approach, represents a means of using remote sensing and spatial analysis in support of sustainable agricultural development.

REFERENCES

CONWAY, GORDON. 1997. *The Doubly Green Revolution: Food for All in the Twenty-First Century*. London: Penguin.

DRIGO, R. 2004. Trends and patterns of tropical land use change. In *Forests, Water and People in the Humid Tropics: Past, Present and Future Hydrological Research for Integrated Land and Water Management*. Cambridge University Press.

DUBÉ, M. G. 2003. "Cumulative effect assessment in Canada: a regional framework for aquatic ecosystems." *Environmental Impact Assessment Review* 23 (6): 723-745.

FOLEY, JONATHAN A., RUTH DEFRIES, GREGORY P. ASNER, CAROL BARFORD, GORDON BONAN, STEPHEN R. CARPENTER, F. STUART CHAPIN, ET AL. 2005. "Global Consequences of Land Use." *Science* 309 (5734) (July 22): 570-574. doi:10.1126/science.1111772.

GLEICK, PETER H. 2003. "Water use." *Annual Review of Environment and Resources* 28 (1) (November): 275-314. doi:10.1146/annurev.energy.28.040202.122849.

GLEICK, PETER H., HEATHER COOLEY, AND MARI MORIKAWA. 2008. *The World's Water 2008-2009: The Biennial Report on Freshwater Resources*. Island Press, December 26.

GORDON, LINE J., GARRY D. PETERSON, AND ELENA M. BENNETT. 2008. "Agricultural modifications of hydrological flows create ecological surprises." *Trends in Ecology & Evolution* 23 (4) (April): 211-219. doi:10.1016/j.tree.2007.11.011.

GOVERNMENT OF SASKATCHEWAN. 2010. *State of the Watershed Report*. Saskatchewan Watershed Authority. http://www.swa.ca/StateOfTheWatershed/Default.asp?type=WatershedReport.

HEATHCOTE, ISOBEL W. 2009. *Integrated watershed management: principles and practice*. John Wiley and Sons, January 26.

HOBSON, KEITH A., ERIN M. BAYNE, AND STEVE L. VAN WILGENBURG. 2002. "Large-Scale Conversion of Forest to Agriculture in the Boreal Plains of Saskatchewan." *Conservation Biology* 16 (6): 1530-1541. doi:10.1046/j.1523-1739.2002.01199.x.

LESSCHEN, JAN PETER, PETER H VERBURG, AND STEVEN J STAAL. 2005. *Statistical Methods for Analysing the Spatial Dimension of Changes in Land Use and Farming Systems*. International Livestock Research Institute; Wageningen University, LUCC Focus 3 Office. http://books.google.com/books?id=ZaCyMAAACAAJ.

OECD/FAO, AND ORGANISATION FOR ECONOMIC/FOOD AND AGRICULTURE ORGANIZATION OF THE UNITED NATIONS CO-OPERATION AND DEVELOPMENT. 2011. "OECD-FAO Agricultural Outlook 2011-2020" (June 17): 196. doi:http://dx.doi.org/10.1787/agr_outlook-2011-en.

PINTO, B. C. T., F. G. ARAUJO, AND R. M. HUGHES. 2006. "Effects of Landscape and Riparian Condition on a Fish Index of Biotic Integrity in a Large Southeastern Brazil River." *Hydrobiologia* 556 (1) (February): 69-83. doi:10.1007/s10750-005-9009-y.

POSTEL, SANDRA L. 1998. "Water for food production: Will there be enough in 2025?" *Bioscience* 48 (8): 629-637.

———. 2000. “Entering an Era of Water Scarcity: The Challenges Ahead.” *Ecological Applications* 10 (4) (August): 941-948. doi:10.1890/1051-0761(2000)010[0941:EAEOWS]2.0.CO;2.

POSTEL, SANDRA L., G. C. DAILY, AND P. R. EHRLICH. 1996. “Human appropriation of renewable fresh water.” *Science* 271 (5250): 785-788.

RAMANKUTTY, N., EVAN, A. T., MONFREDA, C., FOLEY, J. A. 2006. GLOBAL LAND-COVER CHANGE: RECENT PROGRESS, REMAINING CHALLENGES. IN LAND-USE AND LAND-COVER CHANGE: LOCAL PROCESSES AND GLOBAL IMPACTS. HTTP://DX.DOI.ORG/10.1007/3-540-32202-7.

SCHINDLER, D. W. 2001. “The cumulative effects of climate warming and other human stresses on Canadian freshwaters in the new millennium.” *Can. J. Fish. Aquat. Sci.* 58 (1): 18-29.

SCHINDLER, D. W., AND W. F. DONAHUE. 2006. “An impending water crisis in Canada’s western prairie provinces.” *Proc. Natl. Acad. Sci. U. S. A.* 103 (19): 7210-7216.

SCHINDLER, D. W., P. J. DILLON, AND H. SCHREIER. 2006. “A review of anthropogenic sources of nitrogen and their effects on Canadian aquatic ecosystems.” *Biogeochemistry* 79 (1-2): 25-44.

SEITZ, NICOLE E., CHERIE J. WESTBROOK, AND BRAM F. NOBLE. 2011. “Bringing science into river systems cumulative effects assessment practice.” *Environmental Impact Assessment Review* 31 (3) (April): 172-179. doi:10.1016/j.eiar.2010.08.001.

SNYDER, M.N., S.J. GOETZ, AND R.K. WRIGHT. 2005. “Stream health rankings predicted by satellite derived land cover metrics.” *Journal of the American Water Resources Association* 41 (3): 659-677.

STEFFEN, WILL, REGINA ANGELINA SANDERSON, PETER D. TYSON, JILL JÄGER, PAMELA A. MATSON, BERRIEN MOORE III, FRANK OLDFIELD, ET AL. 2005. *Global Change and the Earth System: A Planet Under Pressure*. 1st ed. 2004. 2nd printing ed. Springer, October 6.

TILMAN, DAVID, KENNETH G. CASSMAN, PAMELA A. MATSON, ROSAMOND NAYLOR, AND STEPHEN POLASKY. 2002. "Agricultural sustainability and intensive production practices." *Nature* 418 (6898): 671-677. doi:10.1038/nature01014.

TILMAN, DAVID, JOSEPH FARGIONE, BRIAN WOLFF, CARLA D'ANTONIO, ANDREW DOBSON, ROBERT HOWARTH, DAVID SCHINDLER, WILLIAM H. SCHLESINGER, DANIEL SIMBERLOFF, AND DEBORAH SWACKHAMER. 2001. "Forecasting Agriculturally Driven Global Environmental Change." *Science* 292 (5515) (April 13): 281-284. doi:10.1126/science.1057544.

VERDONSCHOT, PIET F.M. 2000. "Integrated ecological assessment methods as a basis for sustainable catchment management." *Hydrobiologia* 422-423 (April 1): 389-412. doi:10.1023/A:1017094905369.

YUE, S., P. PILON, AND B. PHINNEY. 2003. "Canadian streamflow trend detection: impacts of serial and cross-correlation." *Hydrol. Sci. J.-J. Sci. Hydrol.* 48 (1): 51-63.

CHAPTER 1 PREFACE

In this first chapter, the reader is introduced to the overall motivation for developing enhanced methods suitable for examining spatial and temporal trends in agricultural land cover and land use at local landscape scales. A concise overview of several key techniques for combining land cover and land use information is provided. Background material that was not possible to include in subsequent, more focused, chapters is provided here to give the reader a more wide-ranging and inclusive summary.

CHAPTER 1

REMOTE SENSING AND GIS METHODS FOR MAPPING LAND COVER AND LAND USE IN AGRICULTRUAL ENVIRONMENTS

1.1 ABSTRACT

Human development has resulted in significant global landscape change. Historically, much of these alterations have occurred in natural environments that are compatible with human activities. In the last 300 years, the intensification of land use practises and wholesale shifts in land cover composition within human dominated landscapes have been linked to various forms of environmental degradation. Increasingly, managers and decision makers are faced with balancing the needs of human development with the range of environmental conditions required to maintain properly functioning ecosystems. This task is especially difficult in environments where the nature of the pollution associated with human activities is diffuse, occurs across large regional areas, and is cumulative in nature. As a first step towards addressing such challenges, development on the landscape must first be identified, tracked, and ultimately related to environmental variables of interest. Furthermore, such relationships must also include pre-development conditions in order to assess the full range of variability between landscape changes and environmental variables of interest.

Progress in the ability to detect changes in land cover composition remotely, using sensors aboard aerial and satellite based platforms, have allowed for the near continuous monitoring and evaluation of landscape change across large areas. When remotely sensed imagery is coupled with records detailing the types and intensity of land use practises occurring on the landscape, it is possible to gain a more detailed depiction of human development, both prior to, and after development has taken place. In this chapter, key advances in image processing and data integration techniques are examined that can be used in supporting sustainable development of agricultural environments at larger, ecologically relevant, landscape scales using remotely sensed imagery and land use data.

1.2 INTRODUCTION

Over the past four decades, the ability to more precisely classify and estimate changes in the composition and extent of land cover has been facilitated by the relatively recent and widespread availability of imagery acquired by sensors on-board aerial and satellite based platforms (Wulder & Franklin 2007). Land cover can be defined as those physical features of interest that can be identified on the landscape (e.g., forest), whereas land use describes how that particular cover type is utilized (e.g., national park versus active logging area). Unfortunately, much of the information associated with land use activities cannot be directly inferred with information that is detectable remotely. For example, within agricultural environments, cropland areas might be readily identified by remotely sensed imagery; however, the associated land use practises of this land cover type may change from year to year (e.g., tillage practises, changes in the amount of fertilizer applied, etc.). Crops requiring intensive fertilizer applications may contribute relatively more to human induced eutrophication than those that do not. Such land use intensity information will likely remain difficult or impossible to directly infer from remotely sensed data alone, but such information remains essential to obtaining a complete understanding of historical human-induced landscape change (Drigo 2004; Lesschen et al. 2005).

Understanding historical changes in land cover and land use is largely dependent on the availability and consistency of appropriate data sources, which represents a significant challenge. For example, while the ability to collect increasingly complex land cover information over large areas has improved in recent decades, the availability of such spatially-consistent data prior to the 1960s is limited in most areas of the world. Aerial photography may extend such land cover records into the early decades of the 20th century, but in many cases, land cover data sources for earlier periods are likely to be qualitative, spatially-constrained, or even non-existent. Similarly, detailed and consistent land use information, such as the data recorded in government censuses, is considered to be of very poor quality prior to the mid-1940s (Ramankutty et al. 2006). Furthermore, while land use data are most often collected at fine

spatial scales (e.g., individual farmsteads), such data are often only made available to the public in aggregated form over much broader spatial extents, often representing administrative units (e.g., census boundaries). Unfortunately, such spatial delineations often bear little or no resemblance to natural boundaries that are ecologically relevant (e.g., watersheds, ecoregions, etc.), and the aggregation process itself can cause valuable fine spatial scale information to be lost.

Land cover and land use data represent complementary, yet distinctly different, information required to better understand human-induced environmental change over current and historical time periods. Increasingly, researchers are examining ways of integrating such disparate datasets (see Liverman 1998; Entwisle 2005; Lambin & Geist 2006). The promise of such an approach is the ability to utilize information that describes the variability and magnitude of land cover change, along with local landscape scale information related to human development activities (e.g., land use information available in census data). Together, such information allows for a richer understanding of how humans impact the landscape, at a variety of spatial and temporal scales. Unfortunately, issues of availability, continuity, and comparability between remotely sensed imagery and ancillary datasets used in such approaches still plague efforts in the reconstruction of historical land cover and land use. Progress in image processing and data integration techniques developed for a variety of remote sensing applications offer a promising means of partially addressing these issues. In this chapter, several advances in image processing and data integration techniques suitable for reconstructing historical land cover and land use are examined with the following goals:

i) Review relevant examples of image processing techniques that demonstrate improvements in land cover discrimination and classification accuracy, with a focus on examples that can effectively utilize multiple sources of remotely sensed imagery;

ii) Examine how data integration techniques can be used to spatially disaggregate land use information (e.g., agricultural census data) using relatively fine spatial resolution land cover information derived from remotely sensed imagery;

iii) Describe how the above two techniques, when used within an object-based image analysis approach facilitated by a Geographical Information System (GIS), and driven by remotely sensed imagery and ancillary datasets, can be used to efficiently create and update consistent land cover and land use maps at finer spatial resolutions than typically available.

When considered together, progress within these above areas represent a viable means of addressing issues of data availability, continuity, and comparability that presently challenge our understanding of change in land cover and land use at a variety of spatial and temporal scales. The emphasis in this review is on agricultural environments as this particular land cover and land use represents a relatively ubiquitous example of human activity in terrestrial environments; however, the techniques and methods outlined here should remain transferable to other settings where the consistency, comparability, and integration of land cover and land use data are of interest.

1.3 IMAGE FUSION FOR ENHANCING THE MAPPING OF LAND COVER IN AGRICULTURAL ENVIRONMENTS

Sensors on-board aerial or satellite based platforms are capable of recording electromagnetic energy at different spatial, temporal, spectral, and radiometric resolutions. "Image fusion" describes a suite of data processing techniques used to integrate multiple digital based images, often from disparate sources, for the purposes of enhancing information from the image(s) that could not otherwise be extracted using a single image alone (Pohl & Van Genderen 1998). So-called "fused" imagery can be used to improve upon a variety of existing remote sensing applications ranging from the visual interpretation of imagery (e.g., "pan-

sharpened" multispectral imagery) to enhancing the ability to extract land cover classes for thematic mapping purposes. In this section, several examples of image fusion are examined. The examples are limited to studies that combine imagery in the optical and microwave portion of the electromagnetic spectrum as this combination has been used extensively to map agricultural landscapes. Furthermore, this sections illustrates the relative advantage of using multiple sources of remotely sensed imagery to improve classification accuracies of agricultural land cover types

In agricultural environments, image fusion techniques involving visual/near-infrared (VNIR) and microwave wavelengths have long been used to improve upon classification accuracies of various land cover types (Ahern et al. 1978). Microwave and VNIR wavelengths interact with objects in the environment differently, and provide unique wavelength dependant information that can increase the ability to discriminate between specific agricultural land cover types of interest when combined (e.g., wheat vs. corn). For vegetation, the amount of backscattering received by a sensor in the relatively longer microwave wavelengths is strongly dependent on the macro structure of the target (size of leaves, stems, branches, and cropping configuration) as well as its moisture content; whereas information received from relatively shorter VNIR wavelengths are more dependent on plant pigmentation, micro structure (intercellular arrangement), and moisture content of the leaf and canopy (Carver et al. 1985; Jensen 2000; Lillesand et al. 2004; Jensen 2005). While VNIR wavelengths for mapping agricultural land cover often achieve higher accuracies when compared to using only microwave wavelengths, many studies have shown that the combination of both types of imagery can achieve higher overall classification accuracies.

For example, Ahern et al. (1978) concluded that multispectral and microwave data, simultaneously gathered from an aerial platform, provided complimentary information that when combined allowed for an increased ability to discriminate between agricultural land cover types as compared to using a single source. In a similar study, Ulaby et al. (1982) found that combining airborne microwave data with VNIR imagery (Landsat), improved the classification accuracy of agricultural land cover types (wheat stubble, corn, pasture, and bare soil) by

approximately 10% on a per pixel basis, and by ~15% when averaged across their studied field (400 x 400 meters). These early studies demonstrate that the fusion of VNIR and microwave imagery can improve the discrimination of crop types.

In later studies, Brisco & Brown (1995) investigated the utility of fusing multi-date airborne Synthetic Aperture Radar (SAR) imagery and multi-spectral imagery (Landsat) for the purposes of mapping agricultural land cover types. Their findings demonstrated that combining these two image sources provided an enhanced ability to discern agricultural land cover types, with SAR imagery better able to distinguish canola from grains and fallow land cover types when compared to VNIR data, especially in the early portion of the growing season, likely due to the relatively higher amounts of backscatter from the macro structure of the broad-leafed crops as compared to the grains and fallow land cover types. Brisco & Brown (1995) also noted that land cover classifications utilizing SAR imagery over multiple dates improved overall classification accuracy from 30% to 74%; however, the same imagery only added a slight improvement to the classification accuracies achieved using multiple-date VNIR classifications (90% versus 92%). While VNIR classifications still outperformed those produced using SAR imagery, the additional improvements in SAR classification accuracies using multiple date SAR imagery was substantial in this study. Similarly, Simone et al. (2002) found that the fusion of multiple-date, multi-polarized SAR (ERS-1) imagery along with multi-spectral imagery (Landsat) sources resulted in a substantial improvement in the average classification accuracy for "cereals" land cover in the early portion of the growing season (16.7% without fusion, compared to 75.0% with fusion).

In a more recent study (McNairn et al. 2009), a single VNIR image dataset (SPOT and Landsat TM) was compared to a single multi-polarized SAR image dataset (RADARSAT and ENVISAT), with both datasets acquired within a 7-day window. Overall classification accuracies for crop land cover types of the VNIR dataset (~70%) outperformed those of the SAR dataset (~45-50%) in a variety of environments; however, when multiple dates of SAR imagery were combined (without VNIR imagery), classification accuracies between 74-84% were possible (McNairn et al. 2009). The use of multi-polarization SAR imagery for classifying agricultural land cover shows a distinct improvement over the results obtained by Brisco & Brown (1995), and

suggests that such an approach offers a comparable ability to classify crop types, as compared to VNIR-only based classifications, when multiple-dates of imagery are used.

While the list of examples above is not exhaustive, the results typify those found throughout the literature on microwave-VNIR image fusion. Improvements to land cover classification accuracy in agricultural environments when fusing multiple date SAR and VNIR imagery can yield substantial improvements, but in general, typical results provide only marginal increases over classification accuracies achieved using single date VNIR data alone. However, since atmospheric conditions (cloud cover, smoke, etc.) often hamper the collection of VNIR imagery, a strategy for image acquisitions that includes the all-weather capabilities of SAR imagery to fill in and/or complement existing VNIR imagery are evident and persuasive when obtaining consistent spatial and temporal coverage of land cover is of interest (McNairn et al. 2009).

In Chapter 3, an example of data fusion using multiple sources of remotely sensed (VNIR) imagery is described. While SAR imagery was available for the more recent time periods examined in this thesis (1990 and beyond), the relative lack of such imagery in earlier time periods precluded its use. Nevertheless, the utility of fusing VNIR and SAR imagery for enhancing the classification accuracy of various agricultural land cover types appears to be well founded especially in operational settings where the all-weather capabilities of SAR can fill-in and/or enhance crop classification efforts (McNairn et al. 2009). Given these findings, operational settings requiring the spatial disaggregation of land use data should employ multi-date VNIR and SAR imagery to supplement and/or enhance the classification of agricultural land cover types, especially in situations where the discrimination between multiple crop types are of interest.

1.4 CREATING CONSISTENT HISTORICAL LAND COVER AND LAND USE MAPS

Linke et al. (2009a) outline an object-based image analysis approach suitable for updating an existing reference thematic map within a "spatio-temporal disturbance-inventory database" (i.e., a GIS) using remotely sensed imagery. Object-based image analysis relies on image segmentation, a process whereby individual pixels are grouped to form larger, often spectrally similar, image objects or segments. These image objects are used as the basis for subsequent image classification. Linke et al. (2009b) demonstrated that small errors ("slivers") introduced through object-based map updating procedures can potentially cause large discrepancies in various landscape metrics, potentially introducing a large source of error over time. To minimize such errors, only areas where change has been detected are subjected to map updating procedures (Feranec et al. 2000; 2007). In their approach, Linke et al. (2009a) calculated the enhanced wetness difference index (EWDI) for each date to determine areas of annual disturbances (Franklin et al. 2001). Areas representing change between dates are converted into polygon objects through image segmentation. Since disturbance information from ancillary and remotely sensed imagery are treated as objects within a GIS, individual disturbance objects can be classified and updated (or backdated) from the original baseline map, and any anomalies that can affect comparison of landscape metrics between multiple dates (e.g., spurious stretch, sliver objects, etc) can be handled and errors minimized (Linke et al. 2009b).

By incorporating object-based image analysis, and only updating areas identified as change, the approach described by Linke et al. (2009a) is well suited to applications that require a long time series of land cover maps that minimizes the amount of error introduced from the updating procedure. In Chapter 4, the map updating logic recommended by Linke et al (2009a) is adapted to a large study area, and utilizes disparate sources of remotely sensed imagery with distinctly different spatial, spectral, and radiometric properties.

1.5 INTEGRATING AGGREGATED LAND USE DATA WITH REMOTELY SENSED LAND COVER IMAGERY

Detailed land use data, collected at fine local spatial scales (e.g., individual farmsteads), are often summarized over large administrative areas (e.g., census boundaries). Typically, data aggregation is done to protect the privacy of individuals' information, but it also serves as a means of summarizing key demographic and agricultural measures of interest over a broad geographical area (e.g., demographic information, amount of fertilizer purchased, number of livestock, etc.). Unfortunately, the size of the boundaries used to disseminate publicly accessible information is often compiled over scales too coarse to ascertain local landscape development activities. In addition, while these administrative boundaries are useful for facilitating analysis relative to jurisdictional needs, such delineations are not well suited for understanding processes that occur over ecologically relevant boundaries (e.g., watersheds, ecozones, soil types, etc.). Information provided in the latter form allow for a better understanding of how human activities might be linked to deteriorating ecological services (e.g., anthropogenic eutrophication). Fortunately, several techniques have been used to "spatially refine" aggregated land use data into a form more suitable to examining local landscape development using ecologically relevant boundaries. In this section, an example of using spatially explicit land cover data derived from remotely sensed imagery to disaggregate land use data is examined.

Perhaps the earliest example of using remotely sensed imagery of land cover to disaggregate land use information was pioneered by Green (1957). In that study, land cover data extracted from aerial photographs were combined with socioeconomic data that measured the relative desirability of residential areas in Birmingham, Alabama. Relevant areas of land cover (e.g., urban and suburban built environments) were identified on aerial photography and associated with housing density and socioeconomic data, such as mean household income, in order to clarify urban patterns in a spatially explicit manner. Using this approach, Green (1957) showed that the higher spatial resolution of urban dwellings depicted

in the aerial photographs could be used to effectively disaggregate the spatially coarse resolution land use data contained within population census data. Since that time, the development of satellite-based platforms, advances in sensor technology, computing power, image processing techniques, and statistical modelling methods have allowed for this approach to further improve similar studies based in urban environments (Lo 1995; Lo & Faber 1997; Chen 2002; Rogan & Chen 2004).

Data integration techniques such as those presented above illustrate that data collected and summarized using different scales can be successfully merged, allowing for aggregated land use information to be made more comparable with relatively fine spatial resolution land cover imagery. In Chapter 5, several examples of spatial disaggregation of agricultural land use information using remotely sensed imagery are examined. In addition, a spatial disaggregation process is conducted over a large study area, with the results compared to typical choropleth mapping results.

1.6 DISCUSSION

Developments in image processing and data integration techniques can aid in the production of land cover and land use maps in agricultural environments. Image fusion techniques allow for increased classification accuracies and the ability to better discriminate between various agricultural land cover types. Such techniques also allow for a more robust means of dealing with the vagaries of atmospheric effects and the subsequent loss of data that hamper land cover classification exercises. Advances in data integration techniques illustrate how land use data aggregated over large areas, such as agricultural census data, can be made more comparable to finer spatial resolution land cover data derived from remotely sensed imagery. When used in concert, these two techniques produce maps of land cover and land use data that are spatially explicit, and therefore, more representative of local landscape development. Lastly, land cover and land use maps produced using the techniques outlined above are further strengthened within an object-based image analysis approach, which allows

for finer grained control over updating existing base map, reducing small, but potentially cumulatively large, errors while improving consistency between a time series of land cover maps. When combined, progress in these three areas represents an innovative means of monitoring and documenting landscape change in agricultural environments.

1.7 CONCLUSION

In this chapter, key advances in image processing, data integration, and GIS techniques using remotely sensed imagery and historical ancillary data were examined. Recent progress in these areas represent significant developments that, when combined, can form the basis of an integrated analytical framework capable of monitoring and assessing changes in land cover and land use over historical time periods at fine spatial scales. Improvements such as these are important in a variety of applications where detailed land cover and land use information are desirable. As human populations continue to grow, greater demands placed on agricultural environments are likely to increase, along with the environmental degradation associated with such development. Further refinement and combination of the techniques described here will allow for a greater understanding of historical land cover and land use change at local landscape scales commensurate with human activity.

1.8 REFERENCES

AHERN, F. J., D. G. GOODENOUGH, A. L. GREY, R. A. RYERSON, AND R. J. VILBIKAITIS. 1978. Simultaneous microwave and optical wavelength observations of agricultural targets. *Canadian Journal of Remote Sensing* 4 (2): 127-142.

BRISCO, B., AND R. J. BROWN. 1995. Multidate SAR/TM synergism for crop classification in western Canada. *Photogrammetric Engineering and Remote Sensing* 61 (8): 1009-1014.

BRYANT, D. G., D. NIELSEN, L. TANGLEY, AND F. F. I. (WORLD R. INSTITUTE). 1997. *The last frontier forests*. World Resources Institute, Forest Frontiers Initiative.

CARVER, K. R., C. ELACHI, AND F. T. ULABY. 1985. MICROWAVE REMOTE SENSING FROM SPACE. *Proceedings of the IEEE* 73 (6): 970-996.

CHEN, K. 2002. An approach to linking remotely sensed data and areal census data. *International Journal of Remote Sensing* 23 (1): 37.

CIHLAR, J., L. HUNG, L. ZHANQING, C. JING, H. POKRANT, AND H. FENGTING. 1997. Multitemporal, Multichannel AVHRR Data Sets for Land Biosphere Studies--Artifacts and Corrections. *Remote Sensing of Environment* 60: 35-57.

DRIGO, R. 2004. Trends and patterns of tropical land use change. In *Forests, Water and People in the Humid Tropics: Past, Present and Future Hydrological Research for Integrated Land and Water Management*. Cambridge University Press.

FRANKLIN, S.E., M. B. LAVIGNE, L. M. MOSKAL, M.A. WULDER, AND T. M. MCCAFFREY. 2001. Interpretation of forest harvest conditions in New Brunswick using Landsat TM enhanced wetness difference imagery (EWDI). *Canadian Journal of Remote Sensing* 27 (2): 118-128.

FERANEC, JAN, G. HAZEU, S. CHRISTENSEN, AND G. JAFFRAIN. 2007. Corine land cover change detection in Europe (case studies of the Netherlands and Slovakia). *Land Use Policy* 24 (1): 234-247.

FERANEC, JÁN, M. SÚRI, J. OT'AHEL', T. CEBECAUER, J. KOLÁR, T. SOUKUP, D. ZDENKOVÁ, ET AL. 2000. Inventory of major landscape changes in the Czech Republic, Hungary, Romania and Slovak Republic 1970s - 1990s. *International Journal of Applied Earth Observation and Geoinformation* 2 (2): 129-139.

GREEN, N. E. 1957. Aerial photographic interpretation and the social structure of the city. *Photogrammetric Engineering* 23 (1): 89-96.

JENSEN, J. R. 2000. *Remote sensing of the environment*. Prentice Hall.

———. 2005. *Introductory Digital Image Processing: A Remote Sensing Perspective*. 3rd ed. Prentice Hall series in geographic information science. Upper Saddle River, N.J: Pearson/Prentice Hall.

KERR, J. T., AND J. CIHLAR. 2003. Land use and cover with intensity of agriculture for Canada from satellite and census data. *Glob. Ecol. Biogeogr.* 12 (2): 161-172.

LAMBIN, E. F., AND H. GEIST. 2006. *Land-Use and Land-Cover Change: Local Processes and Global Impacts*.

LESSCHEN, J. P., P. H. VERBURG, AND S. J. STAAL. 2005. *Statistical Methods for Analysing the Spatial Dimension of Changes in Land Use and Farming Systems*. International Livestock Research Institute; Wageningen University, LUCC Focus 3 Office.

LILLESAND, T. M., R. W. KIEFER, AND J. W. CHIPMAN. 2004. *Remote sensing and image interpretation*. Wiley.

LINKE, J., G. J. MCDERMID, D. N. LASKLN, A. J. MCLANE, A. PAPE, J. CRANSTON, M. HALL-BEYER, AND S.E. FRANKLIN. 2009a. A disturbance-inventory framework for flexible and reliable landscape monitoring. *Photogrammetric Engineering and Remote Sensing* 75 (8): 981-995.

LINKE, J.,G.J. MCDERMID, A. PAPE, A. MCLANE, D. LASKIN, M. HALL-BEYER, AND S.E. FRANKLIN 2009b. The influence of patch-delineation mismatches on multi-temporal landscape pattern analysis. *Landscape Ecology* 24 (2): 157-170.

LIVERMAN, D. M. 1998. *People and Pixels Linking Remote Sensing and Social Science*. Washington, D.C.: National Academy Press.

LO, C. P. 1995. Automated population and dwelling unit estimation from high-resolution satellite images: a GIS - approach. *International Journal of Remote Sensing* 16 (1): 17.

LO, C. P., AND B. J. FABER. 1997. Integration of landsat thematic mapper and census data for quality of life assessment. *Remote Sensing of Environment* 62 (2): 143-157.

POHL, C., AND J. L. VAN GENDEREN. 1998. Review article Multisensor image fusion in remote sensing: concepts, methods and applications. *International Journal of Remote Sensing* 19 (5): 823.

RAMANKUTTY, N., L. GRAUMLICH, A. FRÉDÉRIC, A. DIOGENES, C. ABHA, R.S. DEFRIES, J. FOLEY, H. GEIST, R. HOUGHTON, K. KLEIN GOLDEWIJK, E. LAMBIN, A. MILLINGTON, K.

RAMUSSEN, R.S. REID, B.L. TURNER II, 2006. Global Land-Cover Change: Recent Progress, Remaining Challenges. In *Land-Use and Land-Cover Change: Local Processes and Global Impacts*.

ROGAN, J., AND D. CHEN. 2004. Remote sensing technology for mapping and monitoring land-cover and land-use change. *Progress in Planning* 61 (4): 301-325.

SIMONE, G., A. FARINA, F. C. MORABITO, S. B. SERPICO, AND L. BRUZZONE. 2002. Image fusion techniques for remote sensing applications. *Information Fusion* 3 (1): 3-15.

STEFFEN, W., R. A. SANDERSON, P. D. TYSON, J. JÄGER, P. A. MATSON, B. M. III, F. OLDFIELD, ET AL. 2005. *Global Change and the Earth System: A Planet Under Pressure*. 1st ed. 2004. 2nd printing ed. Springer.

ULABY, F. T., R. Y. LI, AND K. S. SHANMUGAN. 1982. Crop Classification Using Airborne Radar and Landsat Data. *IEEE Transactions on Geoscience and Remote Sensing* GE-20 (1): 42-51.

WULDER, M. A., AND S.E. FRANKLIN. 2007. *Understanding forest disturbance and spatial pattern*. CRC Press.

CHAPTER 2 PREFACE

In this chapter, a comparison between pixel-based and object-based image analysis is conducted to ascertain the relative strengths and weaknesses of each approach. In addition, several relatively newer machine learning algorithms used to classify remotely sensed imagery are assessed, with emphasis placed on their ability to provide visually optimal depictions of selected land cover types while achieving high overall classification accuracies. As the selected image analysis approach and classification algorithm produce output that represents the underlying basis for subsequent analyses, the assessment process utilized both a statistically rigorous approach and a detailed visual assessment. The results of the comparison, and the outlined detailed assessment process, serve as the basis for image analysis conducted in subsequent chapters of this thesis.

CHAPTER 2

A COMPARISON OF PIXEL-BASED AND OBJECT-BASED IMAGE ANALYSIS WITH SELECTED MACHINE LEARNING ALGORITHMS FOR THE CLASSIFICATION OF AGRICULTURAL LANDSCAPES USING SPOT-5 HRG IMAGERY[*]

[*] The published contents of this chapter appear with permission from Elsevier Inc. The version that appears in this document has been modified to maintain consistency and formatting between chapters, and as such, it contains different content than the original material. Readers are encouraged to refer to the original publication:

DURO, D.C., FRANKLIN, S.E., DUBÉ, M.G. (2012). A comparison of pixel-based and object-based image analysis with selected machine learning algorithms for the classification of agricultural landscapes using SPOT-5 HRG imagery. *Remote Sensing of Environment* (118): pp. 259-272.

All work reported in this chapter, including the review of the literature, experimental design, analysis and discussion of the results, and writing of the text, was carried out by the Ph.D. candidate. As supervisors, Drs. S.E. Franklin and M.G. Dubé reviewed all or parts of the work.

2.1 ABSTRACT

Pixel-based and object-based image analysis approaches for classifying broad land cover classes over agricultural landscapes are compared using three supervised machine learning algorithms: decision tree (DT), random forest (RF), and the support vector machine (SVM). Overall classification accuracies between pixel-based and object-based classifications were not statistically significant ($p>0.05$) when the same machine learning algorithms were applied. Overall classification accuracy for pixel-based image analysis approaches ranged from 87.6 to 89.3%, and 88.8% to 94.2% for object-based image analysis approaches. Using object-based image analysis, there was a statistically significant difference in classification accuracy between maps produced using the DT algorithm compared to maps produced using either RF ($p=0.0116$) or SVM algorithms ($p=0.0067$). Using pixel-based image analysis, there was no statistically significant difference ($p>0.05$) between results produced using different classification algorithms. Classifications based on RF and SVM algorithms provided a more visually adequate depiction of wetland, riparian, and crop land cover types when compared to DT based classifications, using either object-based or pixel-based image analysis. In this study, pixel-based classifications utilized fewer variables (15 vs. 300), achieved similar classification accuracies, and required less time to produce than object-based classifications. Object-based classifications produced a visually appealing generalized appearance of land cover classes. Based exclusively on the basis of overall classification accuracy, there was no advantage to preferring one image analysis approach over another for the purposes of mapping broad land cover types in agricultural environments using medium spatial resolution earth observation imagery.

2.2 INTRODUCTION

The classification of land use and land cover (LULC) from remotely sensed imagery can be divided into two general image analysis approaches: i) classifications based on pixels, and ii) classifications based on objects. While pixel-based analysis has long been the mainstay for classifying remotely sensed imagery, object-based image analysis has become increasingly

commonplace over the last decade (Blaschke, 2010). Whether pixels or objects are used as underlying units for the purposes of classifying remotely derived imagery, the information contained within and among these units can be subjected to a variety of classification algorithms. Previous comparative studies have been conducted that examine the relative performance of different classification algorithms using pixel-based, and/or object-based image analysis. A brief summary of selected comparisons is provided below.

2.2.1 ALGORITHM COMPARISONS USING PIXEL-BASED OR OBJECT-BASED CLASSIFICATIONS

Using pixel-based based image analysis on Landsat Thematic Mapper (TM) data, Huang et al. (2002) compared thematic mapping accuracies produced using four different classification algorithms: support vector machines (SVMs), decision trees (DTs), a neural network classifier, and the maximum likelihood classifier (MLC). Their results suggested that the accuracy of SVM-based classifications generally outperformed the other three classification algorithms. Pal (2005) compared the accuracies of two supervised classification algorithms using Landsat Enhanced Thematic Mapper (ETM+) data: SVMs and Random Forests (RFs) (Breiman, 2001), and found that they performed equally well. Gislason et al. (2006) compared a RF approach to a variety of decision tree-like algorithms using pixel-based image analysis of Landsat MSS data. They found that the selected tree-like algorithms tested performed similarly, but that the RF algorithm outperformed the standard implementation of Breiman et al.'s (1984) DTs; however, their findings also showed that the RF algorithm performed slightly less well than a modified DT algorithm (boosted 1R). Carreiras et al. (2006) examined several classification algorithms, which included standard DTs, quadratic discriminant analysis, probability-bagging classification trees (PBCT), and k-nearest neighbors (K-NN) using pixel-based analysis of spatially coarse (1 km pixels) SPOT-4 VEGETATION imagery. Their results, verified by 10-fold cross-validation, showed that the PBCT algorithm produced the best overall classification accuracy. Brenning (2009) compared eleven classification algorithms using a pixel-based image analysis, and Landsat ETM+ imagery, for the detection of rock glaciers. This extensive study found that penalized

linear discriminant analysis (PLDA) yielded significantly better mapping results as compared to all other classifiers, including both SVMs and RFs. Using Landsat TM and ETM+data, Otukei and Blaschke (2010) compared the MLC, SVM, and DT algorithms in a pixel-based approach, and found DTs performed better than MLC and SVM. In an earlier study, Laliberte et al. (2006) used an object-based approach on Quickbird imagery to compare K-NN with DT algorithms. Their study found that DTs produced better overall classification accuracies than the K-NN algorithm, but that the former was more difficult to implement as compared to the latter.

2.2.2 ALGORITHM COMPARISONS BETWEEN PIXEL-BASED AND OBJECT-BASED CLASSIFICATIONS

Relatively recent comparisons between the results of pixel-based and object-based image analysis have also been conducted. For example, Yan et al.(2006) compared pixel-based image analysis using MLC and object-based image analysis using K-NN on Terra Advanced Spaceborne Thermal Emission and Reflection Radiometer (ASTER) imagery. In their study, the authors claimed that the overall accuracy of the object-based K-NN classification drastically outperformed the pixel-based MLC classification (83.25% and 46.48%, respectively). Yu et al. (2006) used high spatial resolution digital airborne imagery and compared a pixel-based classification based on MLC with an object-based classification using K-NN, using a DT as a mechanism for feature selection in both cases. Their study showed that the 1-NN object-based classification outperformed the pixel-based MLC classification by 17%, although calculation of the average classification accuracy of each of the 48 vegetation classes listed was only 51% for the object-based K-NN classification, and 61.8% for the pixel-based classification using MLC. Platt and Rapoza (2008) compared K-NN and MLC for both pixel-based and object-based classifications, with and without the addition of expert-based knowledge, using multi-spectral IKONOS imagery. Their results revealed that the object-based NN classification using expert knowledge had the best overall classification (78%), while the best pixel-based classification using MLC (without expert knowledge) achieved an overall accuracy of 64%. Castillejo-González et al. (2009) compared pixel-based and object-based classifications in agricultural environments

using multispectral Quickbird imagery and a variety of classification algorithms. The best pixel-based classification used non-pan-sharpened imagery and the MLC algorithm, while the best purely object-based classification used pan-sharpened imagery and MLC, with both approaches achieving high overall accuracies of 89.6% and 93.69%, respectively. Their study also revealed that the two best results, using non-pan-sharpened imagery and MLC, showed a small difference in classification accuracy between pixel-based and object-based image analysis (89.60% and 90.66%, respectively); however, the difference between these same approaches grew considerably when using pan-sharpened imagery (82.55% and 93.69%, respectively). Myint et al. (2011) used Quickbird imagery to classify urban land cover. They compared results from a MLC pixel-based classification with an object-based classifier using K-NN and a series of fuzzy membership functions.

The object-based classification (90.4%) outperformed the pixel-based classification (67.6%) in overall accuracy for their original image; however, in their test image, the differences between the object-based and pixel-based approaches were reduced to less than 10% (95.2 and 87.8%, respectively). Finally, in a recent study, Dingle Robertson and King (2011) compared pixel-based and object-based image analysis for classifying broad agricultural land cover types for two time periods (1995 and 2005) using Landsat-5 TM imagery. They compared land cover maps produced using MLC (pixel-based) and K-NN (object-based) algorithms and found that the difference in overall accuracy between these classification approaches was not statistically significant. Despite these findings, an intensive visual analysis of their post-classification analysis revealed that the object-based classification using K-NN depicted areas of change more accurately than the pixel-based classification using MLC.

In general, the above comparisons between pixel-based and object-based classifications reveal that the latter typically outperform the former when comparing overall classification accuracy using a variety of remotely sensed imagery in settings ranging from agricultural to urban land cover classes. However, unlike the studies examining either pixel-based or object-based classifications in isolation, many comparison studies often rely on relatively simple

classification algorithms (e.g., K-NN) for the object-based classification, and probabilistic based algorithms (e.g., MLC) for the pixel-based classification, the latter of which is less suited to datasets that are non-normally distributed, or that contain categorical data (Franklin & Wulder, 2002).

The present study aims to bridge the gap between these previous comparisons by examining both pixel-based and object-based classification approaches, with a selection of relatively modern and robust supervised machine learning algorithms: decision trees (DTs), random forests (RFs), and support vector machines (SVMs). We conduct a visual and statistical assessment of the classification outputs using medium spatial resolution (10 m) multi-spectral imagery from the SPOT-5 HRG sensor. For the purposes of this study, six broad land cover classes were mapped in a riparian area undergoing intensive agricultural development in western Canada. We assessed each image analysis approach, and each of the selected machine learning algorithms, for their ability to accurately portray these selected land cover types. Recommendations are made in the context of mapping of agricultural landscapes for the purposes of general land cover mapping and monitoring in agricultural environments using medium spatial resolution earth observation imagery.

2.3 METHODS

2.3.1 STUDY AREA

The study area is located along the South Saskatchewan River approximately 90 km east of the provincial border of Alberta-Saskatchewan (Figure 1). The approximately 80 sq. km study area is a subset of a much larger drainage basin selected by researchers attempting to understand how long-term (~30 years) land cover change and land use practices typical of the southern half of the western Prairie Provinces of Canada might impact the integrity of aquatic ecosystem composition and function. Similar large drainage areas have been previously selected by others to assess potential impacts caused by development on aquatic ecosystems over time (e.g., Squires et al., 2009), and represent an appropriate scale and unit of measurement for conducting cumulative environmental effects assessments on aquatic

ecosystems (Dubé, 2003; Duinker & Greig, 2006; Noble, 2008; Seitz et al., 2011). Indeed, over the past century, environmental impacts in the region due to agricultural development have replaced much of the native vegetation and has filled an estimated 40% of small wetland areas (Huel, 2000), facilitating the gradual introduction of crops and improved pasture lands that dominate much of the prairies today. The selected study area is typical of agricultural activity conducted near riparian and wetland environments in the region. Such environments have been linked to a range of species and environmental processes, the flow of nutrients between terrestrial and aquatic ecosystems, and are the focus of agricultural management practices for protecting water quality in agricultural environments (Cooper et al., 1995; Gordon et al., 2008; Gregory et al., 1991; Naiman & Décamps, 1997; Thompson & Hansen, 2001; US EPA, 2005). Climate in the Prairie Ecozone is characterized by long and cold winters, with summers being relatively short, but often very warm. The region receives little precipitation and is relatively dry as a result, with semi-arid regions existing in the southern portions of the province (e.g., The Great Sand Hills).

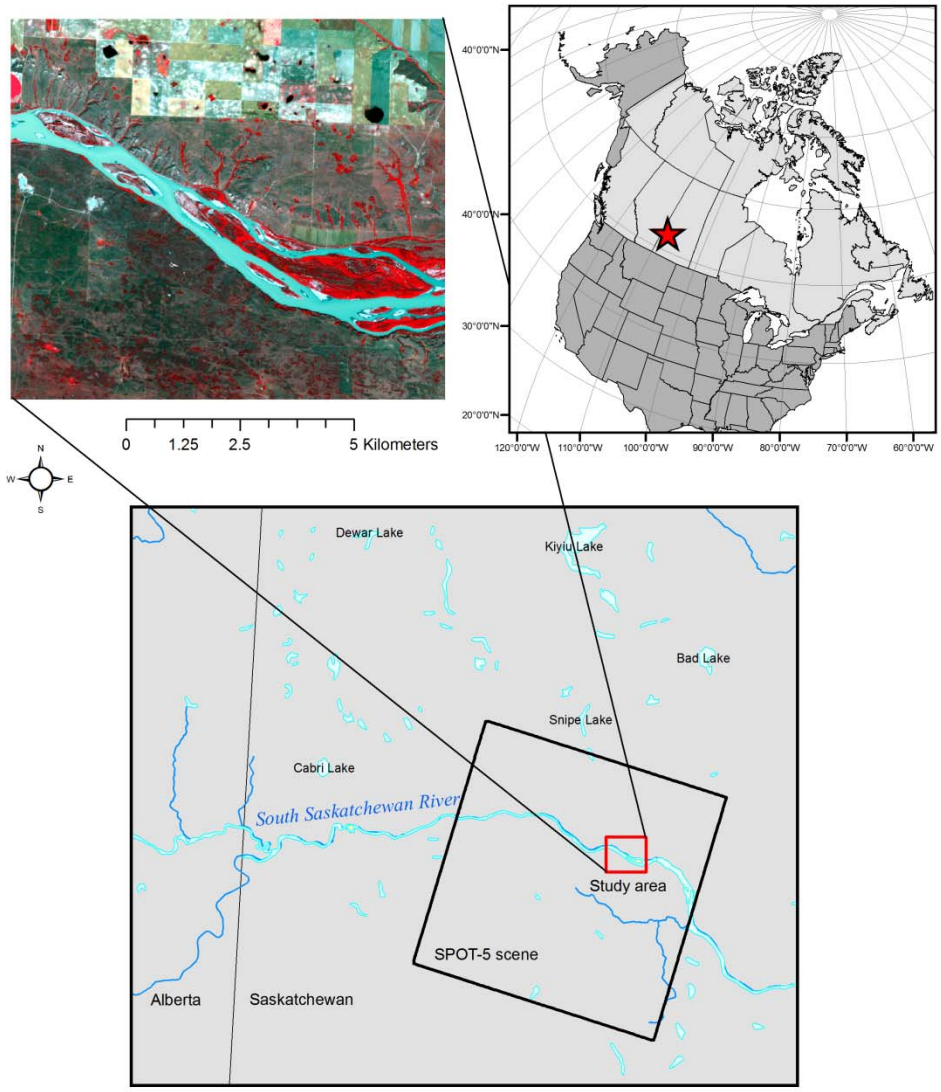

Figure 1: Study area encompassing the South Saskatchewan River (Saskatchewan, Canada). Inset shows SPOT-5 10 m HRG false color image of study area (R = NIR, G = Red, B =Green).

2.3.2 DATA SETS AND PROCESSING

2.3.2.1 ANCILLARY DATASETS

Several tiles of the Canadian Digital Elevation Data (CDED) digital elevation model (DEM) were downloaded from the GeoBase online spatial data portal (www.geobase.ca). At latitudes of less than 68° N, the CDED DEM has a horizontal post spacing of approximately 23 m (North–south) × 16–11 m (East–west). After projection into Albers Equal Area Conic and nearest-neighbor resampling, the CDED DEM was converted to square 16×16 m pixels. An Albers-Equal Area Conic was selected as the final projection for all data used in this chapter due to known area preserving characteristics of this projection, and because using a standard Universal Transverse Mercator projection would have spanned multiple zones, introducing potential projection-related challenges in the final map output. Together with elevation above sea level, slope and aspect, topographic features (e.g., ridge, channel, plane) (Pike, 2000) were calculated from the CDED DEM and included as variables in the classification process. Other ancillary datasets (e.g., road networks, geodetic monuments, administrative boundaries, etc.) were downloaded from the GeoSask online spatial data portal (www.geosask.ca), and used as reference layers for geometric and orthographic corrections of satellite imagery.

2.3.2.2 REMOTE SENSING IMAGERY

Panchromatic (2.5 m) and multispectral (10 m) imagery from the Système Pour l'Observation de la Terre (SPOT-5) satellite were obtained from the Alberta Terrestrial Imaging Corporation (www.imagingcenter.ca). The SPOT-5 imagery was collected on August 28, 2005. High resolution digital color aerial orthoimagery (60 cm pixels) obtained in the same year as the SPOT-5 imagery was downloaded from the Saskatchewan Geospatial Imagery Collaborative (www.flysask.ca) online data portal. The panchromatic imagery was orthorectified using a rational polynomial coefficient model of the SPOT-5 sensor and the CDED DEM mosaic, in conjunction with ground control points (n>=30)obtained from ancillary layers (road network

and geodetic monuments). Image-to-map registration yielded a root-mean-square error (RMSE) of 0.3 pixels using a 1st order polynomial transformation when applied to the panchromatic imagery. The multispectral imagery was then registered to the panchromatic imagery, achieving an RMSE of less than 0.5 pixels using a 1st order polynomial transformation. A visual assessment confirmed that all image sources were aligned with ancillary data layers of higher spatially accuracy (e.g., road network, quarter section plots, etc.). The multispectral SPOT-5 scene was examined for a study area suitably representative of an environment undergoing agricultural development, and a 630×553 pixel subset (348,390 pixels) of the full SPOT-5 scene was then selected for analysis (Figure 1).

Radiometric processing was applied to the SPOT-5 multispectral imagery, and the Normalized Difference Vegetation Index (NDVI) layer was computed and included in the analysis (Rouse et al. 1973). Calibrated digital numbers (DNs) were first converted to top-of-atmosphere reflectance following procedures outlined by Chander et al. (2009) with updated sensor calibration coefficients for both SPOT-5 HRG sensors provided by the Centre National d'Études Spatiales (CNES, 2009), and updated exoatmospheric solar irradiance coefficients using the Thuiller spectrum (Thuillier et al., 2003) provided by G. Chander (personal communication, Sept. 2010). Absolute atmospheric correction of the imagery was not performed due to the lack of simultaneously acquired ground based spectral data or appropriate meteorological data available in the study area. Instead, a relative correction using the Dark-Object Subtraction (DOS) method was used to alleviate atmospheric scattering effects (Chavez, 1988). The angular second moment texture measure, from computed co-occurrence matrices, was calculated for each of the SPOT-5 multispectral bands and NDVI layer. Texture measures have been found to increase overall classification accuracies using SPOT imagery (Franklin & Peddle 1990), and have been shown to improve the quality of the image segmentation process (Ryherd & Woodcock, 1996). The angular second moment texture measure (Haralick et al. 1973), a measure related to the degree of homogeneity among neighbouring pixels (Baraldi and Parmiggiani 1995), was included in our analysis as it has been shown to be important for discriminating between different crop types (Peña-Barragán et al.

2011). The four bands of SPOT-5 multispectral imagery were placed in a single data set along with the calculated NDVI layer, texture measures, DEM, and related landscape variables. This combined data set, or "image stack", consisted of 15 individual layers, or predictor variables (Table 1) suitable for differentiating between the selected land cover types. Pixel-based variables were selected from this stack based on previous experience in classifying land cover types in the study area. The object-based classification used several layers from the pixel-based image stack as input to the image segmentation process, and as input layers for the calculation of "object features".

Table 1: Image layers used in pixel-based classifications.

Spectral reflectance	Vegetation indices	Landscape variables	Texture measure[1]
Green	NDVI	Elevation	Green
Red		Slope degrees	Red
NIR		Aspect degrees	NIR
SWIR		Topgraphic class[2]	SWIR
			NDVI
			DEM
[1]- "Angular second moment" texture calculated for the listed image layers			
[2]- Topographic classes: Plain, Ridge, Channel (Pike 2000)			

2.3.3 IMAGE SEGMENTATION AND OBJECT FEATURE SELECTION

Image segmentation represents a fundamental first step in object-based image analysis, as the image objects (or image segments) resulting from this process form the basis of an object-based image classification (Castilla & Hay, 2008). In this study, image segmentation was performed using the multi-resolution segmentation (MRS) algorithm found in the 64-bit version of eCognition Developer 8 (Trimble, 2010a). The MRS algorithm uses a bottom-up image segmentation approach that begins with pixel sized objects which are iteratively grown through pair-wise merging of neighboring objects based on several user-defined parameters (scale, colour/shape, smoothness/compactness) that are weighted together to define a homogeneity

criterion; together, these parameters define a stopping threshold of within-object homogeneity based on underlying input layers, and thus define the size and shape of resulting image objects (Baatz & Schäpe, 2000; Benz et al., 2004; Trimble, 2010b). Of the parameters used by the MRS algorithm, the selection of an appropriate value for the scale parameter is considered the most important, as this value controls the relative size of the image objects, which has a direct effect on the classification accuracy of the final map (e.g., Kim et al., 2008; Myint et al., 2011; Smith, 2010). In general, smaller values for the scale parameter produce relatively smaller image objects, while larger values produce correspondingly larger objects. An examination of the available literature reveals that a quantitative, semi-automated approach for the selection of optimum values for image segmentation parameters using genetic algorithms exists (e.g., Bhanu et al., 1995), but that such semi-automated methods are not yet fully implemented in mainstream image segmentation software (e.g., Definiens' eCognition; but, see Costa et al., 2008; Drăgut et al., 2010). In this study, the selection of appropriate input layers and values for individual parameters used by the MRS algorithm was guided by previous experience and by using an iterative trial-and-error approach often employed by others conducting object-based image analysis (Dingle Robertson & King, 2011; Yan et al., 2006; Yu et al., 2006; Mathieu et al., 2007; Myint et al., 2011). The values for image segmentation parameters used in this study are found in Table 2. Definitions of each parameter defined by the MRS algorithm are described elsewhere (Baatz & Schäpe, 2000; Benz et al., 2004; Trimble, 2010b).

Table 2: Parameter values used in multi-resolution segmentation (MRS) algorithm

Scale	Color/Shape	Smoothness/Compactness	# of Objects	Median area of objects (sq. m)
5	0.9/0.1	0.5/0.5	6,583	9401
15	0.9/0.1	0.5/0.5	937	69243
30	0.9/0.1	0.5/0.5	273	241434
*-Image layers used: NDVI, DEM, and slope (weighted equally)				

The image segmentation process was considered complete once image objects were produced that visually corresponded to meaningful real-world objects of interest (e.g., fields of crop, sinuous strip of riparian vegetation, circular patches of wetland vegetation, linear road segments, etc.). Image objects produced using the smallest scale parameter (Figure 2b) were

sufficiently small enough to delineate fine scale features of interest within the study area such as narrow channels of riparian vegetation, or fringes of wetland vegetation located around pools of water. The two additional, coarser image segmentation scales (Figure 2c and d) were included in the object-based classification to depict larger objects of interest (e.g., crop fields). The use of image object information derived from multiple image segmentation scales has been shown elsewhere to produce better overall classification accuracies (Smith, 2010), and better classification accuracies for individual land cover classes (Myint et al., 2011). Image objects produced at the finest image segmentation scale served as the underlying building blocks, or "image segments" (Castilla & Hay, 2008), used for the object-based classification, although information obtained from image objects produced at all three image segmentation scales (Figures 2b–d) was utilized in the object-based classifications.

Following the image segmentation process, variables were selected for use in the object-based classification. The object-based image analysis software used in this chapter refers to such variables as "object features" (Trimble, 2010a), which is a term adopted throughout the rest of the text when referring to variables used by object-based classifications. Object features allow for contextual relationships between image objects to be incorporated into the object-based image analysis. For example, relationships between several smaller sub-objects (e.g., groups of individual crops) contained within a single image object (e.g., crop field) produced using a larger image segmentation scale, can be used for discriminating between land cover types (Myint et al., 2011). In such cases, the information being considered represents an "object texture feature" (see Table 3). Several types of object features are available within the eCognition software and are described elsewhere (Trimble, 2010a).

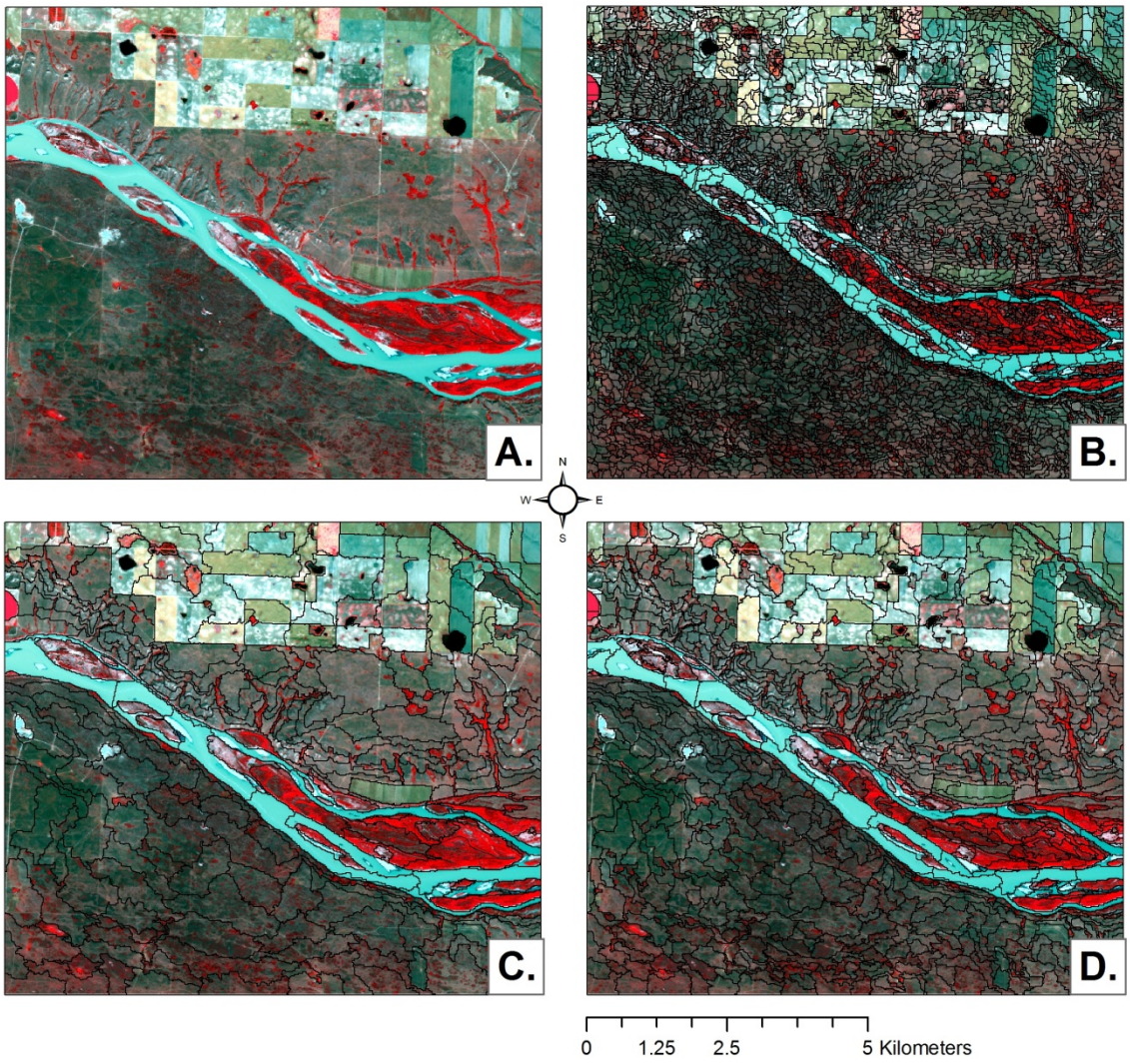

Figure 2: Comparison of image segmentation levels used in object-based classification: A) SPOT-5 10 m HRG false color image of study area (R—NIR, G—Red, B—Green); B) Image segmentation (MRS scale 5); C) Image segmentation (MRS scale 15); D) Image segmentation (MRS scale 30).

Selecting object features for use in object-based image analysis can be a subjective process based on past experience and user knowledge (e.g., Laliberte et al., 2007), or one driven by a feature selection algorithm prior to final classification (e.g., Yu et al., 2006; Van Coillie et al., 2007). In this chapter, past experience with object-based classifications in the study area was used to guide the selection of object features (Table 3). Detailed definitions of each object feature are described elsewhere (Trimble, 2010b).

Table 3: Object features used in object-based classifications

Table 3: Object features *	
Object layer features	*Description*
Mean	Mean value of an image object
Standard deviation	Standard deviation of image object
Mean difference to neighbours	The difference between mean values of an image object and neighboring image objects.
Mean difference to scene	The difference between the mean input layer value of an image object and the mean input layer value of the scene
Mean difference to super-objects	The difference between the mean input layer value of an image object and the mean input layer value of its superobject. Distance of 1.
Std. dev. difference to super-object	The difference of the std. dev. input layer value of an image object and the std. dev. input layer value of its super-object. Distance of 1.
Object texture features	*Description*
Mean of sub-objects	Standard deviation of the different input layer mean values of the sub-objects. Distance of 1.
Avg. mean diff to neighbors of sub-objects	The contrast inside an image object expressed by the average mean difference of all its sub-objects for a specific input layer. Distance of 1.
* Object features listed were calculated for each of the 15 image layers listed in Table 1	

The total number of object-features considered in a multi-scale object-based classification can be considerable since information is calculated per image object, and can be calculated at each segmentation scale for each of the input layers. In this study, information based on all 15 input layers (Table 1), 3 image segmentation scales (Table 2), and 8 object features (Table 3) were used in the object-based classification. The total number of object features considered (360) in the object-based image analyses was reduced to 300 as the calculation of values for certain object features required that certain conditions are met. For example, in this study, “object texture features” (Table 3) were selected that calculate values for an individual image object based on their underlying sub-objects, which are created at lower image segmentation scales. However, image objects produced at the finest image segmentation scale represent the finest level of detail, and therefore cannot be used to calculate sub-object information.

The total number of object features available to the object-based classifications greatly outnumbers the number of variables used in pixel-based classifications (300 versus 15, respectively). The ability to utilize and link information from image objects delineated at multiple scales inherent in the underlying imagery is often presented as one of the advantages of object-based image analysis (Blaschke, 2010). Accordingly, multiple image segmentation scales were used for object-based classifications, which is an approach that has been adopted in other recent studies comparing pixel-based and object-based classifications (e.g., Yan et al., 2006; Myint et al., 2011; Whiteside et al., 2011). While utilizing disparate numbers of potential predictor variables may hamper a strict comparison between image analysis approaches, it nonetheless represents a more typical comparison, as object-based classifications often utilize multiple image segmentation scales even if a single object-feature type is utilized (e.g., mean layer value; see Table 3).

2.3.4 SAMPLING DATA, ACCURACY ASSESSMENT, AND MAP COMPARISON

In this study, high spatial resolution aerial orthophotos and panchromatic satellite imagery were used to collect ground reference data, as contemporaneous field-based samples were not available within the selected study area. A stratified random sampling approach was utilized to adequately sample land cover classes of interest (e.g., narrow channels of riparian vegetation) that were relatively underrepresented within the study area. An initial land cover map produced using an unsupervised ISODATA clustering algorithm was created to provide an initial stratification of the study area. Four multispectral bands from the SPOT-5 imagery were used to produce the initial stratified classification using 20 spectral classes. Six broad land cover classes were selected for the purposes of this comparison study: crop land, mixed grasslands, exposed rock/soil, riparian and wetland vegetation, and water (cloud and shadow were not present in the study area). The 20 spectral classes produced by the ISODATA algorithm were grouped into the six selected land cover types. Spectral classes remaining from the ISODATA classification that did not clearly fit into the selected six land cover types were classified as “no

data" and excluded from further analysis. The generalized ISODATA classification was then converted into a polygon based map and imported into a GIS for further analysis.

Using image objects produced at the finest segmentation scale (Table 2), and the polygon-based ISODATA classification, a stratified random sample of image objects within the six land cover types was performed. A total of 690 image objects were selected (115 per land cover type). Image objects produced using the MRS algorithm – even using small image segmentation scale values – can vary in size considerably (see Table 2), and may contain more than a single land cover type. Image objects were visually examined using a combination of SPOT-5 panchromatic and multispectral data, along with color aerial orthoimagery, to assess the homogeneity of the land cover types present within individual image objects. Those image objects that contained more than one of the six broad land cover types were rejected, leaving 679 samples in total. These samples were then split into training and testing set using proportional stratified random sampling, which allowed for both sets of data to retain the overall class distributions of the six selected land cover types present in the original data set. Approximately two-thirds of the samples (437) were used to train the machine learning algorithms, reserving approximately one-third (242) as a test set used exclusively for accuracy assessment and statistical comparisons between classifications. The test set was not used to train or tune parameters associated with the machine learning algorithms examined in this study. Model building and tuning of individual parameters used by the machine learning algorithms was accomplished through repeated k-fold cross-validation based on the training data set only.

To obtain training and testing samples for the pixel-based classification that were commensurate with training and testing image objects, a single point within each of the selected image objects was randomly selected. As each of the image objects used for training and testing were visually screened for land cover homogeneity, any point within the image object would correspond to the underlying land cover type already identified for the image

object. This procedure ensured that both the object-based and pixel-based classifications used training and testing data gathered from the same locations.

Two measures for assessing the accuracy of thematic maps classified from remotely sensed imagery are commonly reported: i) overall accuracy and ii) the Kappa coefficient of inter-rater agreement (Congalton, 1991; Congalton & Green, 1998). Overall accuracy has the advantage of being directly interpretable as the proportion of pixels classified corresponds to probabilities related to a given thematic map's reported commission and omission accuracy (Stehman, 1997), while the Kappa coefficient has been used to assess statistical difference between classifications (Congalton, 1991). Studies often assess the performance of multiple classification algorithms utilizing the same testing and training samples (Foody, 2004). In such cases, the assumption that each classification was independently assessed is violated (Cohen, 1960) – i.e.,that the number of samples being compared are independent – and therefore, a statistical comparison using Kappa coefficient values is unwarranted (Foody, 2004). In such circumstances, it has been recommended that either a Monte Carlo permutation test of related κ coefficient values (McKenzie et al., 1996), or McNemar's test for paired-sample nominal scale data (Agresti, 2002; Zar,2009), be used to assess whether statistically significant differences between classifications exists (Foody, 2004). The latter approach has been used by others to statistically compare object-based and pixel-based classifications (e.g., Dingle Robertson & King, 2011;Yan et al., 2006; Whiteside et al., 2011), and is therefore adopted here for comparability.

For each classification, a confusion matrix is presented, along with its overall accuracy (i.e., the percentage of correctly classified land cover types), and user's and producer's accuracy (Congalton & Green, 1998). As recommended by others, overall accuracy measures are reported using 95% confidence intervals (Morissette & Khorram, 1998; Foody, 2009). The McNemar test was used to assess the following goals of comparison: 1) whether a statistically significant difference exists between pixel-based and object-based classifications that utilize the same machine learning algorithm; and, 2) whether a statistically significant difference exists between different machine learning algorithms when using either pixel-based or object-based

image analysis. The McNemar test was run without Yates' correction for continuity for small sample sizes, as this correction is generally not recommended (Foody, 2004; Zar, 2009). Both the individual accuracy assessments and statistical comparisons are based on the independent test set.

2.3.5 TUNING OF MACHINE LEARNING ALGORITHM PARAMETERS

Model building, tuning, and accuracy assessments of were performed using version 2.12 of the 64-bit version of R, a multi-platform, open-source language and software for statistical computing (R Development Core Team, 2010). Several add-on packages were used within R for creating each of the machine learning algorithms used in this study: decision tree (DT), random forest (RF), and the support vector machine (SVM). Classifications based on DT models used The Recursive PARTitioning or "rpart" package (Therneau & Ripley, 2010), which is largely based on the classification and regression tree (CART) algorithm originally developed by Breiman et al. (1984). The classifications built with the RF algorithm used the "randomForest" package (Liaw & Wiener, 2002), which is based on the original RF algorithm and software code developed by Breiman and Cutler (Breiman, 2001; Breiman & Cutler, 2007). Classifications using models based on the SVM algorithm (Cortes & Vapnik,1995; Vapnik, 1998) used the "kernlab" package (Karatzoglou et al.,2004). In all, three classification algorithms were tested: DT, RF, ad SVM.

All classification models were developed using the "caret" package within R (Kuhn, 2008), which allowed for a single consistent environment for training each of the machine learning algorithms and tuning their associated parameters. A repeated k-fold cross-validation resampling technique was used to create and optimize classification models for both pixel-based and object-based classifications using all three machine learning algorithms. Resampling by k-fold cross-validation begins by partitioning a sample into k subsamples of roughly equal size, with k-1 subsamples used as a training set, and a single subsample left out as a test set. Using this approach, a classification model using each of the three machine learning algorithms is built using the training set and assessed against the single leftover test set. This process is

repeated k times (“folds”), whereby each of the k subsamples serves a turn as a test set, ensuring that all subsamples are used as part of the training and testing sets. Results for each fold are then combined to select the model with the highest average accuracy. Similar cross-validation techniques have been used by others to compare the performance of multiple classifiers using earth observation imagery (e.g., Friedl & Brodley, 1997; Huang et al.,2002; Brenning, 2009, 2010).

Several adjustable “tuning parameters” used by each of the machine learning algorithms to optimize classification performance were examined using 10-fold cross validation, which is the number of folds recommended when comparing the performance of machine learning algorithms (Kohavi, 1995). “Optimal” values for tuning parameters were selected using three repetitions of a 10-fold cross-validation based on the original training data set, with the original test removed completely from the cross-validation process (i.e., the original test set was not used for training or tuning any of the classification models). Tuning parameters were considered optimized based on classification models that achieved the highest overall classification during the cross validation process. Specific details on tuning parameters used by the three machine learning algorithms examined in this study are listed in the following sections.

2.3.5.1 DECISION TREE BASED MODELS

For DT based classifications, several values were examined for the “maximum depth” tuning parameter, which controls the maximum depth of any single node in the tree. When using the “caret” package, an initial DT model is fit to all of the training data to obtain the maximum depth of any node; this value is then used to obtain an upper bound on values considered during subsequent model building using cross validation (Kuhn, 2011). In general, using a larger maximum depth value will allow for a relatively complex tree to be built, with a potential increase in overall classification accuracy, whereas lower maximum depth values tend to build less complex trees, with potentially lower overall classification accuracies. By increasing

the number of branching nodes (i.e., decision rules), the DT algorithm is capable of grouping a larger number of distinct observations present within a dataset. By default, the "rpart" package uses 10-fold cross validation of the training data to internally obtain classification error rates (Therneau & Ripley, 2010). When using "rpart" the appropriate sized tree is obtained using the "1 SE rule" established by Breiman et al. (1984), whereby the smallest-sized tree whose cross validation error is within 1 standard error of the minimum cross validation error is selected. The tree is then pruned using the "cost complexity" (cp) value that corresponds to the size of tree found using the "1 SE rule". The cp parameter controls the condition at which non-informative splits are pruned from the tree (Therneau & Ripley, 2010). Using the "caret" package, the default cp value (0.01) used by the "rpart" package was maintained, and only the maximum depth parameter was tuned for DT based classifications.

2.3.5.2 RANDOM FOREST BASED MODELS

For random forest (RF) based classifications, the default number of trees (500) was selected since values larger than the default are known to have little influence on the overall classification accuracy (Breiman & Cutler, 2007). The other adjustable RF tuning parameter, the mtry parameter, controls the number of variables randomly considered at each split in the tree building process, and is believed to have a "somewhat sensitive" influence on the performance of the RF algorithm (Breiman & Cutler, 2007). For categorical classifications based on the RF algorithm, the default value for the mtry parameter is $\sqrt{n}$, where p equals the number of predictor variables within a data-set (Liaw & Wiener, 2002).

2.3.5.3 SUPPORT VECTOR MACHINE BASED MODELS

Classifications based on the support vector machine (SVM) algorithm used the radial basis function (RBF) kernel. Other kernels were not considered in this study. The parameters used by the SVM algorithm have been shown to influence overall classification accuracy (Burges, 1998).

The two model tuning parameters for SVM models using the RBF kernel in the "kernlab" package are "cost" (C) and "sigma" (σ). Increasing the former leads to larger penalties for prediction errors, which may produce an over-fitted model (Alpaydin, 2004); whereas increasing the latter parameter affects the shape of the separating hyperplane (Huang et al., 2002), which may also influence overall classification accuracy. An analytical method for directly estimating σ from the training data has been implemented in the kernlab package using the "sigest" function (Karatzoglou et al., 2004). The "caret" package estimates an appropriate value for the σ parameter using the sigest function by default; therefore, only the C parameter was tuned when running the SVM algorithm with the RBF kernel (Kuhn, 2011).

2.4 RESULTS

2.4.1 TUNING OF MACHINE LEARNING ALGORITHM PARAMETERS

For DT-based classifications, values ranging from 1 to 8 were examined for the "maximum depth" tuning parameter. Based on the highest overall classification accuracy (i.e., the percentage of correctly classified samples) achieved by pixel-based and object-based models (85.4% and 83.3%, respectively) a maximum depth value of 8 was selected for both pixel-based and object-based classifications models. Several values for the mtry tuning parameter (2–4, 6–8, 10–12, 14) were examined for the pixel-based RF classification. For the pixel-based RF classification, the highest classification accuracy value (91.1%) was obtained with an mtryvalue of 7. A total of 10 mtry parameter values (2, 35, 68, 101, 134, 167, 200, 233, 266, and 300) were examined for the object-based RF classifications. Based on the highest classification accuracy obtained (93.1%), an mtry value of 68 was selected for the object-based RF classification. For the pixel-based and object-based classifications using the SVM algorithm, a total of 10 values for the C parameter (0.25, 0.5, 1, 2, 4, 8, 16, 32, 64, and 18) were examined. The value for the σ parameter was held constant at 0.0928 for pixel-based classifications, and at 0.00361 for object-based classifications. Pixel-based and object-based classifications using the SVM algorithm (overall accuracy of 89.8% and 91.4%, respectively) were obtained using C parameter values of 8 and 1, respectively. Models with optimized tuning parameter values

were used to produce the subsequent image classifications, associated accuracy assessments, and map comparisons.

2.4.2 VISUAL EXAMINATION OF THEMATIC MAPS

Pixel-based and object-based image classifications using the three examined machine learning algorithms are depicted in Figures 3 and 4, respectively. Post classification clean up (e.g., pixel-based filtering, GIS-based adjustment of classes, etc.) of the final thematic maps was not performed. A visual overview of the pixel-based classifications is presented first, followed by object-based classifications, and a comparison of outputs produced using both image analysis approaches and all three machine learning algorithms. The following six broad land cover types were classified using the above classification algorithms and image analysis approaches: crop, mixed grassland, exposed rock/soil, wetland, riparian, and water. These land cover types are visually assessed in the following sections.

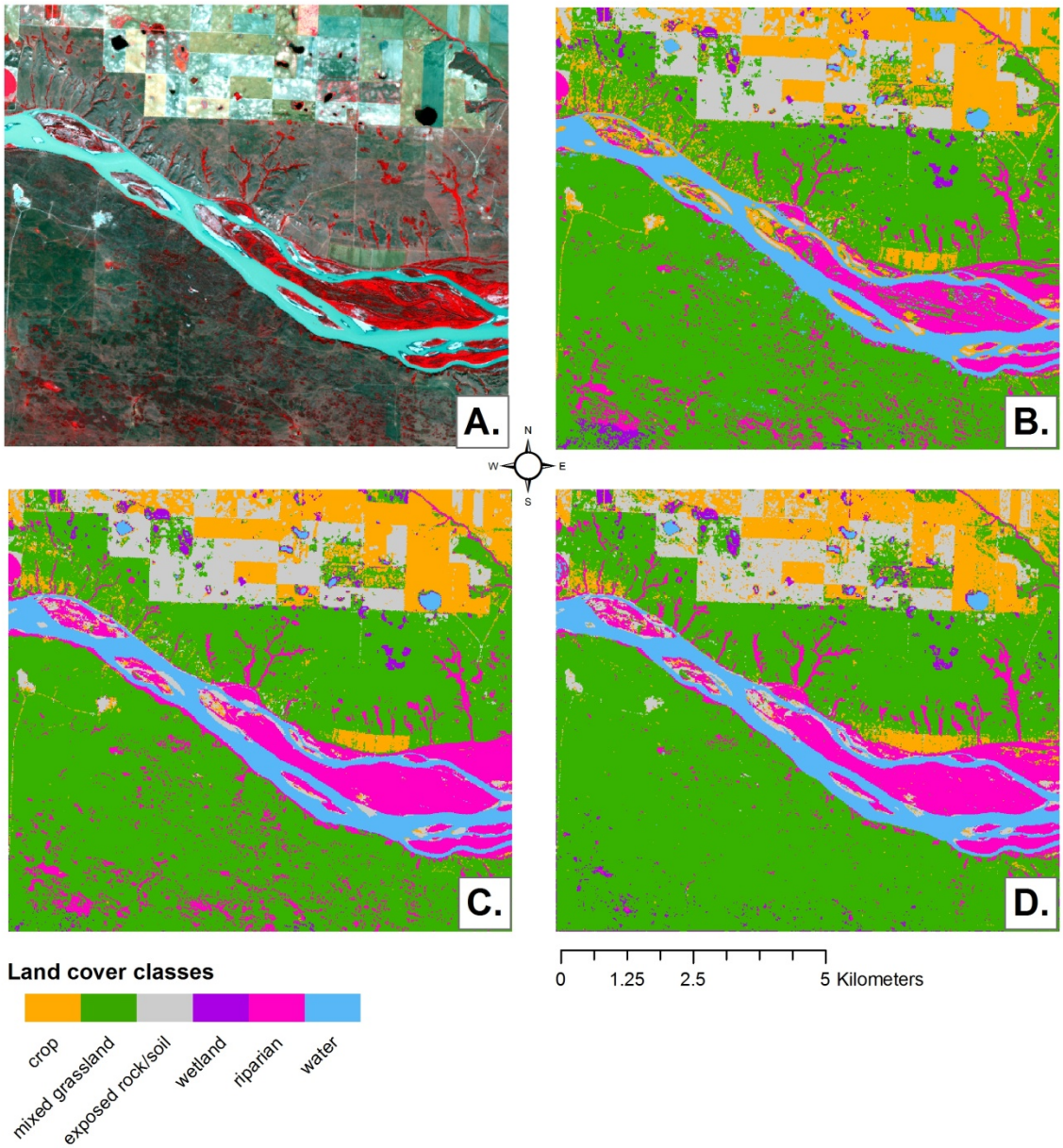

Figure 3: Comparison of pixel-based classifications: A) SPOT-5 10 m HRG false color image of study area (R—NIR, G—Red, B—Green); B) Decision tree based classification; C) Random forest based classification; D) Support vector machine based classification.

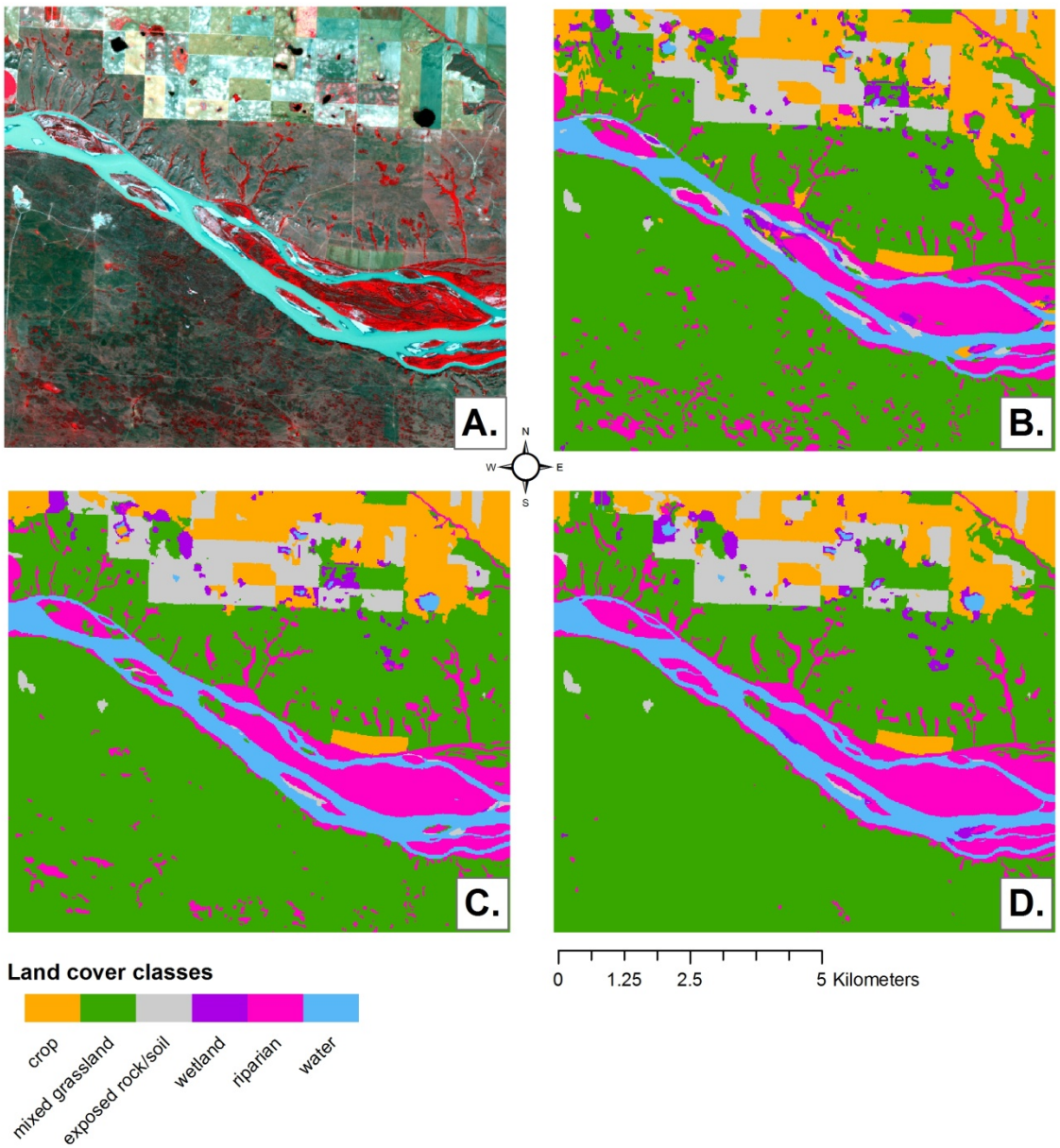

Figure 4: Comparison of object-based classifications: A) SPOT-5 10 m HRG false color image of study area (R-NIR, G-Red, B-Green); B) Decision tree based classification; C) Random forest based classification; D) Support vector machine based classification.

2.4.3 PIXEL-BASED CLASSIFICATIONS

For the pixel-based classifications (Figure 3), the major visual difference interpreted between thematic maps produced by the three different algorithms was the amount of wetland or riparian land cover depicted in the southern quarter of the study area. For tree-based classifications (Figures 3b and 3c), the south-western corner of the study area depicts riparian vegetation, whereas the map produced by the SVM algorithm (Figure 3d) depicts this area as dominated by mixed grasslands dotted primarily with wetlands. A visual inspection of this area using available high spatial resolution imagery and color orthoimagery revealed that this area is predominantly covered in vegetation typical of a mixed grasslands land cover type, although small stream channels can be seen filled with vegetation, indicating the presence of a riparian land cover class. Small areas of wetland vegetation are also present in the high resolution imagery. Two predominant patches of exposed rock/soil, shown as blue-white patches on the left portion of Figure 3a, are best classified by the SVM algorithm, while both the RF and DT algorithms depict these areas with patches of crop land. In general, while all three pixel-based classifications produced a similarly speckled “salt-and-pepper” appearance, the DT and RF based classifications showed noticeably less of this speckle in the depiction of large crop land areas (e.g., see north-eastern corner of Figure 3c). Overall, the pixel-based classification using the SVM algorithm (Figure 3d) appears to contain less speckle compared to the DT and RF classifications. The classification based on the SVM algorithm appears to show fewer errors of commission in the classification of mixed grassland vegetation along the north-western area, especially along channels containing riparian vegetation on the north side of the river.

2.4.4 OBJECT-BASED CLASSIFICATIONS

As with the pixel-based classification, the major visual difference interpreted between thematic maps produced using object-based image analysis (Figure 4), is in the relative amount of wetland, riparian and mixed grassland land cover depicted in the southern half of the study area. For tree-based classifications (Figures 4b and 4c), the southern half of the study area

depicts larger patches of riparian vegetation, whereas the SVM algorithm (Figure 4D) depicts this area as predominantly mixed grassland. The thematic maps based on DT and SVM algorithms (Figures 4b and 4c) show several noticeable errors of commission, namely the misclassification of riparian land cover as wetland within the main river channel. All three object-based classifications misclassified small areas of riparian and exposed/rock soil land cover located along the riverbank as mixed grasslands. The two object-based classifications using the RF and SVM algorithm show little indication of commission error when classifying crop land alongside riparian channels on the northern slope of the river channel, whereas several patches of misclassified crop land are present in this area of the object-based DT classification map. Wetland vegetation present in the northern part of the study area appears well defined by all three object-based classification algorithms, although several errors of commission are noticeable in large inundated fields.

2.4.5 VISUAL COMPARISON OF PIXEL-BASED AND OBJECT-BASED CLASSIFICATIONS

In general, all land cover maps show a reasonably accurate visual depiction of the broad land cover types of interest in this area. When the same machine learning algorithm is compared, both pixel-based and object-based classifications showed similar patterns. For example, the predominance of mixed grassland areas in the southern portion of the study area was noticeably higher in pixel-based and object-based classifications that utilized the SVM algorithm when compared to classifications based on tree-based algorithms. Wetland and riparian areas were generally well defined, although different algorithms and image analysis approaches differed slightly in their specific depictions of these land cover types. Wetland areas appeared to be best represented by the SVM based classifications, particularly when using the object-based approach, which accurately portrayed vegetation encircling areas of open water, although this quality is present when using tree-based classifications to varying degrees. Likewise, the depiction of riparian vegetation was relatively consistent across approaches and algorithms, with pixel-based classifications producing the most visually accurate depictions

along steep ridges and narrow channels. Crop land was best depicted by object-based classifications due to the generalized appearance, however the less speckled appearance of croplands using pixel-based RF and DT based classifications were also considered adequate. Pixel-based classifications based on RF and SVM algorithms produced more visually accurate depictions of sand bars (exposed rock/soil land cover type) in riparian areas than any of the object-based classifications.

2.4.6 ACCURACY ASSESSMENT AND STATISTICAL COMPARISONS

An accuracy assessment was performed for each classification produced in this study to evaluate how well predictions based on the optimized models, generated using repeated k-fold cross validation, compared against the independent test data. Table 4 contains detailed confusion matrices of classification accuracies based on the test data. Overall, both pixel-based and object-based classifications performed similarly with respect to overall classification accuracy. In general, all land cover types achieved over 80% user's accuracy, with the exception of wetland land cover types, which scored below 80% when using pixel-based image analysis, or object-based image analysis using the DT algorithm. Producer's accuracy for several land cover types was relatively consistent for both pixel-based and object-based classifications, but specific differences between machine learning algorithms were apparent. For example, producer's accuracy for the crop land cover type was consistently over 80% for both pixel-based and object-based classifications, except when using the SVM classifier, where it decreased to 75% for both image analysis approaches. All pixel-based classifications achieved a producer's accuracy of 77.27% for wetland land cover types, while object-based classifications using the RF and SVM algorithm achieved over 95% for this class. Pixel-based classifications that utilized the DT algorithm had the lowest overall classification accuracy (87.6%), followed by SVM (89.26%), and RF (89.67%) classifications (Figure 5). The same general trend was observed for object-based classifications, with the DT algorithm obtaining the lowest overall classification accuracy (88.84%), followed by RF (93.39%) and SVM (94.21%) algorithms. Exact 95% confidence limits, calculated on the results obtained with the “hold-out” test data set, reveal a wide variability

and overlap in overall accuracy reported between pixel-based and object-based classifications. Based on these results, the lowest performing classification model (pixel-based DT) potentially scored within the range of the best performing RF and SVM classifications (Figure 5).

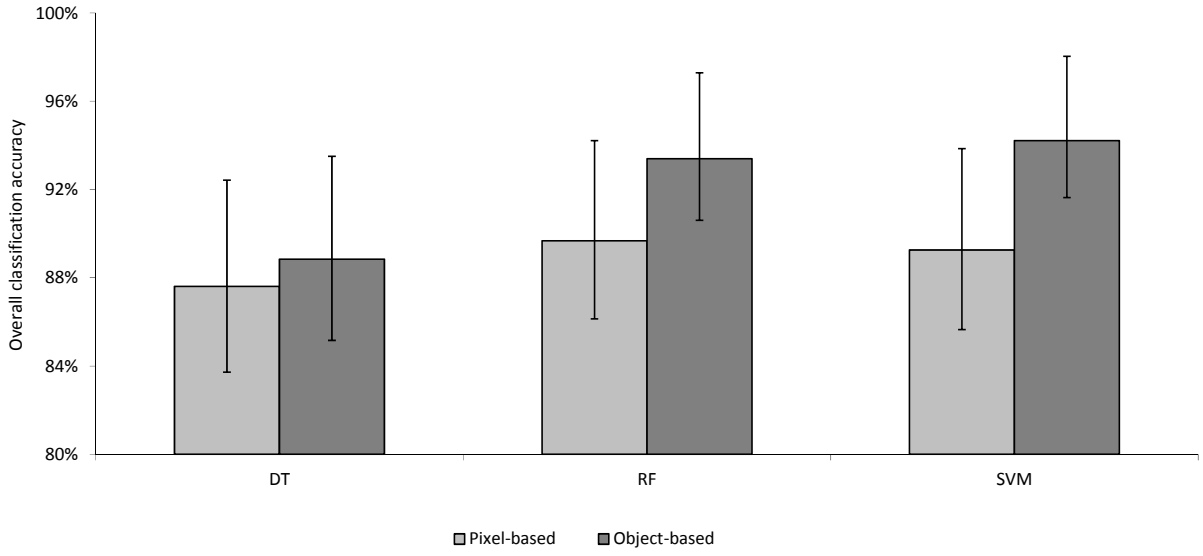

Figure 5: Comparison of overall classification accuracy (percent correct) of pixel-based and object-based classifications using three supervised machine learning algorithms: Decision Tree (DT), Random Forest (RF), and Support Vector Machine (SVM). Results based on "hold-out" test set. Exact 95% confidence intervals plotted.

Based on a comparison between predictions made with optimized classification models built using repeated k-fold cross-validation and the “hold-out” test data, the McNemar test indicated that the observed difference between pixel-based and object-based classifications was not statistically significant ($p>0.05$) when the same machine learning algorithm was used (e.g., DT classification model using pixel-based or object-based image analysis). With pixel-based image analysis, the observed difference in classification accuracy between all three machine learning algorithms was not statistically significant ($p>0.05$). For object-based classifications, a statistically significant difference ($p=0.05$) in classification accuracy between models using DT and RF algorithms ($p=0.011$), and DT and SVM algorithms ($p=0.006$) was observed. The difference in overall classification accuracy between object-based classifications utilizing the RF and SVM algorithms was not statistically significant ($p>0.05$).

Table 4: Confusion matrices and associated classifier accuracies based on test data. CL=crop land, MG=mixed grasslands, RS=exposed rock/soil, RP=riparian, WA=water, WL=wetland; Oa=overall classification accuracy, Pa=producer's accuracy, Ua=user's accuracy, CI=confidence interval.

Pixel-based, Decision Tree								
	CL	*MG*	*RS*	*RP*	*WA*	*WL*	**Total**	**Ua**
CL	27	3	0	0	0	2	32	84.38%
MG	1	60	1	5	0	3	70	85.71%
RS	1	0	13	0	0	0	14	92.86%
RP	3	4	0	72	0	0	79	91.14%
WA	0	1	0	1	23	0	25	92.00%
WL	0	1	0	4	0	17	22	77.27%
Total	32	69	14	82	23	22	**242**	
Pa	84.38%	86.96%	92.86%	87.80%	100.00%	77.27%		
						Oa:	87.60%	
						lower 95% CI:	82.78%	
						upper 95% CI:	91.48%	

Object-based, Decision Tree								
	CL	*MG*	*RS*	*RP*	*WA*	*WL*	**Total**	**Ua**
CL	26	0	1	0	0	0	27	96.30%
MG	1	63	1	1	1	3	70	90.00%
RS	1	0	12	0	1	1	15	80.00%
RP	3	4	0	80	1	2	90	88.89%
WA	0	0	0	0	18	0	18	100.00%
WL	1	2	0	1	2	16	22	72.73%
Total	32	69	14	82	23	22	**242**	
Pa	81.25%	91.30%	85.71%	97.56%	78.26%	72.73%		
						Oa:	88.84%	
						lower 95% CI:	84.18%	
						upper 95% CI:	92.52%	

Pixel-based, Random Forest								
	CL	*MG*	*RS*	*RP*	*WA*	*WL*	**Total**	**Ua**
CL	27	2	0	0	0	0	29	93.10%
MG	1	61	1	0	0	3	66	92.42%
RS	1	1	13	0	0	0	15	86.67%
RP	3	3	0	80	0	2	88	90.91%
WA	0	0	0	0	19	0	19	100.00%
WL	0	2	0	2	4	17	25	68.00%
Total	32	69	14	82	23	22	**242**	
Pa	84.38%	88.41%	92.86%	97.56%	82.61%	77.27%		
						Oa:	89.67%	
						lower 95% CI:	85.13%	
						upper 95% CI:	93.20%	

Object-based, Random Forest								
	CL	*MG*	*RS*	*RP*	*WA*	*WL*	**Total**	**Ua**
CL	27	1	0	0	1	0	29	93.10%
MG	0	65	1	0	0	1	67	97.01%
RS	1	0	13	0	0	0	14	92.86%
RP	3	3	0	82	0	0	88	93.18%
WA	0	0	0	0	18	0	18	100.00%
WL	1	0	0	0	4	21	26	80.77%
Total	32	69	14	82	23	22	**242**	
Pa	84.38%	94.20%	92.86%	100.00%	78.26%	95.45%		
						Oa:	93.39%	
						lower 95% CI:	89.49%	
						upper 95% CI:	96.17%	

Pixel-based, Support Vector Machine								
	CL	*MG*	*RS*	*RP*	*WA*	*WL*	**Total**	**Ua**
CL	24	2	1	1	0	1	29	82.76%
MG	4	63	2	0	1	1	71	88.73%
RS	1	1	11	0	0	0	13	84.62%
RP	2	1	0	81	0	3	87	93.10%
WA	0	0	0	0	20	0	20	100.00%
WL	1	2	0	0	2	17	22	77.27%
Total	32	69	14	82	23	22	**242**	
Pa	75.00%	91.30%	78.57%	98.78%	86.96%	77.27%		
						Oa:	89.26%	
						lower 95% CI:	84.66%	
						upper 95% CI:	92.86%	

Object-based, Support Vector Machine								
	CL	*MG*	*RS*	*RP*	*WA*	*WL*	**Total**	**Ua**
CL	24	0	1	0	0	0	25	96.00%
MG	3	68	1	0	0	0	72	94.44%
RS	1	0	11	0	0	0	12	91.67%
RP	3	1	0	82	0	0	86	95.35%
WA	0	0	0	0	21	0	21	100.00%
WL	1	0	1	0	2	22	26	84.62%
Total	32	69	14	82	23	22	**242**	
Pa	75.00%	98.55%	78.57%	100.00%	91.30%	100.00%		
						Oa:	94.21%	
						lower 95% CI:	90.40%	
						upper 95% CI:	96.80%	

2.5 DISCUSSION

In general, classifications produced using either pixel-based or object-based image analysis created similar and visually acceptable depictions of the broad land cover classes present within the study area. As expected, compared to the pixel-based classifications, the object-based classifications offered a more generalized visual appearance and more contiguous depiction of land cover, which perhaps better represents how land cover interpreters and analysts actually perceive the landscape (Stuckens et al., 2000). In some cases, the generalized depiction of land cover classes produced by object-based image analysis may account for the apparent preference for object-based classifications over slightly better performing pixel-based classifications (e.g., Dorren et al., 2003). Nevertheless, additional processing of pixel-based imagery, either prior to or after classification, can also produce similar generalized representations of land cover, so such differences may in fact be largely trivial, at least when considering the use of medium spatial resolution imagery (10–30 m pixels). When comparing overall classification accuracy (percentage of classes correctly predicted), there is an apparently consistent, but small (1–4%), improvement when using object-based image analysis over pixel-based image analysis (see Table 4 and Figure 5). However, the large variability depicted by the exact 95% confidence intervals suggests that the sample size of the "hold-out" test data set (242) was too small for assessing such differences; therefore, any apparent trend reported here should be considered tentative.

Deciding on a sampling effort that is economically feasible and logistically possible, with one that allows for statistically rigorous comparisons is a major consideration in operational settings where resources are often limited (Congalton, 1991).A sample size that is too large can waste valuable resources that provide unnecessary precision, whereas a sampling effort that is too small may not be capable of resolving any statistically meaningful differences when comparing classification accuracies (Foody, 2009). Despite the lower sample size of the test set and associated wider confidence limits, the McNemar test revealed that, when utilizing the same machine learning algorithm, the observed difference between pixel-based and object-

based classification accuracy was not significant at the 5% level. The findings in this study suggest that, on the basis of achieving better overall classification accuracy for this application, there is no statistical basis for preferring pixel-based to object-based image analysis, when utilizing the same machine learning algorithm. In addition, when using pixel-based image analysis, there was no statistically significant difference observed at the 5% level of significance between classification accuracies achieved by any of the machine learning algorithms. These findings are largely corroborated by the large overlap in confidence intervals depicted in Figure 5.

Nonetheless, when using object-based image analysis, statistically significant differences ($p<0.05$) were observed for classification accuracies achieved by SVM and RF algorithms when compared to DT-based classifications. Unfortunately, the McNemar test as implemented here cannot be used for one-sided hypothesis testing (Foody, 2004), and the wide degree of overlap in the 95% confidence intervals for overall accuracy (Figure 5) suggests that definitively asserting which classification algorithm or image analysis approach is capable of producing higher classification accuracies would be problematic based on the "hold-out" test set used in this study.

Other studies have indicated that both RF and SVM algorithms can achieve similar overall classification accuracies, which are typically greater than those obtained using DT based algorithms. For example, Pal (2005) found that both SVM and RF algorithms produced similar classification accuracies. Gislason et al. (2006) reported that RF based models achieved higher classification accuracies than those produced by standard DT (i.e., DTs that did not utilize bagged or boosting algorithms). These results differed from those reported by Otukei and Blaschke (2010) who found that DTs generally performed better than classifications produced using SVM. As with this study, the previous examples were based on medium- and relatively coarse-spatial resolution imagery (Landsat MSS, TM, ETM+) and used similar broad land cover classes; however, these comparisons relied on comparing overall classification accuracy values

(i.e., the percentage of correctly classified samples) rather than using statistical comparison as employed here and elsewhere (e.g., Foody 2009).

When comparing overall accuracies between object-based and pixel-based classifications of Landsat-5 TM imagery, Dingle Robertson and King (2011) found no statistical difference between approaches. However, two studies (Yan et al., 2006; Whiteside et al., 2011) found that differences in overall classification accuracies produced using object-based image analysis were statistically significant ($p=0.001$, and $p=0.01$, respectively) than pixel-based image analysis, with both studies using medium spatial resolution EO imagery (ASTER and SPOT-5 HRG, respectively). Contrary to the side-by-side comparison conducted in this study, these previous studies compared different classifiers (e.g., MLC and K-NN) and image analysis methods, making direct comparisons difficult. Furthermore, as illustrated in this study, examination of confidence intervals around the overall classification accuracy assessments can reveal significant overlap in overall accuracies between image analysis approaches, confounding the interpretation of two-sided tests of significance such as McNemar's test (Foody, 2009), which have also been used in previous comparisons (e.g., Dingle Robertson & King, 2011; Yan et al., 2006; Whiteside et al., 2011). Potential remedies include collecting a larger “hold-out” test sample to assess whether the large overlap in confidence intervals would remain, along with an appropriate means of testing a one-sided hypothesis for such a comparison. Unfortunately, the collection and use of an adequately sized “hold-out” test set might be prohibitive to assemble for logistical or financial reasons, and would represent an “inefficient use of data”, as these data are, by definition, not utilized by the classifier (Kohavi, 1995). Implementing a repeated k-fold cross-validation, as illustrated in this study, with a larger dataset may provide statistically rigorous results without “wasting” data, while at the same time allowing for one-sided hypothesis testing to be performed (e.g., Kuhn, 2008).

From a practical production standpoint, the setup and execution of object-based classifications were more labor intensive as compared to their pixel-based counterparts. Much of the difference in execution time encountered was due to a lack of commercially available

software for image analysis that implemented the machine learning algorithms examined in this study. This lack of a streamlined production environment multiplied the number of software packages needed and the amount of data transfers required. In addition, many of the present comparisons between pixel-based and object-based classifications of EO imagery in the available literature to date appear to rely on commercially available software solutions that provide relatively outdated and/or less advanced classification methods. The present study, along with others (e.g., Brenning, 2009,2010), fill this void by providing a methodological basis for conducting statistically rigorous comparisons between classification outputs generated from EO imagery using freely available open-source software (e.g., R Development Core Team, 2010). Regardless of which software packages are used, differences in execution time between pixel-based and object-based image analysis still remain. For example, the time spent selecting object-based variables (i.e., "object features") is roughly similar to that involved in selecting variables for a pixel-based classification; however, the additional time needed to select appropriate parameters for the underlying image segmentation is not trivial, especially if the tasks include mapping large overlapping scenes of imagery in an operational setting. Future development and adoption of more quantitative approaches for selecting optimal image segmentation parameters (e.g., Costa et al., 2008; Drăgut et al., 2010) will hopefully reduce the time required for this important step, while at the same time producing superior results to the qualitative trial-and-error methods that are typically practiced now. In addition, faced with potentially hundreds of object features from which to select, the use of more advanced feature selection algorithms in object-based image analysis is gaining increasing attention (e.g., Yu et al., 2006; Chan & Paelinckx, 2008).

Considered together, object-based image analysis will likely remain more labor intensive compared to pixel-based image analysis, which is a factor that should be evaluated carefully when conducting image analysis of EO imagery in an operational environment. While classification accuracy is an important attribute to consider, in circumstances where there are few overall statistical differences between image analysis approaches, other preferences may take precedence. For example, DT based models may be preferable because of their ability to

generate visually interpretable node-based diagrams of the binary decision logic used to arrive at the final classification. Conversely, the potentially higher overall classification accuracies gained by using the RF algorithm may be preferable despite the lack of a similar visual representation offered by the DT algorithm.

While statistically significant differences in overall classification accuracy were not observed in this study between pixel-based and object-based image analysis when utilizing the same machine learning algorithm, there may be other compelling reasons for selecting one image analysis approach over another. For example, object-based image analysis may prove to be more appropriate in situations that rely on the logic of updating and backdating image objects within a versatile GIS environment (e.g., Linke et al., 2009; Linke & McDermid, 2011). As previously mentioned, end users may prefer the generalized appearance of object-based classification maps as compared to pixel-based classification maps, even when pixel-based accuracy assessments are shown to be superior (Dorren et al., 2003). Such examples illustrate that the selection of an image analysis approach, or selection of an individual classification algorithm, may not always be driven by overall classification accuracy.

2.6 CONCLUSIONS

Classification of EO imagery using pixel-based and object-based image analysis was performed using three machine learning algorithms. No statistical difference between object-based and pixel-based classifications was found when the same machine learning algorithms were compared. When conducting object-based image analysis, RF or SVM algorithms produced classification accuracies that were statistically different compared to DT based algorithms. No statistical significant between pixel-based classifications were found. Based on visual assessments and interpretation of land cover distribution, all classifications were capable of depicting the broad land cover types selected for this study with similar, and acceptable, classification accuracies. More visually adequate overall depictions of riparian, wetland, and crop land cover types were attributed to RF and SVM based classifications, whereas DT based

classifications contained noticeably more omission and commission errors in these classes. Object-based classifications were comparatively more time consuming to produce than their pixel-based counterparts. Based solely on overall classification accuracy, there appeared to be no advantage in selecting a particular image analysis approach. However, in light of the challenges presented in the Introduction and Chapter 1 of this thesis, and in the interest of recommending an approach suitable for meeting the operational needs of regional environmental reporting frameworks, a rational for preferring a particular image analysis approach and classification algorithm examined in this chapter are offered below.

First, the fundamental working unit and mapping output of object-based image analysis are easily integrated into present vector-based Geographical Information Systems. This seamless exchange of information allows for further spatially explicit analysis to be conducted without the need for convert from a pixel-based format, a process that can lead to the loss of information and/or the introduction of error. Second, the Random Forest (RF) classifier achieved high overall classification accuracies as compared to the decision tree (DT) algorithm. While perhaps not as interpretable as the binary decision logic diagrams produced by decision tree (DT) algorithm, the RF classifier is capable of generating feature importance scores, which can provide insight into which variables are relatively more important to per-class (and per-model) classification accuracies. The ability to handle large number of variables relative to the number of observations further suggests that the RF classifier is well suited to object-based image analysis, where the amount of variables used (as demonstrated in this chapter) can number in the hundreds. In the following chapter, these recommendations to further explore object-based image analysis and the RF classifier are examined in more depth.

2.7 REFERENCES

AGRESTI, A. (2002). Categorical data analysis. : John Wiley and Sons.

ALPAYDIN, E. (2004). Introduction to machine learning. : MIT Press.

BAATZ, M., & SCHÄPE, A. (2000). Multiresolution segmentation—an optimization approach for high quality multi-scale image segmentation. In J. Strobl, T. Blaschke,& G. Griesebner (Eds.), Angewandte Geographische Informationsverarbeitung XII(pp. 12–23). Wichmann-Verlag, Heidelberg.

BARALDI, A. and PARMIGGIANI, F., 1995, An investigation of the textural characteristics associated with gray level co-occurrence matrix statistical parameters. *IEEE Transactions on Geoscience and Remote Sensing,* 33, pp. 293-304.

BENZ, U. C., HOFMANN, P., WILLHAUCK, G., LINGENFELDER, I., & HEYNEN, M. (2004). Multi-resolution, object-oriented fuzzy analysis of remote sensing data for GIS-ready information. ISPRS Journal of Photogrammetry and Remote Sensing, 58(3–4), 239–258.

BHANU, B., LEE, S., & MING, J. (1995). Adaptive image segmentation using a genetic algorithm. IEEE Transactions on Systems, Man, and Cybernetics, 25(12), 1543–1567.

BLASCHKE, T. (2010). Object based image analysis for remote sensing. ISPRS Journal ofPhotogrammetry and Remote Sensing, 65(1), 2–16.

BREIMAN, L. (2001). Random Forests. *Machine Learning*, 45, 5–32.

BREIMAN, L.,& CUTLER, A.(2007). RANDOMFORESTS — CLASSIFICATION DESCRIPTION: RANDOMFORESTS AVAILABLE AT: HTTP://STAT-WWW.BERKELEY.EDU/USERS/BREIMAN/RANDOMFORESTS/CC_HOME.HTM [ACCESSED JANUARY 12, 2011]

BREIMAN,L.,FRIEDMAN,J.,STONE,C.,& OLSHEN,R.(1984).Classificationand regression trees,Belmont, California, U.S.A. : Chapman & Hall/CRC Available at:. http://www.amazon.ca/exec/obidos/redirect?tag=citeulike09-20&path=ASIN/0412048418 [Accessed January 12, 2011]

BRENNING, A. (2009). Benchmarking classifiers to optimally integrate terrain analysis and multispectral remote sensing in automatic rock glacier detection. Remote Sensing of Environment, 113(1), 239–247.

BRENNING, A. (2010). Land cover classification by multisource remote sensing: Comparing classifiers for spatial data. In H. Locarek-Junge, & C. Weihs (Eds.), Classification as a tool for research (pp. 435–443). Berlin, Heidelberg: Springer Berlin Heidelberg Available at: http://www.springerlink.com/content/x55n3g1314766146/ [Accessed October 4, 2011]

BURGES, C. (1998). A tutorial on Support Vector Machines for Pattern Recognition. Data Mining and Knowledge Discovery, 2(2), 121–167.

CARREIRAS, J. M. B., PEREIRA, J. M. C., CAMPAGNOLO, M. L., & SHIMABUKURO, Y. E. (2006). Assessing the extent of agriculture/pasture and secondary succession forest in the Brazilian Legal Amazon using SPOT VEGETATION data. Remote Sensing of Environment, 101(3), 283–298.

CASTILLA, G., & HAY, G. J. (2008). Image objects and geographic objects. In Blaschke Thomas, S. Lang, & Geoffrey J. Hay (Eds.), Object-based image analysis (pp. 91–110). Berlin, Heidelberg: Springer Berlin Heidelberg Available at:. http:// www.springerlink.com/content/g403k30318784w36/ [Accessed October 1, 2011]

CASTILLEJO-GONZÁLEZ, I. L., LÓPEZ-GRANADOS, F., GARCÍA-FERRER, A., PEÑA-BARRAGÁN, J. M. JURADO-EXPÓSITO, M., DE LA ORDEN, M. S, ET AL. (2009). Object- and pixel-based analysis for mapping crops and their agro-environmental associated measures using QuickBird imagery. Computers and Electronics in Agriculture, 68(2), 207–215.

CHAN, J., & PAELINCKX, D. (2008). Evaluation of Random Forest and Adaboost tree-based ensemble classification and spectral band selection for ecotope mapping using airborne hyperspectral imagery. Remote Sensing of Environment, 112(6), 2999–3011.

CHANDER, G., MARKHAM, B. L., & HELDER, D. L. (2009). Summary of current radiometric calibration coefficients for Landsat MSS, TM, ETM+, and EO-1 ALI sensors. Remote Sensing of Environment, 113(5), 893–903.

CHAVEZ, P. S., JR. (1988). An improved dark-object subtraction technique for atmospheric scattering correction of multispectral data. Remote Sensing of Environment, 24(3), 459–479.

CNES (2009). SPOT image quality performances. Available at:. http://www.spotimage. com/automne_modules_files/standard/public/p551_29f05cbeaf21f085aab8a439d6fb4e 14Performance_QI_Spot2009.pdf [Accessed January 11, 2011]

COHEN, J. (1960). A coefficient of agreement for nominal scales. Educational and psychological measurement, 20(1), 37–46.

CONGALTON, R. G. (1991). A review of assessing the accuracy of classifications of remotely sensed data. Remote Sensing of Environment, 37(1), 35–46.

CONGALTON, R. G., & GREEN, K. (1998). Assessing the accuracy of remotely sensed data: Principles and practices (1st ed.): CRC Press.

COOPER, A. B., SMITH, C. M., & SMITH, M. J. (1995). Effects of riparian set-aside on soil characteristics in an agricultural landscape: Implications for nutrient transport and retention. Agriculture, Ecosystems & Environment, 55(1), 61–67.

CORTES, C., & VAPNIK, V. (1995). Support-vector networks. Machine Learning, 20(3), 273–297.

COSTA,G.A.O.P.,FEITOSA,R.Q.,CAZES,T.B.,&FEIJÓ,B.(2008).Genetic adaptation of segmentation parameters. In Thomas Blaschke, S. Lang, & Geoffrey J. Hay (Eds.), Object-based image analysis (pp.679–695). Berlin, Heidelberg: Springer Berlin Heidelberg Available at:. http://www.springerlink.com/content/l7367p41j61715w5/ [Accessed July 27, 2011]

DINGLE ROBERTSON, L., & KING, D. J. (2011). Comparison of pixel- and object-based classification in land cover change mapping. International Journal of Remote Sensing, 32 (6), 1505–1529.

DORREN, L. K. A., MAIER, B., & SEIJMONSBERGEN, A. C. (2003). Improved Landsat-based forest mapping in steep mountainous terrain using object-based classification. Forest Ecology and Management, 183(1), 31–46.

DRĂGUT, L., TIEDE, D., & LEVICK, S. R. (2010). ESP: a tool to estimate scale parameter for multiresolution image segmentation of remotely sensed data. International Journal of Geographical Information Science, 24(6), 859.

DUBÉ, M. G. (2003). Cumulative effect assessment in Canada: a regional framework for aquatic ecosystems. Environmental Impact Assessment Review, 23(6), 723–745.

DUINKER,P.,& GREIG,L.(2006).The impotence of cumulative effects assessment in Canada: Ailments and ideas for redeployment. Environmental Management, 37(2), 153–161.

FOODY, G. M. (2004). Thematic map comparison: Evaluating the Statistical significance of differences in classification accuracy. Photogrammetric Engineering and Remote Sensing, 70(5), 627–634.

FOODY, G. M. (2009). Sample size determination for image classification accuracy assessment and comparison. International Journal of Remote Sensing, 30(20), 5273-5291.

FRANKLIN, S. E., & PEDDLE, D. R. (1990). Classification of SPOT HRV imagery and texture features. International Journal of Remote Sensing, 11(3), 551–556.

FRANKLIN, S. E., & WULDER, M. A. (2002). Remote sensing methods in medium spatial resolution satellite data land cover classification of large areas. Progress in Physical Geography, 26(2), 173–205.

FRIEDL, M. A., & BRODLEY, C. E. (1997). Decision tree classification of land cover from remotely sensed data. Remote Sensing of Environment, 61(3), 399–409.

GISLASON, P. O., BENEDIKTSSON, J. A., & SVEINSSON, J. R. (2006). Random Forests for land cover classification. Pattern Recognition Letters, 27(4), 294–300.

GORDON, L. J., PETERSON, G. D., & BENNETT, E. M. (2008). Agricultural modifications of hydrological flows create ecological surprises.Trends in Ecology & Evolution, 23(4),211–219.

GREGORY, S., SWANSON, F.., MCKEE, W., & CUMMINS, K. (1991). An ecosystem perspective of riparian zones. BioScience, 41(8).

HARALICK, R. M., SHANMUGAM, K. and DINSTEIN, I., 1973, Textural Features for Image Classification. *IEEE Transactions on Systems, Man and Cybernetics,* 3, pp. 610-621.

HUANG, C., DAVIS, L. S., & TOWNSHEND, J. R. G. (2002). An assessment of support vector machines for land cover classification. International Journal of Remote Sensing, 23 (4), 725–749.

HUEL, D. (2000). Managing Saskatchewan Wetlands: A landowner's guide. Available at: http://www.swa.ca/Publications/Documents/ManagingSaskatchewanWetlands.pdf [Accessed November 11, 2011]

KARATZOGLOU, A., SMOLA, A., HORNIK, K., & ZEILEIS, A. (2004). kernlab – An S4 Package for Kernel Methods in R. Journal of Statistical Software, 11(9), 1–20.

KIM, M., MADDEN, M., & WARNER, T. (2008). Estimation of optimal image object size for the segmentation of forest stands with multispectral IKONOS imagery. Object-based image analysis (pp. 293–307). Berlin, Heidelberg: Springer Berlin Heidelberg Available at: http://www.springerlink.com/content/u7741201m568u327/ [Accessed January 11, 2011]

KOHAVI, R. (1995). A study of cross-validation and bootstrap for accuracy estimation and model selection. International joint conference on artificial intelligence (pp. 1137–1143). Available at:. http://citeseerx.ist.psu.edu/viewdoc/summary? doi=10.1.1.48.529

KUHN, M. (2008). Building predictive models in R using the caret package. Journal Of Statistical Software, 28(5), 1–26.

KUHN, M. (2011). The caret package. Available at:. http://cran.r-project.org/web/packages/caret/vignettes/caretTrain.pdf [Accessed October 3, 2011]

LALIBERTE, A. S., FREDRICKSON, E. L., & RANGO, A. (2007). Combining decision trees with hierarchical object-oriented image analysis for mapping arid rangelands. Photogrammetric Engineering and Remote Sensing, 73(2), 197–207.

LALIBERTE, A.S., KOPPA, J.S., FREDRICKSON, E.L., RANGO, A. (2006). Comparison of nearest neighbor and rule-based decision tree classification in an object-oriented environment. In: IEEE international Geoscience and Remote Sensing Symposium Proceedings, July 31-August 4, 2006, Denver, Colorado.

Liaw, A., & Wiener, M. (2002). Classification and regression by randomForest. R News, 2(3), 18–22.

LINKE, J., & MCDERMID, G. J. (2011). A conceptual model for multi-temporal landscape monitoring in an object-based environment. Selected Topics in Applied Earth Observations and Remote Sensing. IEEE Journal of, 4(2), 265–271.

LINKE, J., MCDERMID, G. J., LASKIN, D. N., MCLANE, A. J., PAPE, A., CRANSTON, J., ET AL. (2009). A disturbance-inventory framework for flexible and reliable landscape monitoring. Photogrammetric Engineering and Remote Sensing, 75(8), 981–995.

MATHIEU, R., ARYAL, J., & CHONG, A. K. (2007). Object-based classification of Ikonos imagery for mapping large-scale vegetation communities in urban areas. Sensors, 7(11), 2860–2880.

MCKENZIE, D. P., MACKINNON, A. J., PÉLADEAU, N., ONGHENA, P., BRUCE, P. C., CLARKE, D. M., HARRIGAN, S., MCGORRY, P.D. (1996). Comparing correlated kappas by resampling: Is one level of agreement significantly different from another? Journal of Psychiatric Research, 30(6), 483–492.

MORISSETTE, J. T., & KHORRAM, T. A. (1998). Exact binomial confidence interval for proportions. Photogrammetric Engineering and Remote Sensing, 64.

MYINT, S. W., GOBER, P., BRAZEL, A., GROSSMAN-CLARKE, S., & WENG, Q. (2011). Per-pixel vs. object-based classification of urban land cover extraction using high spatial resolution imagery. Remote Sensing of Environment, 115(5), 1145–1161.

NAIMAN, R., & DÉCAMPS, H. (1997). The ecology of interfaces: Riparian Zones. Annual Review of Ecology and Systematics, 28(1), 621–658.

NOBLE, B. F. (2008). Strategic approaches to regional cumulative effects assessment: a case study of the Great Sand Hills, Canada. Impact Assessment and Project Appraisal, 26, 78–90.

OTUKEI, J. R., & BLASCHKE, T. (2010). Land cover change assessment using decision trees, support vector machines and maximum likelihood classification algorithms. International Journal of Applied Earth Observation and Geoinformation, 12 (Supplement 1), S27–S31.

PAL, M. (2005). Random forest classifier for remote sensing classification. International Journal of Remote Sensing, 26(1), 217.

PEÑA-BARRAGÁN, J. M., NGUGI, M. K., PLANT, R. E. and SIX, J., 2011, Object-based crop identification using multiple vegetation indices, textural features and crop phenology. *Remote Sensing of Environment,* 115, pp.1301-1316.

PIKE, R. J. (2000). Geomorphometry —Diversity in quantitative surface analysis. Progress in Physical Geography, 24(1), 1–20.

PLATT, R. V., & RAPOZA, L. (2008). An evaluation of an object-oriented paradigm for land use/land cover classification. The Professional Geographer, 60(1), 87.

R DEVELOPMENT CORE TEAM (2010). R: A language and environment for statistical computing, Vienna, Austria. Available at: http://www.R-project.org/

ROUSE, J.W., R.H. HAAS, J.A. SCHELL, AND D.W. DEERING (1973). “MONITORING VEGETATION SYSTEMS IN THE GREAT PLAINS WITH ERTS.” IN PROCEEDINGS OF THE THIRD ERTS SYMPOSIUM, 1:309–317. WASHINGTON DC, 1973.

RYHERD, S., & WOODCOCK, C. (1996). Combining spectral and texture data in the segmentation of remotely sensed images. Photogrammetric Engineering and Remote Sensing, 62(2), 181–194.

SEITZ, N. E., WESTBROOK, C. J., & NOBLE, B. F. (2011). Bringing science into river systems cumulative effects assessment practice. Environmental Impact Assessment Review, 31(3), 172–179.

SMITH, A. (2010). Image segmentation scale parameter optimization and land cover classification using the Random Forest algorithm. Journal of Spatial Science, 55(1), 69.

SQUIRES, A. J., WESTBROOK, C. J., & DUBÉ, M. G. (2009). An approach for assessing cumulative effects in a model river, the Athabasca River Basin. Integrated Environmental Assessment and Management (pp. 1).

STEHMAN, S. V. (1997). Selecting and interpreting measures of thematic classification accuracy. Remote Sensing of Environment, 62(1), 77–89.

STUCKENS, J., COPPIN, P. R., & BAUER, M. E. (2000). Integrating contextual information with per-pixel classification for improved land cover classification. Remote Sensing of Environment, 71(3), 282–296.

THERNEAU, T. M., & RIPLEY, B. A. (2010). rpart: Recursive Partitioning. Available at: http://CRAN.R-project.org/package=rpart

THOMPSON, W. H., & HANSEN, P. L. (2001). Classification and management of riparian and wetland sites of the Saskatchewan prairie ecozone and parts of adjacent subregions. Available at: http://www.swa.ca/Publications/Documents/ClassificationManagementRiparianWetlandSites.pdf [Accessed July 1, 2011]

THUILLIER, G., HERSÉ, M., LABS, D., FOUJOLS, T., PEETERMANS, W., GILLOTAY, D., ET AL. (2003).The solar spectral irradiance from 200 to 2400 nm as measured by the SOLSPEC spectrometer from the ATLAS and EURECA missions. Solar Physics, 214(1), 1–22.

TRIMBLE (2010A). eCognition® Developer 8.64.0 reference book. Available at:. http://www.definiens.com/ [Accessed January 11, 2011]

TRIMBLE (2010B). eCognition® Developer 8.64.0 user guide. Available at:. http://www.definiens.com/ [Accessed January 11, 2011]

US EPA (2005). National management measures to protect and restore wetlands and riparian areas for the abatement of nonpoint source pollution. Available at: http://water.epa.gov/polwaste/nps/wetmeasures/index.cfm [Accessed July 26, 2011]

VAN COILLIE, F. M. B., VERBEKE, L. P. C., & DE WULF, R. R. (2007). Feature selection by genetic algorithms in object-based classification of IKONOS imagery for forest mapping in Flanders, Belgium. Remote Sensing of Environment, 110(4), 476–487.

VAPNIK, V. (1998). Statistical learning theory. : Wiley-Interscience Available at:. http://www.amazon.ca/exec/obidos/redirect?tag=citeulike09-20&path=ASIN/0471030031 [Accessed July 28, 2011].

WHITESIDE, T. G., BOGGS, G. S., & MAIER, S. W. (2011). Comparing object-based and pixel-based classifications for mapping savannas. International Journal of Applied Earth Observation and Geoinformation, 13(6), 884–893.

YAN, G., MAS, J. F., MAATHUIS, B. H. P., XIANGMIN, Z., & VAN DIJK, P. M. (2006). Comparison of pixel-based and object-oriented image classification approaches-A case study in a coal

fire area, Wuda, Inner Mongolia, China. International Journal of Remote Sensing, 27, 4039–4055.

YU, Q., GONG, P., CLINTON, N., BIGING, G., KELLY, M., & SCHIROKAUER, D. (2006). Object-based detailed vegetation classification with airborne high spatial resolution remote sensing imagery. Photogrammetric Engineering and Remote Sensing, 72(7), 799–811.

ZAR, J. H. (2009). Biostatistical analysis (5th ed.): Prentice Hall.

CHAPTER 3 PREFACE

Random Forests, one of the machine learning algorithms used for classifying remotely sensed imagery in the previous chapter, exhibited promising characteristics when applied to large datasets typical of multi-scale object-based image analysis. As noted in Chapter 1, the fusion of multiple sources of remotely sensed imagery can often lead to better discrimination between land cover types and an increase in overall classification accuracies. In this chapter, the Random Forest algorithm is explored in greater depth and is used to classify remotely sensed information derived from two satellite-based platforms. In addition, a feature selection algorithm, based on Random Forests, is used to select relevant predictors from several dozen object-based variables. Such data reduction and fusion techniques can provide potentially valuable insight into what spatial scales and spectral information are most relevant for discriminating between selected land cover types.

CHAPTER 3

MULTI-SCALE OBJECT-BASED IMAGE ANALYSIS AND FEATURE SELECTION OF MULTI-SENSOR EARTH OBSERVATION IMAGERY USING RANDOM FORESTS [†]

[†] The published contents of this chapter appear with permission from Taylor & Francis Ltd. The version that appears in this document has been modified to maintain consistency and formatting between chapters, and as such, it contains different content than the original material. Readers are encouraged to refer to the original publication:

DURO, D.C., FRANKLIN, S.E., DUBÉ, M.G. (2012). Multi-scale object-based image analysis and feature selection of multi-sensor earth observation imagery using random forests. *International Journal of Remote Sensing* (33): pp. 4502-4526.

All work reported in this chapter, including the review of the literature, theoretical and experimental design, analysis and discussion of the results, and writing of the text, was carried out by the Ph.D. candidate. As supervisors, Drs. S.E. Franklin and M.G. Dubé reviewed all or parts of the work.

3.1 ABSTRACT

The random forest (RF) classifier is a relatively new machine learning algorithm that can handle data sets with large numbers and types of variables. Multi-scale object-based image analysis (MOBIA) can generate dozens, and sometimes hundreds, of variables used to classify earth observation (EO) imagery. In this study, a MOBIA approach is used to classify the land cover in an area undergoing intensive agricultural development. The information derived from the elevation data and imagery from two EO satellites are classified using the RF algorithm. Using a wrapper feature selection algorithm based on the RF, a large initial data set consisting of 418 variables was reduced by ~60%, with relatively little loss in the overall classification accuracy. With this feature-reduced data set, the RF classifier produced a useable depiction of land cover in the study area and achieved an overall classification accuracy of greater than 90%. Variable importance measures produced by the RF algorithm provided an insight into which object features were relatively more important for classifying individual land-cover types. The MOBIA approach outlined in this study achieved the following: (i) consistently high overall classification accuracies (>85%) using the RF algorithm in all models examined, both before and after feature reduction; (ii) feature selection of a large data set with little expense to the overall classification accuracy; and (iii) increased interpretability of classification models due to the feature selection process and the use of variable importance scores generated by the RF algorithm.

3.2 INTRODUCTION

3.2.1 OBJECT-BASED IMAGE ANALYSIS

Object-based image analysis of earth observation (EO) imagery has become increasingly prevalent over the last decade (Blaschke 2010). Uptake of object-based image analysis can be partially ascribed to the increasing availability and use of sub-meter imagery (Lang 2008), as

such very high spatial resolutions tends to increase intra-class spectral variability, which is an issue when using pixel-based image analysis with classification algorithms that rely on parametric statistical techniques to separate spectral classes (Chen et al. 2004, Yu et al. 2006, Lu and Weng 2007). Additionally, the popularity of object-based image analysis can be seen in light of efforts to alleviate issues associated with using pixel-based data as an underlying unit of measurement (see Fisher 1997, Townshend et al. 2000), and as a means of more intuitively incorporating information on features of interest that may exist at multiple spatial scales within an image scene (Strahler et al. 1986, Hay et al. 2002).

Compared to traditional pixel-based approaches, multi-scale object-based image analysis (MOBIA) often entails the use of dozens, and sometimes, hundreds of variables. This difference is largely due to the use of object features, which are variables used to summarize information from the original input layers (e.g., multi-spectral bands, vegetation indices, digital elevation model, etc.). Selected object features are used for subsequent object-based classification and are calculated for individual image objects, which are produced in a preceding image segmentation process (e.g., see Section 3.3.3 for details). Image segmentation can be conducted at a variety of scales related to the underlying input data, creating many smaller image objects, or fewer larger image objects. When using multiple image segmentation scales, object features that describe relationships between image objects created at different segmentation scales can be used to provide additional contextual information, which is potentially useful to multi-scale landscape analysis and classification applications. Such object-based image analysis has been called “multi-scale segmentation/object relationship modelling” (Burnett and Blaschke 2003), and has been used in various forms by others for the purposes of classifying EO imagery (e.g., Watts et al. 2009; Kim et al. 2011; Leibovici and Jackson 2011).

3.2.2 CLASSIFICATION ALGORITHMS FOR MOBIA

While MOBIA provides a potentially attractive approach for extracting information from EO imagery, the large number of variables and data types that are often utilized requires the use of suitable analytical methods to extract meaningful information from the underlying imagery. Common methods used for MOBIA of EO imagery have tended to focus on using heuristically simple classification algorithms, or "classifiers", such as k-nearest neighbour (k-NN), or parametric statistical techniques such as maximum-likelihood classification (MLC). The MLC classifier is believed to be unsuited to the classification of data types that may violate various assumptions of parametric statistical techniques, such as categorical or non-normally distributed data sets (Benediktsson et al. 1990; Gong 1996; Bruzzone et al. 1999; Franklin and Wulder 2002). Despite these reservations, MLC is still often used in studies comparing various classifiers, ostensibly as a benchmark due to its many decades of use for classifying EO imagery. The MLC algorithm tends to perform relatively poorly in overall classification accuracy when compared to more modern nonparametric machine learning classifiers (e.g., decision tree, support vector machine, random forest), which has been demonstrated in a variety of recent comparative studies (Yan et al. 2006; Yu et al. 2006; Platt and Rapoza 2008; Na et al. 2010; Otukei and Blaschke 2010; Myint et al. 2011). Despite these findings, the MLC algorithm has been found to perform better the k-NN classifier in pixel-based comparisons where the feature space (i.e., number of input variables) was not optimized (Platt and Rapoza 2008). In a study comparing machine learning algorithms (Mallinis et al. 2008), the k-NN classifier, commonly used in OBIA, was compared with a decision tree (DT) classifier. The comparison found that the DT classifier outperformed the k-NN classifier, a finding echoed in an earlier study (Laliberte et al. 2006). Chan and Paelinckx (2008) compared the use of two tree-based ensemble algorithms (Adaboost DT and random forest) against a neural network algorithm for classifying airborne hyperspectral imagery containing 126 bands. Both tree-based ensemble classifiers achieved similar results, and outperformed the neural network classifier; however, the random forest (RF) classifier was found to be faster to train and more stable than the Adaboost DT classifier.

The above studies suggest that classification algorithms that are well suited to MOBIA-based application are those that are not restricted by parametric based assumptions (like MLC), are capable of utilizing a variety of data types and sources (like DT), and that employ more sophisticated heuristics than the k-NN classifier.

3.2.2.1 RANDOM FOREST

The RF classifier described by Breiman (2001) is a relatively new non-parametric machine learning algorithm that can handle a variety of data types and has become adopted in a wide variety of applications (Svetnik et al. 2004, Peters et al. 2007, Watts et al. 2009, Na et al. 2010). As the name implies, the RF classifier utilizes several DTs, whereby predictions made by individual trees are averaged across the entire forest (Breiman and Cutler 2007). Such ensemble-based classification algorithms combine predictions made by several individually trained classifiers (e.g., DT) to achieve classification accuracies that are frequently more accurate than what can be achieved using a single classifier alone (Maclin and Opitz 1999, Prasad et al. 2006). The RF algorithm is capable of handling large numbers of variables (v) relative to the number (n) of observations (Svetnik et al. 2004). These so-called "small *n*, large *v*" data sets, referred to by others as the "curse of dimensionality" (Melgani and Bruzzone 2004), often characterize applications involving MOBIA of EO imagery, and are especially relevant in instances where the number of variables (object features) may equal, or even exceed, the number of training samples being considered. Such performance characteristics make the RF classifier a attractive choice for MOBIA of EO imagery.

Recently, Sesnie et al. (2008) used importance measures generated by RF to identify relationships between predictor variables and ecological categories, and as a means of eliminating predictors of minor consequence to overall classification accuracy, in an approach similar to the one adopted for this study. Ghimire et al. (2010) combined the Getis statistic, a measure of local spatial dependence, and RF classifier to incorporate spatial dependence into a pixel-based classification. Their findings showed that a spatial RF, using various window sizes to

calculate the Getis statistic, outperformed the non-spatial RF when classifying several land cover types using Landsat Enhance Thematic Mapper Plus (ETM+) imagery. The RF classifier has also been used to create predictive maps of tree species using several ecological variables under a range of potential future climate scenarios (Prasad et al. 2006). This latter study found that the RF classifier performed slightly better than regression tree analysis, bagging trees, and multivariate adaptive regression splines, based on a variety of measures.

In this study, a MOBIA approach and RF classifier are used to classify multi-source, multi-sensor EO imagery. While the RF algorithm has been applied to multi-source classification of EO imagery in pixel-based approaches (Pal 2005; Gislason et al. 2006), this study utilizes multiple types of EO imagery obtained at variable spatial and spectral resolutions, along with other ancillary data utilizing MOBIA. A similar approach has been previously used to classify urban and rural land cover whereby information from different sensors were used in *a priori* fashion for creating image objects for specific land cover types (Forghani et al. 2007). In contrast, this study employs a feature selection procedure, based on the RF classifier, and variable importance measures generated by the RF classifier, to derive which variables and sensor specific image sources are important for the classification of individual land cover types. The MOBIA approach outlined in this study answers the following questions: (i) what kind of classification accuracies can be expected when using the RF algorithm to classify a multi-source, multi-sensor dataset, both before and after feature reduction? (ii) What effects does feature selection have on classification accuracies? (iii) What are the benefits of using feature selection and the RF classifier for MOBIA of EO imagery?

3.3 METHODS

3.3.1 STUDY AREA

The study area is situated in Saskatchewan along a section of the South Saskatchewan River approximately 80 km east of the provincial border between Alberta and Saskatchewan, Canada (see Figure 6). Economic activity within the area is dominated by agricultural industries

with an emphasis on dryland farming, although irrigation is used on a limited basis. Various crop types are grown and harvested in the region including several cereal crop species (e.g., wheat, barley, oat, rye, triticale), oilseed species (e.g., canola, flax, mustard, sunflower), and a variety of leguminous "pulse crops" (e.g., peas, lentils, chickpeas, dry beans). Livestock farming is also practised in the region, either in the form of intensive cattle feedlots, or as ranching operations covering large areas of rangeland. The climate is characterized by long cold winters with relatively short warm summers. Mean annual precipitation in the area is less than 350 mm, with portions classified as semiarid (e.g., Great Sand Hills, Saskatchewan). Threats to water quality and quantity from cumulative environmental effects caused by development and climate change are of increasing concern in the region (Schindler 2001, Schindler and Donahue 2006).

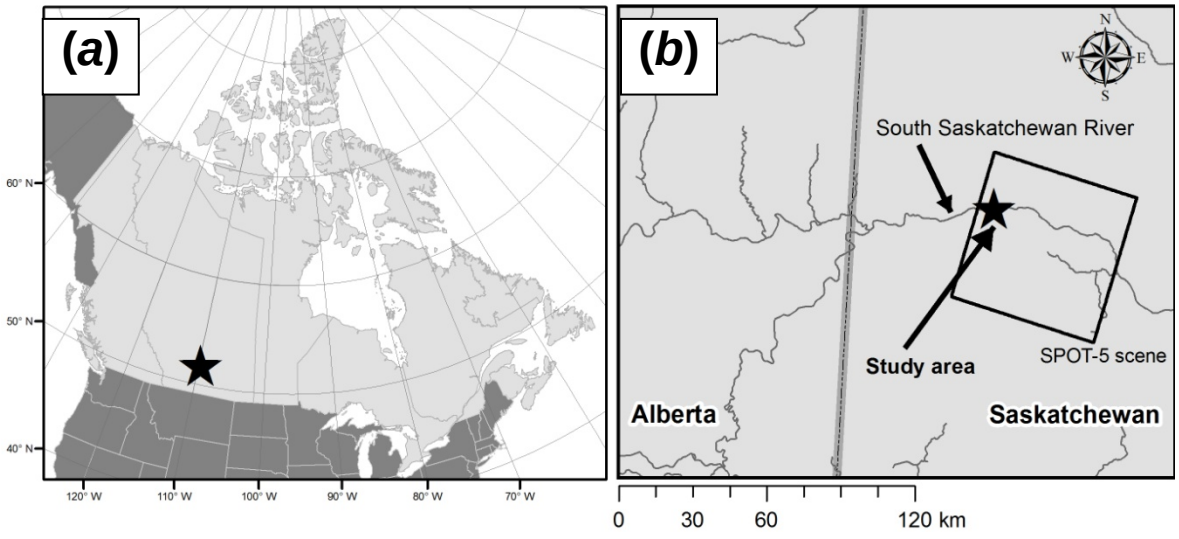

Figure 6: a) Location of study area in south-western Saskatchewan, Canada. b) Location of study area in relation to full SPOT-5 scene.

3.3.2 DATASETS AND PRE-PROCESSING

Two sources of remotely sensed imagery were obtained for this study: Landsat-5 Thematic Mapper (TM) data, and SPOT-5 High Resolution Geometric (HRG) data. A 2.5 m panchromatic scene and a 10 m multi-spectral scene (August 28, 2005) of the study area was

obtained from the SPOT-5 satellite, along with a 30 m multi-spectral scene from Landsat-5 (August 22, 2008). The Landsat series of satellites have a long history of use in agricultural applications (Rouse et al. 1973), with the TM sensor recently being used for mapping grizzly bear habitat in agricultural environments (Collingwood et al. 2009; Wang et al. 2010), and wildfire susceptibility in semi-arid rangeland environments (Chen et al. 2011), which are environments similar to those found in the study area. The SPOT-5 HRG sensor is the most widely used Landsat-like alternative and has been found to be at least as accurate as Landsat in comparisons of land cover classification accuracy (Powell et al. 2007). Recently, the HRG sensor onboard SPOT-5 has been used to classify within-field crop types and estimates of crop yields (Yang et al. 2009, Conrad et al. 2010).

Control points used to georectify the satellite imagery were derived from several sources of ground survey data (e.g., national road network, geodetic controls points, and cadastral boundary layers). Using a first order polynomial transformation, all data sets were geometrically rectified to the higher spatial precision of the ground survey data with registration errors of less than 0.4 RMSE in all cases. Several tiles of the Canadian Digital Elevation Data digital elevation model (DEM) covering our study area were downloaded (www.geobase.ca) and processed. The use of a DEM and derived topographic variables has been used to increase classification accuracy of EO imagery (Franklin 1987) and as a means of correcting for illumination and topographic effects (Franklin and Giles 1995). All imagery and DEM files were transformed to a common projection (Albers Equal Area Conic, North American Datum 1983) for subsequent processing steps. The DEM has a horizontal post spacing of approximately 23 m (North-South) x 16-11 m (East-West) at the latitude of the study area. A mosaic of the separate tiles of the DEM was created, and converted to 16 x 16 m pixels using nearest-neighbour resampling. The latter processing step was performed in order to avoid software related issues when using analyzing datasets with square and non-square pixels. Slope and aspect were derived from the DEM, along with measures of topographic features (e.g., channel, ridge, plain) (Pike 2000). The DEM and derived topographic variables were included in our analysis to better discriminate areas of upland riparian vegetation which often follow a

specific topographic morphology (e.g., narrow stream channels that drain into a larger river). DEMs have been used in this capacity by others as input variables in ecological models for predicting vegetation composition (Moore et al. 1991; Franklin 1995; Miller and Franklin 2002).

In order to better compare spectral information from two separate sources and dates of remotely sensed imagery, the calibrated 8-bit digital numbers for SPOT-5 and Landsat-5 spectral bands were converted to 32-bit floating point exoatmospheric reflectance data (see Chander et al. 2009). Landsat-5 imagery was selected as the basis for the relative radiometric correction due to the widely available information and calibration history of the sensor. The SPOT-5 scene was radiometrically normalized relative to the Landsat-5 scene through a linear transformation based on spectrally invariant objects (Schott et al. 1988). This process involved simple thresholding of spectral bands to isolate and mask out areas of water and vegetation to locate spectrally invariant pixels common between scenes (e.g., large gravel pits, paved roads, large sand dunes, etc.) (Clark et al. 2011). A linear transformation was applied to each band of the target imagery (SPOT-5 HRG) to match the mean and standard deviation of the spectrally invariant pixels found in the base image (Landsat-5 TM). The Normalized Difference Vegetation Index (NDVI) was calculated for both the SPOT-5 and Landsat-5 imagery. The NDVI was selected based on previous studies that found it useful for classifying crop types (Price et al. 1997, Doraiswamy et al. 1998), assessing agricultural productivity (Hill and Donald 2003, Wardlow 2008, Yang et al. 2009), and as an indicator of watershed condition (Griffith et al. 2002), in agricultural settings similar to those found in our study area. The angular second moment texture measure (Haralick et al. 1973), a measure related to the degree of homogeneity among neighbouring pixels (Baraldi and Parmiggiani 1995), was included in our analysis as it has been shown to be important for discriminating between different crop types (Peña-Barragán et al. 2011). The angular second moment texture measure was calculated on the pixel-based NDVI layers derived from SPOT-5 and Landsat-5 multispectral bands. A listing of all input layers used in this study is in Table 5.

Table 5: List of variables selected for image segmentation and calculation of object features.

Data sources	Input variables
SPOT-5 HRG	
	Panchromatic [1]
	Green
	Red
	Near-infrared
	Short-wave infrared
	NDVI [1,2]
	NDVI-angular 2nd moment texture
Landsat-5 TM	
	Blue
	Green
	Red
	Near-infrared
	Short-wave infrared
	Mid-infrared
	NDVI [3,4]
	NDVI-angular 2nd moment texture
DEM	
	Elevation
	Slope
	Aspect
	Channel
	Ridge
	Plain
[1] used as input for Level 1 image segmentation (see Table 2)	
[2] used as input for Level 2 image segmentation	
[3] used as input for Level 3 image segmentation	
[4] used as input for Level 4 image segmentation	
Note: all variables listed were used in the calculation of selected object features (see Table 3)	

3.3.3 IMAGE SEGMENTATION AND OBJECT FEATURE SELECTION

3.3.3.1 SELECTION OF IMAGE SEGMENTATION PARAMETERS

Image segmentation represents the fundamental first step in a MOBIA of EO imagery, as this procedure defines the size and shape of image objects that will contain the aggregated information from original input layers, which are ultimately used for classification. The selection of appropriate image segmentation parameters tends to vary between projects as these values depend on the selected application, underlying input imagery, and the environment under analysis (Addink et al. 2007, Blaschke 2010, Myint et al. 2011). Image segmentation was performed using the multi-resolution segmentation (MRS) algorithm found in Definiens' eCognition Developer 8 software (Trimble 2010a). The MRS algorithm merges individual pixels with their neighbours based on several parameters that define within-object homogeneity (Baatz and Schape 1999; Benz et al. 2004). Prior to assigning values for parameters that control the image segmentation algorithm, the user must select which input layers are used by the MRS algorithm and whether differing weights should be applied to each data source. In this study, equal weightings were applied to all input imagery in order to equally weigh the fine spatial scale panchromatic data along with the NDVI layers derived from both the SPOT-5 and Landsat-5 sensors. Lippitt et al. (2012) found that the use of spectral transformations (e.g., NDVI) improved the overall accuracy of image segmentations for certain targets as compared to using untransformed spectral data alone. Table 5 indicates which input layers were used by the MRS algorithm for image segmentation.

The three main user-defined parameters for the MRS algorithm are shape-colour, compactness-smoothness, and scale. The paired shape-colour and compactness-smoothness parameters range from 0 to 1, as a weighting between each of the paired parameters. For example, a low value for the shape parameter (e.g., 0.1) is balanced by a larger emphasis on spectral ("colour") information (e.g., 0.9), with both weights always summing to one. Similarly, the compactness-smoothness parameter controls whether image objects with similar spectral characteristics should share smooth borders, or whether image objects should be more

compact overall (Trimble 2010b). Of all the user defined parameters within the MRS algorithm, the scale parameter is considered to be the most important for the classification of EO imagery as this value controls the relative size of image objects and has a direct effect on overall classification accuracy (Blaschke 2003; Meinel and Neubert 2004; Kim et al. 2008; Liu and Xia 2010; Smith 2010; Myint et al. 2011).

Image objects created using the MRS algorithm can be nested hierarchically, whereby lower levels containing many smaller image objects (e.g., tree crowns), can be linked to larger, "super-objects" above them (e.g., forest stand), and vice versa. Smaller image objects obtained by using lower values for the image segmentation scale parameter have been shown to produce better overall classification accuracies compared to using a single larger image segmentation scale (Smith 2010, Myint et al. 2011). However, these same studies have also demonstrated that the use of several image segmentation scales improves overall classification accuracy as compared to using a single image segmentation scale.

In this study, image segmentation scales were selected in an approach similar to Frohn et al. (2011) and Peña-Barragán et al. (2011), whereby smaller image objects derived at finer image segmentation scales were used to form the basis of a hierarchical, multi-scale object-based classification. In other words, image objects created at the finest image segmentation scale do not necessarily represent real-world objects of interest, but are instead sufficiently small to represent such objects when combined. These "image segments" represent the fundamental building blocks of an object-based classification (Castilla and Hay 2008). Image objects created at coarser image segmentation scales were used to provide information on larger real-world objects of interest (e.g., crop fields, channels of riparian vegetation, etc.).

The selection of image segmentation parameters and input bands was based on an iterative trial-and-error approach whereby image segmentations parameters and input variables were systematically varied and the resulting image segmentations visually assessed for their ability to depict real-world objects of interest. While time-consuming and qualitative, this trial-and-error approach is often utilized in object-based classifications (e.g., Laliberte et al. 2007, Mathieu et al. 2007, Dingle Robertson and King 2011, Myint et al. 2011, Pu et al. 2011). A

more quantitative approach for selecting optimal image segmentation parameters based on underlying input variables has been developed (Costa et al. 2008), but was not applied in this study due to time constraints required to properly assess and adapt this approach. Table 6 outlines the values selected for image segmentation parameters along with selected summary statistics for image objects produced at each segmentation level, and Table 5 details the specific bands used for each segmentation level.

Table 6: Values for image segmentation parameters used in the multi-scale, multi-sensor, object-based classification.

Segmentation Level	Scale	Shape/ Colour	Compactness/ Smoothness	# of Objects	Median Area of Objects (m^2)
1	10	0.1/0.9	0.5/0.5	92813	721
2	20	0.1/0.9	0.5/0.5	18306	3525
3	40	0.1/0.9	0.5/0.5	5382	11040
4	60	0.1/0.9	0.5/0.5	2251	30160
Note: see Table 1 for variables used in the image segmentation process					

3.3.3.2 SELECTION OF IMAGE OBJECT FEATURES

Following the segmentation of input layers by the MRS algorithm, several object features were selected. The selection of the appropriate object features in an object-based classification can be based on past experience and user knowledge (e.g., Laliberte et al. 2007), or can utilize feature selection algorithms (e.g., Yu et al. 2006, Chan and Paelinckx 2008, Genuer et al. 2010). In this study, both strategies were adopted: past experience with conducting object-based classification in the study area was used to guide the initial selection of object features, with the RF-based feature selection algorithm (see Section 3.3.6) used to select only those object features deemed "relevant" to the overall land cover classification model. Table 7 lists the two types of object features used in this study. These object features were calculated for all input layers at each segmentation scale, resulting in a total of 440 object features (22

input variables x 5 object features x 4 segmentation scales). The total number of object features was reduced to 418, as object features that consider sub-object values were not calculated at the finest image segmentation scale.

Table 7: List of object features initially used by all land cover classification models: a) "layer features", and; b) "texture features" used in the object-based classification (adapted from Trimble 2010).

Object feature type:	
(*a*) Layer features	**Description**
Mean	Mean value of object for a specific input variable
Standard deviation	Standard deviation of object for a specific input variable
Mean difference to neighbours	The difference between mean values of an image object and neighboring image objects.
Mean difference to super-objects	The difference between the mean value of an image object for a specific input layer and the mean value of it's super-object
(*b*) Texture features	**Description**
Mean of sub-objects	Standard deviation of the mean value of sub-objects for a given superobject
Note: above object features were calculated for all input variables listed in Table 1	

3.3.4 TRAINING AND TESTING DATA

Training and testing data for the study area was obtained from visually interpreting 60 cm aerial colour orthophotos and 2.5 m panchromatic SPOT-5 imagery. An unsupervised ISODATA clustering algorithm was applied to the four bands of SPOT-5 multi-spectral imagery for the purposes of creating an initial land cover map suitable for conducting a stratified random sample. The stratified random sample is the recommended approach when attempting to avoid under-sampling small but possibly important areas of interest (e.g., riparian vegetation in small narrow channels) when sample sizes are small (Congalton 1991). This procedure yielded 20 classes that were generalized to five selected broad land cover types: crop land, mixed grasslands, areas of exposed rock/soil, riparian, and water. Spectral classes produced by the ISODATA classification that did not correspond to one of the five selected land cover types

were labelled as “unclassified”. The remaining spectral classes that represented the five land cover types were then labelled accordingly. A stratified random sample with equal proportions was performed within the five land cover types obtained from the ISODATA classification, yielding a total of 1,000 samples (200 samples per land cover type). These sample points were assessed visually over a 30 m x 30 m area using the SPOT-5 panchromatic and colour aerial photos obtained in the same month and year as the SPOT-5 and Landsat-5 multispectral imagery. Sample points were visually examined to ensure that labels assigned by the generalized ISODATA classification were correct, with mislabelled samples adjusted where necessary.

These sample points and labels were then spatially joined to image objects created at the finest image segmentation scale. This was accomplished using a spatial query within a GIS to determine which samples were completely contained by image objects. The spatially joined image objects were visually reassessed using aerial photos and panchromatic SPOT-5 imagery to ensure that the joined image object represented the land cover labels assigned in the previous procedure. The number of samples was reduced due to multiple sample points occupying the same image object, or points lying on image object boundaries. Training and test data were drawn from the remaining samples through a stratified random sample. This procedure ensured that similar sample proportions for each land cover type were used for both training and testing purposes. Of the remaining 986 samples, 70% were used for training and 30% for testing purposes. Testing data was set aside exclusively for the purposes of assessing classification accuracy.

3.3.5 OBJECT-BASED CLASSIFICATION

Information from all image objects obtained at each segmentation scale was extracted from the Definiens software for further processing in various relational database and GIS software. The development of the classification model was performed using R, a multi-

platform, open-source language and software for statistical computing (R Development Core Team 2010).

3.3.6 FEATURE SELECTION

In this study, the multiplicative effect of considering several input variables, object features, and image segmentation scales led to the creation of a large number of potential predictor variables (i.e., “object features”). When analyzing "small *n*, large *v*" data sets, traditional statistical classifiers (e.g., multiple linear regression and k-NN) cannot be used reliably without feature selection, with more advanced classification algorithms (e.g., artificial neural networks and support vector machine) often requiring feature selection when there are large numbers of irrelevant predictor variables (Svetnik et al. 2004). While the RF classifier is capable of handling large numbers of variables and relatively low number of observations, it may be advantageous to reduce the number of variables that need to be considered for reasons of practicality (i.e., reduced computation time), and/or determining which variables are deemed irrelevant to predicting the feature of interest (Guyon and Elisseeff 2003). The RF classifier has previously been used as a means of conducting feature selection in pixel-based image analyses of earth observation imagery (Chan and Paelinckx 2008, Dye et al. 2011, Ismail and Mutanga 2011), and is used here in the context of MOBIA.

Two problems are associated with reducing data set dimensionality for the purposes of classification (Nilsson et al. 2007): finding a minimal set of variables that are optimal for classification (the “minimal-optimal” problem), versus finding all variables relevant to the target variable (the “all-relevant” problem). As computational time was not an issue, feature selection was carried out to minimize "irrelevant" variables, and improve model interpretability, while maintaining overall classification accuracy. Current feature selection techniques fall under two categories (Kohavi and John 1997, Guyon and Elisseeff 2003): 1) filter approaches, which use selection methods that are independent of the classifier, and define the relevancy of variables based only on the training data; and, 2) wrapper approaches, that search for the subset of

variables that produce the highest classification accuracy using the training data and the classifier as part of the evaluation. Wrapper approaches are believed to produce better results than filter approaches (Kohavi and John 1997), and so the latter is excluded in this study.

In this study, feature selection was performed using the “Boruta” package for R (Kursa and Rudnicki 2010), a wrapper algorithm that uses the RF classifier to determine variable relevancy using the following heuristic (adapted from Kursa and Rudnicki 2010): “shadow variables” are introduced for each of the original variables, which are created by randomly shuffling the original observations for each variable. A RF classifier is applied to the data set, which is now composed of the original variables and their randomly shuffled shadow counterparts. The Boruta algorithm assesses Z-scores of the original RF variable importance score (see Section 3.2.2.1) against the randomly permuted shadow variables to determine which variables are truly important (Kursa and Rudnicki 2010). Variables that are significantly lower than this maximum Z-score are marked as “unimportant” and removed permanently, while variables that are significantly higher are marked as “important”. Shadow variables are then removed and the process is repeated within the wrapper function until all variables have been deemed “important” or “unimportant”, or until the maximum number of user defined iterations completes. Due to the high fluctuations of Z-scores when using large numbers of variables, the process begins with three initial rounds, which compare only selected shadow variables, whereas remaining rounds compare original variables against all shadow variables. The Boruta algorithm was run on the training data set, which had a total of 418 variables and 689 observations. Parameters for the Boruta algorithm were as follows: confidence level was set at 0.999 and the algorithm was set into "force mode", whereby all shadow variables were retained at each run.

3.3.7 MODEL DEVELOPMENT AND VARIABLE IMPORTANCE

The RF classifier used in this study is based on the "randomForest" package in R (Liaw and Wiener 2002). The RF algorithm is based on an ensemble of unpruned decision trees, which are

each grown to their maximum size using a different sample of two-thirds of the original training data, with the remaining one-third held back as "out-of-bag" (OOB) samples used as an internal estimate of error of overall classification accuracy (Breiman and Cutler 2007). It is reported that this "out-of-bag" (OOB) error estimate is unbiased in many tests (Breiman 2001). In this study, final classification accuracy is always reported using the separate “hold-out” test data set (Section 3.3.4), and not the OOB data.

Unlike traditional DT algorithms which examine all variables at each splitting node of the tree, the RF algorithm considers a random number of variables at each split. For the classification of categorical based variables, the majority vote among all trees in the ensemble (i.e., the “forest”) determines the prediction for a given observation. Individual unpruned trees within the forest are considered to be low bias and high variance (i.e., over fitted) models, but the averaging that takes place over hundreds, or many thousands, of trees within the forest lowers variance and reduces bias of the individual trees (Breiman 2001).

The RF algorithm is relatively simple to run “off the shelf” as only two user defined parameters are required: 1) the number of trees to be grown; and, (2) the number of variables which are randomly selected for determining splits at each node in individual trees. While tuning algorithms exist for determining such values, the default parameters have been shown to provide good classification results on datasets containing thousands of predictor variables (Liaw and Wiener 2002). Changes to the number of trees had little effect on the overall classification accuracies for all models used in this study, so this number was left at its default value (500). The mtry parameter, which controls the number of variables randomly considered at each split in the tree building process, is said to have a somewhat sensitive effect on the performance of the random forest algorithm (Breiman and Cutler 2007). Initial runs of the RF classifier on the training data revealed that several levels of this value had no appreciable effect on overall classification accuracy, so the default value was used for all models assessed in this study ($\sqrt{n}$, where n equals the number of variables).

In this study, emphasis is place on the results obtained from applying the RF classifier to the entire multi-source, multi-sensor data set that has undergone the feature selection

procedure outlined in Section 3.3.6. Variable importance is assessed using the "mean decrease in accuracy" measure found in the "randomForest" package (Liaw and Wiener 2002). Variable importance in RF is based on the following heuristic: prediction errors based on the OOB samples are recorded for each tree, and again after randomly shuffling OOB samples. The difference between prediction accuracy of the OOB samples versus permuted OOB samples is averaged over all trees, and then normalized by the standard deviation of the differences (Liaw and Wiener 2002). Variables with larger scores are thought to be more important to the classification than variables with lower scores. It should be noted that the feature selection algorithm also uses the "mean decrease in accuracy" measure, but does so by comparing Z-scores between original and randomly permuted "shadow" variables (see Section 3.3.6). Several classifications were performed in order to assess the relative effect of the feature selection process, and multiple sources of EO imagery, on classification accuracy. This was accomplished using the full dataset, and two modifications thereof: 1) SPOT-5 based variables removed, 2) Landsat-5 based variables removed. Classification accuracy before and after feature selection was assessed by examining the percentage of predictions classified as correct relative to the reference data set.

3.4 RESULTS

3.4.1 IMAGE SEGMENTATION

The results of the four selected image segmentation scales are shown in Figure 7 over a detailed subset within the study area. By design, image objects produced at the finest segmentation scale conform to small patches of spectrally similar pixels and do not necessarily conform to any real-world object of interest, although patches of mixed grassland are well delineated in the bottom left corner of Figure 7a. At coarser image segmentation scales, real-world features of interest are depicted as large generalized image objects. For example, areas of riparian vegetation (depicted as bright red vertical areas in Figure 7) are segmented with large contiguous boundaries in Figures 7c and 7d, correctly representing long channels of riparian vegetation. Areas of exposed soil/rock are best delineated with contiguous boundaries

in Figure 2b, which can be seen by the correct delineation of an exposed sandbar within the river channel (white oval object next to sandbar covered in riparian vegetation).

3.4.2 FEATURE SELECTION

The Boruta algorithm was applied to the full multi-source, multi-sensor data set. A total of 130 runs of the algorithm resulted in sizeable reduction of variables (i.e., object features). Of the original 418 variables contained in the entire multi-source, multi-sensor data set ("full model"), 160 variables were confirmed as “relevant”, 190 as “unimportant”, and 68 as “tentative”. In addition to leaving out irrelevant variables, variables marked as tentative were excluded from further analysis. A diagnostic plot depicting the fluctuation of variable importance after several iterative runs of the Boruta algorithm is found in Figure 8. The number of variables deemed unimportant dropped off markedly after approximately 40 runs of the Boruta algorithm, although fluctuations in Z-scores are noticeable in irrelevant variables at approximately 100 runs. The number of variables considered relevant and tentative remains fairly consistent over all iterations of the Boruta algorithm.

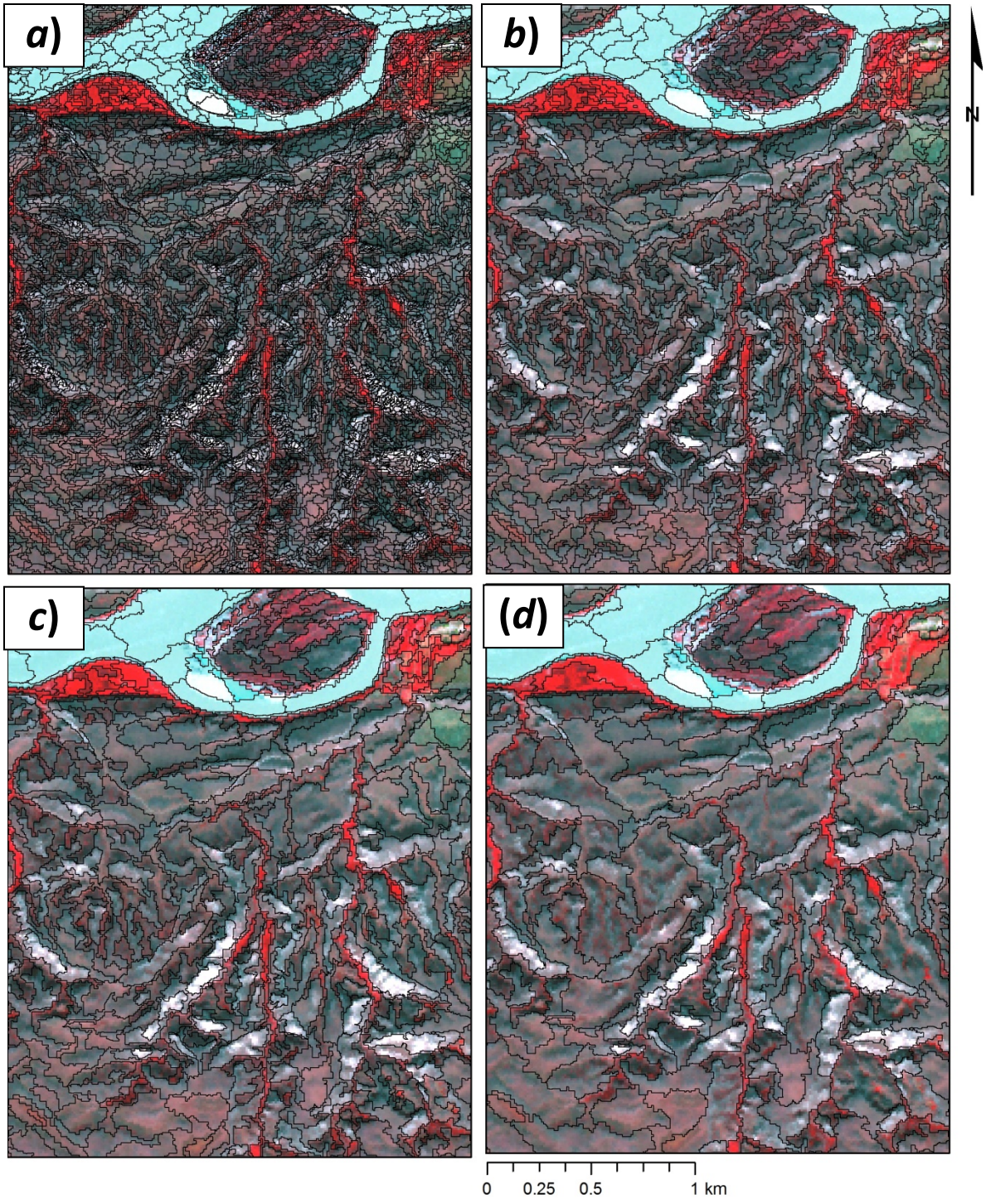

Figure 7: Image segmentation results for a detailed section of the study area at the following image segmentation scales: (a) 10, (b) 20, (c) 40, (d) 60. Standard false colour composite (R=NIR band, G=Red band, B=Green band) of SPOT-5 multispectral imagery (28 August 2005) as background.

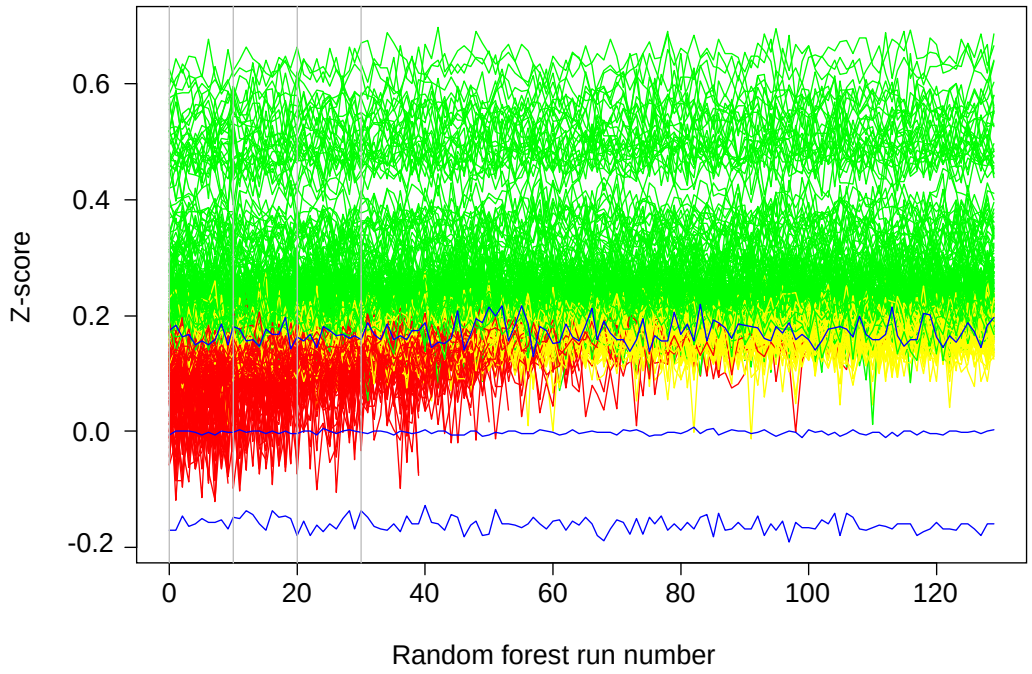

Figure 8: Diagnostic plot showing overall feature selection results after 130 runs of the Boruta algorithm (Kursa & Rudnicki 2010). Green lines represent "relevant" variables, yellow lines "tentative" variables, and red lines "unimportant" variables. The three blue lines along the horizontal axis represent maximum, median, and minimum Z-scores for "shadow variables". Vertical grey lines represent the initial three, less restrictive, runs of the Boruta algorithm. Higher Z-scores indicate relatively more important variables relative to shadow variables.

Figure 9 lists the top 40 object features used by the feature reduced "full model". The types of object features and related input layers that dominated the feature reduced "full model" were predominantly those based on the SPOT-5 derived NDVI, and individual spectral bands of the SPOT-5 and Landsat-5 sensors. Over half of the top 40 object features were dominated by the NDVI and multispectral information, object features based on the texture measure as applied to the SPOT-5 NDVI , and object features based on mean elevation, in the bottom-third of the list. The dominate object feature types were those that calculated mean and standard deviation values, while object features based on relationships between image objects at different image segmentation scales were not present in the top 40 object-features. Object features based on SPOT-5 NDVI and SPOT-5 spectral bands (panchromatic, red, and

green) dominate the top five important variables. Information from the SPOT-5 panchromatic band obtained at the two coarsest image segmentation scales (40 and 60) were in the top ten most important variables. The top three object features based on the Landsat-5 sensor are based on the mean value of image objects derived from the NDVI input variable at all segmentation levels except for 20.

Figure 10 summarizes the change in overall classification accuracy (percentage of correct predictions) before and after the feature selection process under two scenarios: (i) using the full multi-source, multi-sensor dataset, and; (ii) using a subset with sensor specific multi-spectral information removed. All classification models retained the use of other object features (e.g., SPOT-5 panchromatic and DEM-based object features). The number of variables before and after feature selection are as follows (Figure 10): (a) all multi-spectral information included (418 before vs. 160 after), (b) SPOT-5 multi-spectral information only (266 before vs. 129 after), (c) Landsat-5 multi-spectral information only (279 before vs. 177 after). Overall classification accuracy decreased slightly (<0.5%) after feature selection when using multi-spectral information from both SPOT-5 and Landsat-5 sensors. The model based on SPOT-5 multi-spectral information alone showed a slight increase (<0.5%) in overall classification accuracies after feature selection, whereas classification accuracy increased (~1.4%) after eature selection when using Landsat-5 multi-spectral information alone. The maximum difference between overall classification accuracies between models was approximately 3%. Using SPOT-5 multi-spectral information alone produced slightly higher overall classification accuracies (~1.3% maximum difference) than when using a model with multi-spectral information from both satellite sensors.

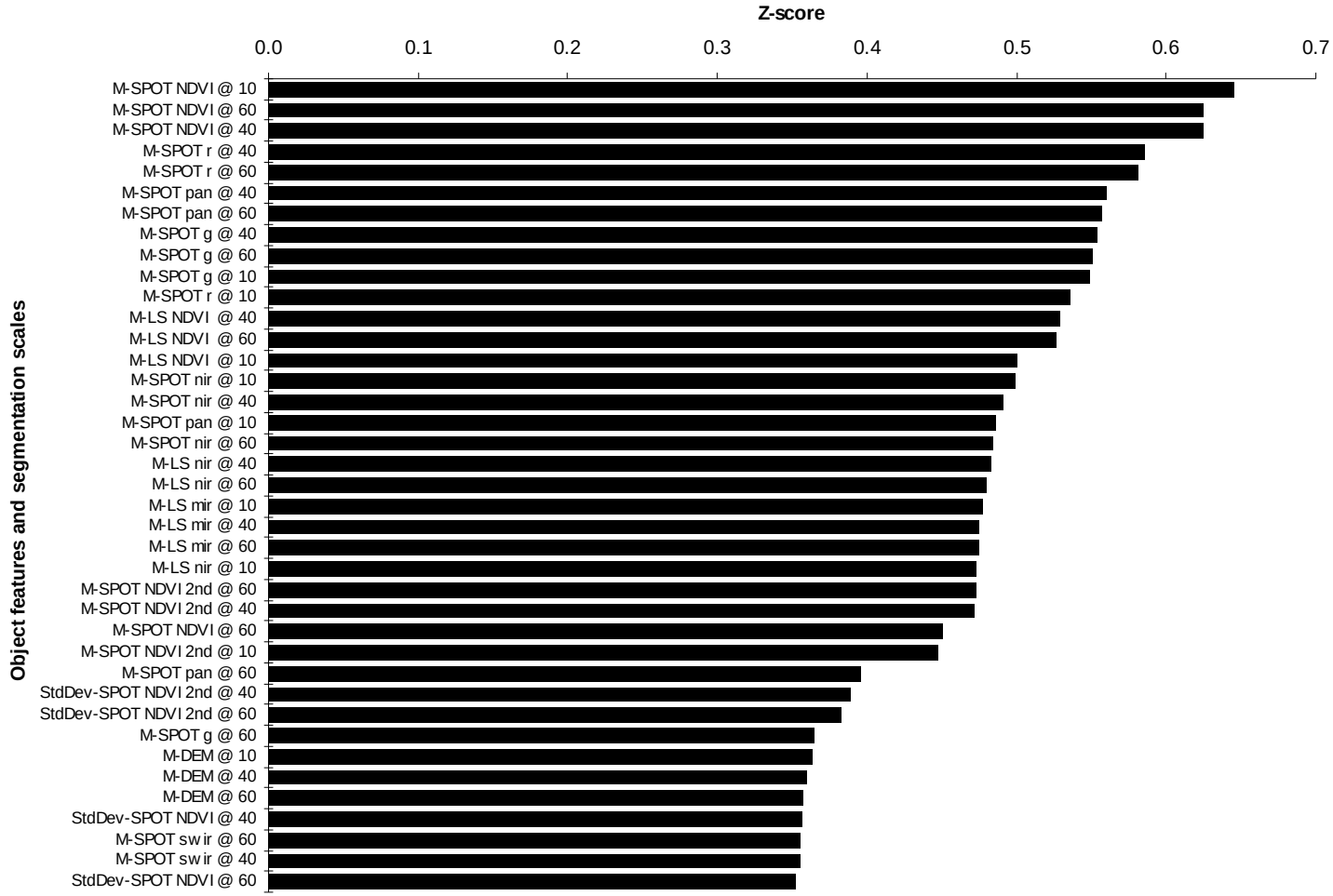

Figure 9: Feature selection results with the top 40 variables (object features) rated by Z-score for the feature reduced "full model" depicted in Figure 10(a). Image segmentation scale is listed after the variable name. Labels prefixed with "M" and "StdDev", refer to object features that calculate the mean and standard deviation of image objects for a particular input layer (see Table 5). The labels "pan", "g", "r", "nir", "nir", "swir", "mir", refer to the panchromatic, green, red, near-infrared, short-wave infrared, and mid-infrared bands, respectively, of SPOT-5 (SPOT) and Landsat-5 (LS) sensors. Variables appended with the suffix label "2nd" represent the angular second order moment texture for that variable.

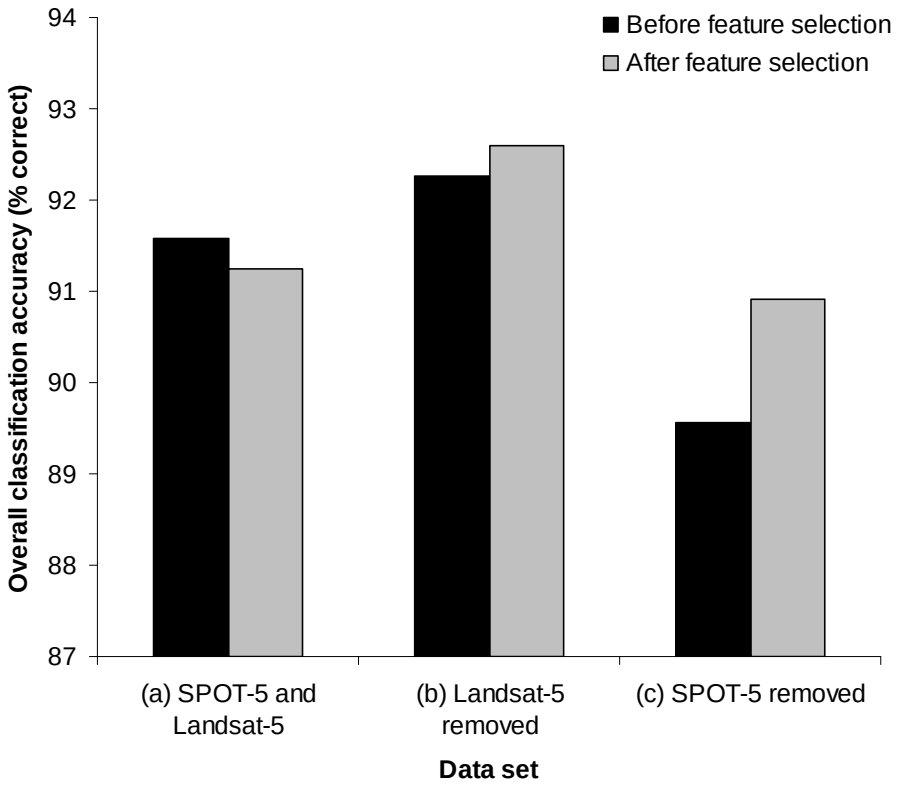

Figure 10: Overall classification accuracy (percentage of predictions correctly classified) before and after feature selection. Results are displayed for classification models that utilize: (a) object features derived from both sensors (i.e., "full data set" model); (b) Landsat-5 multi-spectral based object features removed, and; (c) SPOT-5 multi-spectral based object features removed.

3.4.3 CLASSIFICATION OUTPUT

The classification produced using the feature reduced "full dataset" model, which utilizes multi-spectral and texture information from both satellite sensors, is shown in Figure 11a. Riparian areas appear to be depicted accurately along the banks of the river and within the narrow drainage channels in the northern half of the study area. Errors of commission for riparian land cover are apparent in large rectangular crop fields and along the road found in the southern half of the study area. The narrow drainage channels containing riparian vegetation in the south-western corner of the study area appear to be over represented along ridge lines.

Areas of crop land appear well delineated as rectangular fields, but several errors of omission and commission are visible throughout the image. Commission errors for areas of crop land appear most noticeably in the southern half of the study area where small pockets appear interspersed with riparian and mixed grassland land cover types. Areas of exposed rock/soil appear well delineated in the classified imagery, with narrow road features correctly identified in the northern half of the study area (but not in the south). Recently harvested crop land, or fields left fallow appear bright white and cyan in the false colour composite shown in Figure 11b, and appear well delineated as field-like objects in Figure 11a. Areas of mixed grasslands are depicted reasonably well, although errors of omission are present in the southern half of the study area, where small pockets of concentrated shrubby vegetation (visible in high spatial resolution imagery) are incorrectly classified as riparian vegetation.

A detailed confusion matrix of the classification accuracy of the feature reduced model depicted in Figure 11a is available in Table 8. Based on the percentage of correct predictions, the crop land cover type showed the worst user's and producer's classification accuracy (50 and 63%, respectively). An examination of the confusion matrix reveals that there is a large amount of class confusion between crop land and mixed grassland. All other land cover types achieved user's and producer's accuracy above 83%, with the majority above 88%. The feature-reduced model achieved an overall accuracy of 91.3%, with a lower 95% confidence interval of 87.4%.

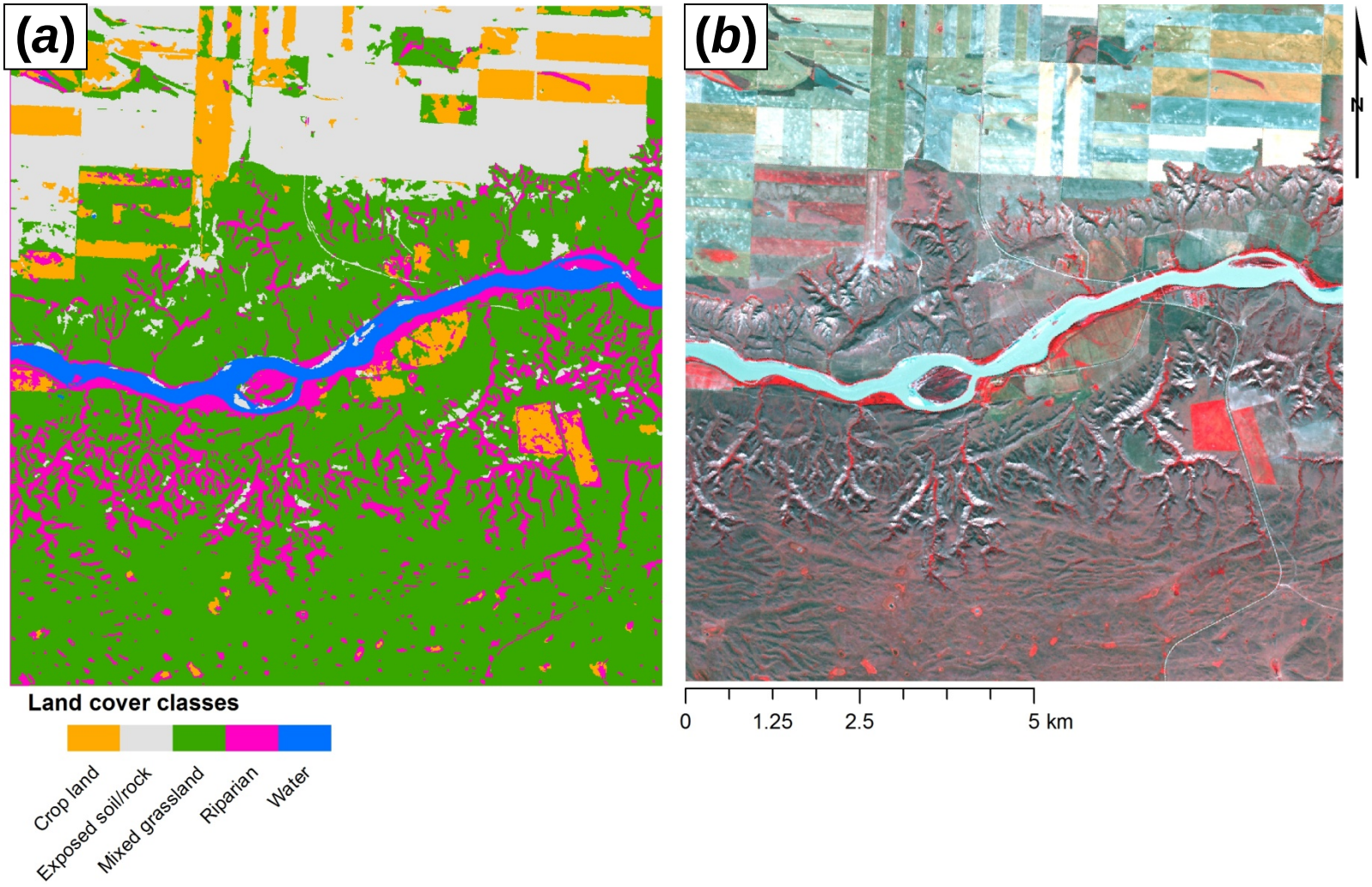

Figure 11: a) Multi-scale, multi-sensor, object-based classification of land cover, and; b) standard false colour composite (R=NIR band, G=Red band, B=Green band) of SPOT-5 multispectral imagery (28 August 2005) for comparison.

Table 8: Confusion matrix (based on reference data) of the feature reduced "full dataset model" (see Figure 11a). Pa = Producer's accuracy; Ua = User's accuracy.

	Predicted Class							
Class	Crop land	Exposed soil/rock	Mixed grasslands	Riparian	Water	**Total**		
Reference Class							Ua	Per-class kappa (Ua)
Crop land	**12**	4	6	2	0	24	50%	0.47
Exposed soil/rock	0	**80**	5	0	0	85	94%	0.92
Mixed grasslands	5	0	**52**	2	0	59	88%	0.85
Riparian	1	0	0	**100**	0	101	99%	0.98
Water	1	0	0	0	**27**	28	96%	0.96
Total	19	84	63	104	27	297		
Pa	63%	95%	83%	96%	100%			
Per-class kappa (Pa)	0.60	0.93	0.78	0.94	1.00			
	Overall accuracy: 91.3% (95% lower and upper confidence limits: 87.4-94.2%)							
	Overall kappa: 0.882 (95% lower and upper confidence limits: 0.838-0.926)							

3.4.4 VARIABLE IMPORTANCE

The top ten variables used to classify four selected land cover types in the feature reduced full-model are displayed in Figure 12. Object-features are ranked by the "Mean Decrease in Accuracy" measure (see Section 3.3.7). All object features listed are based on mean layer values of input variables (see Table 5). The top ten object features for three of the four land cover types are dominated by information derived from the SPOT-5 sensor, with the exception of the crop land cover type, where Landsat-5 based object features were found to be relatively more important than SPOT-5 object features (Figure 12c). Object features based on the SPOT-5 panchromatic input layer are found in the top ten object features listed for all four land cover types, but only at image segmentation scales greater than or equal to 40. Information derived from the SPOT-5 NDVI input layer, and obtained at the two coarsest image segmentation scales (40 and 60), is relatively more important to the classification of mixed grasslands than other object features. Only the riparian land cover type utilized object features based on the angular second moment texture measure, and did so at the finest (10) and coarsest (60) image segmentation scales using the SPOT-5 NDVI input layer (Figure 12a). Except for the mixed grassland land cover type, the relative difference in variable importance between the top 10 object features was relatively small.

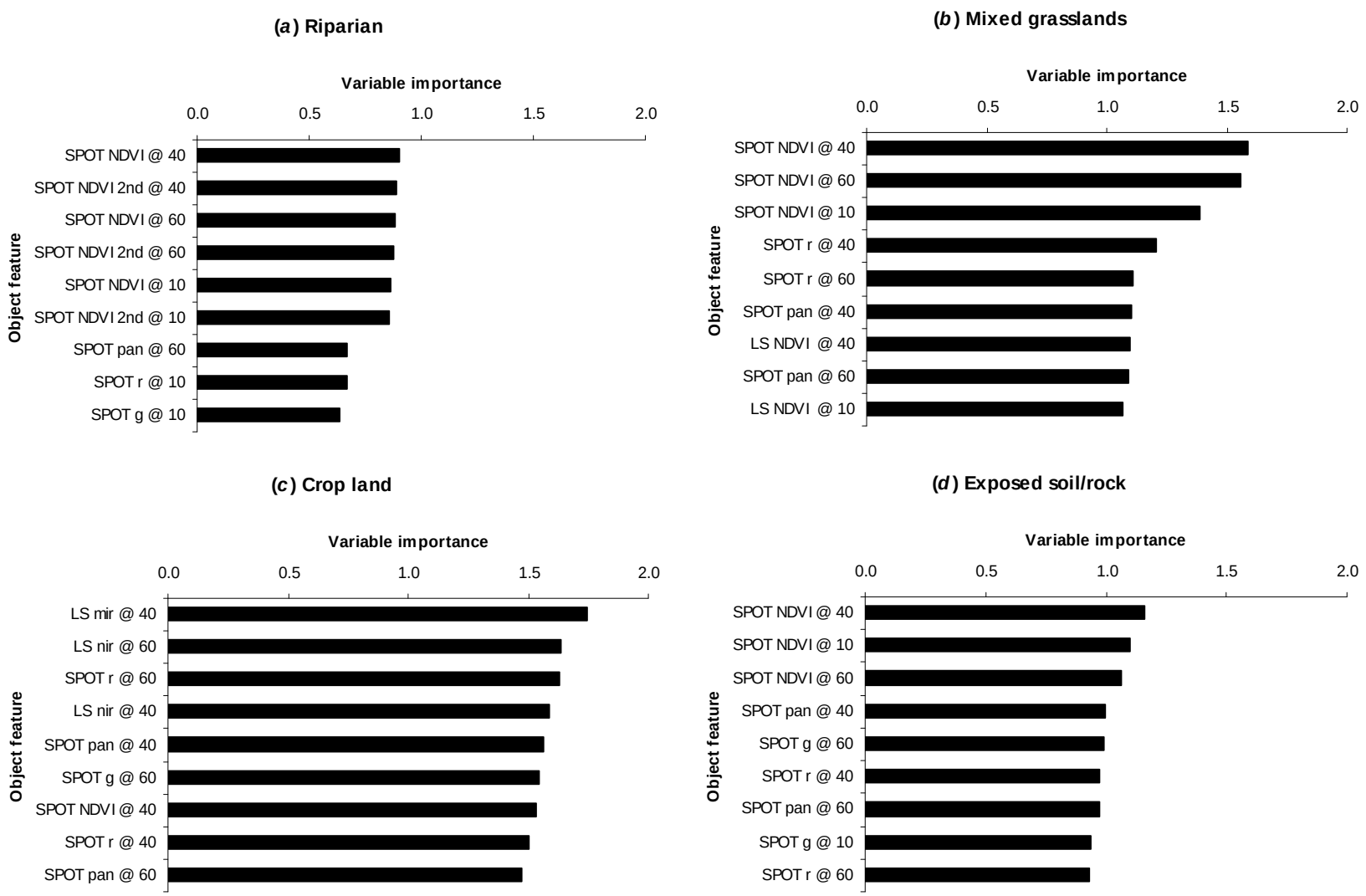

Figure 12: Top ten object features selected by the RF algorithm for classifying four land cover types: a) riparian, b) mixed grassland, c) crop land, and d) exposed soil/rock. The labels "g", "r", "nir", "nir", "swir", "mir", refer to the green, red, near-infrared, short-wave infrared, and mid-infrared bands, respectively, of SPOT-5 (SPOT) and Landsat-5 (LS) sensors. Variables appended with the "2nd" label been calculated using the angular second momen texture measure.

3.5 DISCUSSION

The use of a feature selection algorithm was able to markedly reduce the number of variables used by the RF classifier, while maintaining similar overall classification accuracies. While the reduction in variables resulted in a slight decrease in overall classification accuracy (<0.5%) for classification models that combined both SPOT-5 and Landsat-5 imagery, small increases (<1.5% at most) were noted when using feature reduced models that had Landsat-5 or SPOT-5 multi-spectral information removed (Figure 10). These results suggest that, in terms of overall classification accuracy, the RF classifier was relatively insensitive to the feature selection procedure, which is in agreement with findings made by others (Svetnik et al. 2004). However, the sizeable reduction (30-60%) in "irrelevant" variables allowed for a more tractable interpretation of the final model, with only small differences in overall classification accuracy. From the perspective of conducting MOBIA of EO imagery, where the use of many object features can impede the interpretation of the final classification model, such results reveal a promising avenue for building more parsimonious classification models that maintain overall classification accuracy while increasing model interpretability.

The removal of Landsat-5 multi-spectral bands from the full data set produced slightly higher (at most, 1.5%) overall classification accuracies as compared to the multi-sensor model (Figure 10). Several explanations for this discrepancy are possible, with the most likely related to the image segmentation procedures used in this study. The two finest image segmentation scales (10 and 20) utilized the SPOT-5 NDVI input layer and SPOT-5 panchromatic, while Landsat-5 NDVI input layer was used for the creation of the two coarser image segmentation scales (40 and 60). Larger image segmentation scales were used to produce image objects that were commensurate with the coarser spatial resolution of the Landsat-5 data, as finer image segmentation scales used with the Landsat-5 data produced blocky pixel-like image objects. It is possible that using image objects created by SPOT-5 data at lower image segmentation scales as the basis for image objects created by Landsat-5 data at coarser image segmentation scales may have resulted in image objects that were sub-optimal for the TM based data.

Another potential source of error could be related to the radiometric processing used to normalize the spectral responses between satellite sensors. Image acquisitions from both satellites were within 6 days of each other, which should minimize any differences in vegetation phenology and earth-sun illumination differences between dates. Visual inspection of both sources of imagery did not reveal any noticeable differences in land cover. The off-nadir viewing capability of the SPOT-5 sensor may have confounded the classification accuracy of the multi-sensor model, as sensor view angle is known to influence values obtained when using vegetation indices applied to crop vegetation (Pinter et al. 1987). The higher overall accuracy attributed to the classification model which had the Landsat-5 multi-spectral based information removed may also indicate that the two relatively coarser image segmentation scales were inappropriate; however, the prevalence of these two image segmentation scales in the variable importance plots (Figures 9 and 12) suggest that this is not likely the major source of error. Further refinement of the approach outlined will be necessary to fully understand the relative utility and drawbacks of combining multi-sensor data sets in the MOBIA approach outlined here, as various permutations of image segmentation parameters and input layers are possible.

The classification produced by the feature reduced multi-source, multi-sensor data set provided an acceptable visual depiction of broad land cover classes within the study area. The RF algorithm provided classification accuracies over 91% when using the feature reduced multi-source, multi-sensor data set. Variable importance measures produced by the RF algorithm provided information on which object features and sensor specific information provided relatively more useful information for individual land cover types. In general, the top ten most important variables for each land cover type (Figure 12) revealed a relatively flat response in depicted importance scores (i.e., the top ten object features were relative equal in importance). This finding suggests the possibility that several redundant object features remain, which could be potentially removed through more stringent feature reduction using the Boruta algorithm, and/or a more judicious selection of input variables. Despite the small relative differences in variable importance scores for most land cover type, the mixed grasslands land cover type

(Figure 12b) showed a larger relative difference between the first two object features (based on SPOT-5 NDVI) and the remaining eight object features, with an emphasis on coarse image segmentation scales. Such a result can be potentially explained given the large homogenous areas covered by mixed grasslands within the study area. In other words, due to the relative spectral homogeneity of the mixed grasslands land cover type, object feature information derived at coarser image segmentation scales was relatively more important than the equivalent information at finer image segmentation scales. In contrast, only the riparian land cover type utilized object feature information derived at the finest image segmentation scale (Figure 12a). In addition, only the riparian land cover type utilized the angular second moment texture measure as applied to the SPOT-5 NDVI input variable. These results suggest that areas of riparian vegetation are best described using smaller image objects whose spectral differences contrast their immediate surroundings (e.g., water and exposed soil/rock). Both interpretations fit well with a visual assessment of areas containing riparian vegetation. While these interpretations are only preliminary they serve to illustrate how the variable importance scores produced by the RF algorithm can lead to increased interpretability of classification models produced from MOBIA of EO imagery.

3.6 CONCLUSIONS

In this study, using a MOBIA approach, a classification model based on several hundred object features derived from multiple data sources and two types of EO imagery was created. The feature selection algorithm was able to reduce the size of the datasets examined by up to 60% while still maintaining similar overall classification accuracies. Using the feature reduced multi-source, multi-sensor dataset, the RF classifier achieved an overall classification accuracy greater than 90%. Variable importance measures produced by the RF classifier allowed for the final classification model to be interpreted, providing insight into how image segmentation scales and object features were related to a particular land cover type. Both feature selection and the use of the RF classifier proved useful when conducting MOBIA on EO imagery.

3.7 REFERENCES

ADDINK, E. A., DE JONG, S. M. and PEBESMA, E. J., 2007, The importance of scale in object-based mapping of vegetation parameters with hyperspectral imagery. *Photogrammetric Engineering Remote Sensing,* 73, pp. 905-912.

BAATZ, M. and SCHAPE, A., 2000, Multiresolution segmentation: an optimization approach for high quality multi-scale image segmentation. *Journal of Photogrammetry and Remote Sensing,* 58, pp. 12-23.

BARALDI, A. and PARMIGGIANI, F., 1995, An investigation of the textural characteristics associated with gray level co-occurrence matrix statistical parameters. *IEEE Transactions on Geoscience and Remote Sensing,* 33, pp. 293-304.

BENEDIKTSSON, J. A., SWAIN, P. H. and ERSOY, O. K., 1990, Neural network approaches versus statistical methods in classification of multisource remote sensing data. *IEEE Transactions on Geoscience and Remote Sensing,* 28, pp. 540- 552.

BENZ, U. C., HOFMANN, P., WILLHAUCK, G., LINGENFELDER, I. and HEYNEN, M., 2004, Multi-resolution, object-oriented fuzzy analysis of remote sensing data for GIS-ready information. *ISPRS Journal of Photogrammetry and Remote Sensing*, 58, 239-258.

BLASCHKE, T., 2003, Object-based contextual image classification built on image segmentation. In *2003 IEEE Workshop on Advances in Techniques for Analysis of Remotely Sensed Data,* 27-28 October 2003, Greenbelt, Maryland, pp. 113-119.

BLASCHKE, T., 2010, Object based image analysis for remote sensing. *ISPRS Journal of Photogrammetry and Remote Sensing,* 65, pp. 2-16.

BREIMAN, L., 2001, Random Forests. *Machine Learning,* 45, pp. 5-32.

BREIMAN, L. and CUTLER, A., 2007, Random forests - classification description. Available online at: www.stat.berkeley.edu/~breiman/RandomForests/cc_home.htm (accessed 28 October 2011).

BRUZZONE, L., PRIETO, D. F. and SERPICO, S. B., 1999, A neural-statistical approach to multitemporal and multisource remote-sensing image classification. *IEEE Transactions on Geoscience and Remote Sensing,* 37, pp. 1350-1359.

BURNETT, C. and BLASCHKE, T., 2003, A multi-scale segmentation/object relationship modelling methodology for landscape analysis. *Ecological Modelling,* 168, pp. 233-249.

CASTILLA, G. and HAY, G. J., 2008, Image objects and geographic objects. In *Object-Based Image Analysis*, Blaschke, T., Lang, S. and Hay, G. J. (Eds.), pp. 91-110 (Berlin, Germany: Springer).

CHAN, J. and PAELINCKX, D., 2008, Evaluation of Random Forest and Adaboost tree-based ensemble classification and spectral band selection for ecotope mapping using airborne hyperspectral imagery, *Remote Sensing of Environment,* 112, pp. 2999-3011.

CHANDER, G., MARKHAM, B. L. and HELDER, D. L., 2009, Summary of current radiometric calibration coefficients for Landsat MSS, TM, ETM+, and EO-1 ALI sensors. *Remote Sensing of Environment,* 113, pp. 893-903.

CHEN, D., STOW, D. A. and GONG, P., 2004, Examining the effect of spatial resolution and texture window size on classification accuracy: an urban environment case. *International Journal of Remote Sensing,* 25, pp. 2177-2192.

CHEN, F., WEBER, K. T., ANDERSON, J. and GOKHAL, B., 2011, Assessing the susceptibility of semiarid rangelands to wildfires using Terra MODIS and Landsat Thematic Mapper data. *International Journal of Wildland Fire,* 20, pp. 690-701.

CLARK, B., SUOMALAINEN, J. and PELLIKKA, P., 2011, The selection of appropriate spectrally bright pseudo-invariant ground targets for use in empirical line calibration of SPOT satellite imagery. *ISPRS Journal of Photogrammetry and Remote Sensing*, 66, pp. 429-445.

COLLINGWOOD, A., FRANKLIN, S. E., GUO, X. and STENHOUSE, G., 2009, A medium-resolution remote sensing classification of agricultural areas in Alberta grizzly bear habitat. *Canadian Journal of Remote Sensing,* 35, pp. 23-36.

CONGALTON, R. G., 1991, A review of assessing the accuracy of classifications of remotely sensed data. *Remote Sensing of Environment,* 37, pp. 35-46.

CONRAD, C., FRITSCH, S., ZEIDLER, J., RÜCKER, G. and DECH, S., 2010, Per-field irrigated crop classification in arid central asia using SPOT and ASTER data. *Remote Sensing,* 2, pp. 1035-1056.

COSTA, G. A. O. P., FEITOSA, R. Q., CAZES, T. B. and FEIJÓ, B., 2008, Genetic adaptation of segmentation parameters. In *Object-Based Image Analysis*, Blaschke, T., Lang, S. and Hay, G. J. (Eds.), pp. 679-695 (Berlin, Germany: Springer).

DINGLE ROBERTSON, L. and KING, D. J., 2011, Comparison of pixel- and object-based classification in land cover change mapping. *International Journal of Remote Sensing,* 32, pp. 1505-1529.

DORAISWAMY, P. C., STERN, A. J. and COOK, P. W., 1998, Classification techniques for mapping biophysical parameters in the US southern Great Plains. In *Proceedings of the 1998 International Geoscience and Remote Sensing Symposium,* 6-10 July 1998, Seattle, Washington, pp. 862-866.

DYE, M., MUTANGA, O. and ISMAIL, R., 2011, Examining the utility of random forest and AISA Eagle hyperspectral image data to predict Pinus patula age in KwaZulu-Natal, South Africa. *Geocarto International,* 26, pp. 275-289.

FISHER, P., 1997, The pixel: a snare and a delusion. *International Journal of Remote Sensing,* 18, pp. 679-685.

FORGHANI, A., CECHET, B. and NADIMPALLI, K., 2007, Object-based classification of multi-sensor optical imagery to generate terrain surface roughness information for input to wind risk simulation. In *Proceedings of the 2007 International Geoscience and Remote Sensing Symposium,* 23-28 July 2007, Barcelona, Spain, pp. 3090-3095.

FRANKLIN, J., 1995, Predictive vegetation mapping: geographic modelling of biospatial patterns in relation to environmental gradients. *Progress in Physical Geography,* 19, pp. 474 -499.

FRANKLIN, S. E., 1987, Geomorphometric processing of digital elevation models. *Computers and Geosciences,* 13, pp. 603-609.

FRANKLIN, S. E. and GILES, P. T., 1995, Radiometric processing of aerial and satellite remote-sensing imagery. *Computers and Geosciences,* 21, pp. 413-423.

FRANKLIN, S. E. and WULDER, M. A., 2002, Remote sensing methods in medium spatial resolution satellite data land cover classification of large areas. *Progress in Physical Geography,* 26, pp. 173 -205.

FROHN, R. C., AUTREY, B. C., LANE, C. R. and REIF, M., 2011, Segmentation and object-oriented classification of wetlands in a karst Florida landscape using multi-season Landsat-7 ETM+ imagery. *International Journal of Remote Sensing,* 32, pp. 1471-1489.

GENUER, R., POGGI, J.M. and TULEAU-MALOT, C., 2010, Variable selection using random forests. *Pattern Recognition Letters,* 31, pp. 2225-2236.

GHIMIRE, B., ROGAN, J. and MILLER, J., 2010, Contextual land-cover classification: incorporating spatial dependence in land-cover classification models using random forests and the Getis statistic. *Remote Sensing Letters,* 1, pp. 45-54.

GISLASON, P. O., BENEDIKTSSON, J. A. and SVEINSSON, J. R., 2006, Random Forests for land cover classification. *Pattern Recognition Letters,* 27, pp. 294-300.

GONG, P., 1996, Integrated analysis of spatial data from multiple sources: Using evidential reasoning and artificial neural network techniques for geological mapping. *Photogrammetric Engineering and Remote Sensing,* 62, pp. 513-523.

GRIFFITH, J. A., MARTINKO, E. A., WHISTLER, J. L. and PRICE, K. P., 2002, Interrelationships among landscapes, NDVI, and stream water quality in the US central plains. *Ecological Applications,* 12, pp. 1702-1718.

GUYON, I. and ELISSEEFF, A., 2003, An introduction to variable and feature selection. *Journal of Machine Learning Research,* 3, pp. 1157-1182.

HARALICK, R. M., SHANMUGAM, K. and DINSTEIN, I., 1973, Textural Features for Image Classification. *IEEE Transactions on Systems, Man and Cybernetics,* 3, pp. 610-621.

HAY, G. J., DUBÉ, P., BOUCHARD, A. and MARCEAU, D. J., 2002, A scale-space primer for exploring and quantifying complex landscapes. *Ecological Modelling,* 153, pp. 27-49.

HILL, M. J. and DONALD, G. E., 2003, Estimating spatio-temporal patterns of agricultural productivity in fragmented landscapes using AVHRR NDVI time series. *Remote Sensing of Environment,* 84, pp. 367-384.

SMAIL, R. and MUTANGA, O., 2011, Discriminating the early stages of Sirex noctilio infestation using classification tree ensembles and shortwave infrared bands. *International Journal of Remote Sensing,* 32, pp. 4249-4266.

KIM, M., MADDEN, M. and WARNER, T., 2008, Estimation of optimal image object size for the segmentation of forest stands with multispectral IKONOS imagery. In *Object-Based Image Analysis*, Blaschke, T., Lang, S. and Hay, G. J. (Eds.), pp. 293-307 (Berlin, Germany: Springer).

KIM, M., WARNER, T., MADDEN, M. and ATKINSON, D., 2011, Multi-scale GEOBIA with very high spatial resolution digital aerial imagery: scale, texture and image objects. *International Journal of Remote Sensing,* 32, pp. 2825-2850.

KOHAVI, R. and JOHN, G. H., 1997, Wrappers for feature subset selection. *Artificial Intelligence,* 97, pp. 273-324.

KURSA, M. B. and RUDNICKI, W. R., 2010, Feature selection with the Boruta Package. *Journal Of Statistical Software,* 36, pp. 1-13.

LALIBERTE, A. S., FREDRICKSON, E. L. and RANGO, A., 2007, Combining decision trees with hierarchical object-oriented image analysis for mapping arid rangelands. *Photogrammetric Engineering and Remote Sensing,* 73, pp. 197-207.

LALIBERTE, A., KOPPA, J., FREDRICKSON, E. and RANGO, A., 2006, Comparison of nearest neighbor and rule-based decision tree classification in an object-oriented environment. In *Proceedings of the 2006 International Geoscience and Remote Sensing Symposium,* 31 July - 4 August 2006, Denver, Colorado, pp. 3923-3926.

LANG, S., 2008, Object-based image analysis for remote sensing applications: modeling reality – dealing with complexity. In *Object-Based Image Analysis*, Blaschke, T., Lang, S. and Hay, G. J. (Eds.), pp. 3-27 (Berlin, Germany: Springer).

LEIBOVICI, D. G. and JACKSON, M., 2011, Multi-scale integration for spatio-temporal ecoregioning delineation. *International Journal of Image and Data Fusion,* 2, pp. 105-119.

LIAW, A. and WIENER, M., 2002, Classification and Regression by randomForest. *R News,* 2, pp.18-22.

LIPPITT, C. D., COULTER, L. L., FREEMAN, M., LAMANTIA-BISHOP, J., PANG, W. and STOW, D. A., 2012, The effect of input data transformations on object-based image analysis. *Remote Sensing Letters,* 3, pp. 21-29.

LIU, D. and XIA, F., 2010, Assessing object-based classification: advantages and limitations. *Remote Sensing Letters,* 1, pp. 187-194.

LU, D. and WENG, Q., 2007, A survey of image classification methods and techniques for improving classification performance. *International Journal of Remote Sensing,* 28, pp. 823-870.

MACLIN, R. and OPITZ, D., 1999, Popular Ensemble Methods: An Empirical Study. *Journal Of Artificial Intelligence Research,* 11, pp. 169-198.

MALLINIS, G., KOUTSIAS, N., TSAKIRI-STRATI, M. and KARTERIS, M., 2008, Object-based classification using Quickbird imagery for delineating forest vegetation polygons in a Mediterranean test site. *ISPRS Journal of Photogrammetry and Remote Sensing,* 63, pp. 237-250.

MATHIEU, R., ARYAL, J. and CHONG, A. K., 2007, Object-based classification of Ikonos imagery for mapping large-scale vegetation communities in urban areas. *Sensors,* 7, pp. 2860-2880.

MEINEL, G. and NEUBERT, M., 2004, A comparison of segmentation programs for high resolution remote sensing data. In *International Archives of the ISPRS*, 35, 2004, pp. 1097-1105.

MELGANI, F. and BRUZZONE, L., 2004, Classification of hyperspectral remote sensing images with support vector machines. *IEEE Transactions on Geoscience and Remote Sensing,* 42, pp. 1778-1790.

MILLER, J. and FRANKLIN, J., 2002, Modeling the distribution of four vegetation alliances using generalized linear models and classification trees with spatial dependence. *Ecological Modelling,* 157, pp. 227-247.

MOORE, I. D., GRAYSON, R. B. and LADSON, A. R., 1991, Digital terrain modelling: A review of hydrological, geomorphological, and biological applications. *Hydrological Processes,* 5, pp. 3-30.

MYINT, S. W., GOBER, P., BRAZEL, A., GROSSMAN-CLARKE, S. and WENG, Q., 2011, Per-pixel vs. object-based classification of urban land cover extraction using high spatial resolution imagery. *Remote Sensing of Environment,* 115, pp. 1145-1161.

NA, X., ZHANG, S., LI, X., YU, H. and LIU, C., 2010, Improved land cover mapping using random forests combined with Landsat Thematic Mapper imagery and ancillary geographic data. *Photogrammetric Engineering and Remote Sensing,* 76, pp. 833-840.

NILSSON, R., PENA, J. M., BJORKEGREN, J. and TEGNER, J., 2007, Consistent feature selection for pattern recognition in polynomial time. *Journal of Machine Learning Research,* 8, pp. 589-612.

OTUKEI, J. R. and BLASCHKE, T., 2010, Land cover change assessment using decision trees, support vector machines and maximum likelihood classification algorithms. *International Journal of Applied Earth Observation and Geoinformation,* 12, pp. S27-S31.

PAL, M., 2005, Random forest classifier for remote sensing classification. *International Journal of Remote Sensing,* 26, pp. 217-222.

PEÑA-BARRAGÁN, J. M., NGUGI, M. K., PLANT, R. E. and SIX, J., 2011, Object-based crop identification using multiple vegetation indices, textural features and crop phenology. *Remote Sensing of Environment,* 115, pp.1301-1316.

PETERS, J., BAETS, B. D., VERHOEST, N. E. C., SAMSON, R., DEGROEVE, S., BECKER, P. D. and HUYBRECHTS, W., 2007, Random forests as a tool for ecohydrological distribution modelling. *Ecological Modelling,* 207, pp. 304-318.

PIKE, R. J., 2000, Geomorphometry -diversity in quantitative surface analysis. *Progress in Physical Geography,* 24, pp. 1 -20.

PINTER, P. J., ZIPOLI, G., MARACCHI, G. and REGINATO, R. J., 1987, Influence of topography and sensor view angles on NIR/red ratio and greenness vegetation indices of wheat. *International Journal of Remote Sensing,* 8, pp. 953-957.

PLATT, R. V. and RAPOZA, L., 2008, An evaluation of an object-oriented paradigm for land use/land cover classification. *The Professional Geographer,* 60, pp. 87.

POWELL, S. L., PFLUGMACHER, D., KIRSCHBAUM, A. A., KIM, Y. and COHEN, W. B., 2007, Moderate resolution remote sensing alternatives: a review of Landsat-like sensors and their applications. *Journal of Applied Remote Sensing,* 1, p. 012506.

PRASAD, A. M., IVERSON, L. R. and LIAW, A., 2006, Newer classification and regression tree techniques: bagging and random forests for ecological prediction. *Ecosystems,* 9, pp.181-199.

PRICE, K. P., EGBERT, S. L., NELLIS, M. D., LEE, R.-Y. and BOYCE, R., 1997, mapping land vover in a High Plains agro-ecosystem using a multidate Landsat Thematic Mapper modeling approach. *Transactions of the Kansas Academy of Science (1903-),* 100, pp. 21-33.

PU, R., LANDRY, S. and YU, Q., 2011, Object-based urban detailed land cover classification with high spatial resolution IKONOS imagery. *International Journal of Remote Sensing,* 32, pp. 3285-3308.

R DEVELOPMENT CORE TEAM., 2010, R: A Language and Environment for Statistical Computing. Vienna, Austria. Available online at: www.r-project.org (accessed 28 October 2011).

ROUSE, J., HAAS, R., SCHELL, J. and DEERING, D., 1973, Monitoring vegetation systems in the Great Plains with ERTS. In *Proceedings of the Third ERTS Symposium*, Vol.1, December 1973, Washington, DC (NASA), p. 309-317.

SCHINDLER, D. W., 2001, The cumulative effects of climate warming and other human stresses on Canadian freshwaters in the new millennium. *Canadian Journal of Fisheries and Aquatic Science,* 58, pp. 18-29.

SCHINDLER, D. W. and DONAHUE, W. F., 2006, An impending water crisis in Canada's western prairie provinces. *Proceedings of the National Academy of Sciences of the United States of America,* 103, 7210-7216.

SCHOTT, J. R., SALVAGGIO, C. and VOLCHOK, W. J., 1988, Radiometric scene normalization using pseudoinvariant features. *Remote Sensing of Environment,* 26, pp. 1-14.

SESNIE, S. E., GESSLER, P. E., FINEGAN, B. and THESSLER, S., 2008, Integrating Landsat TM and SRTM-DEM derived variables with decision trees for habitat classification and change

detection in complex neotropical environments. *Remote Sensing of Environment,* 112, pp. 2145-2159.

SMITH, A., 2010, Image segmentation scale parameter optimization and land cover classification using the Random Forest algorithm. *Journal of Spatial Science,* 55, pp. 69-79.

STRAHLER, A. H., WOODCOCK, C. E. and SMITH, J. A., 1986, On the nature of models in remote sensing. *Remote Sensing of Environment,* 20, pp. 121-139.

TOWNSHEND, J. R. G., HUANG, C., KALLURI, S. N. V., DEFRIES, R. S., LIANG, S. and YANG, K., 2000, Beware of per-pixel characterization of land cover. *International Journal of Remote Sensing,* 21, pp. 839-843.

TRIMBLE, 2010a, eCognition® Developer 8.64.0 User Guide.

TRIMBLE, 2010b, eCognition® Developer 8.64.0 Reference Book.

WANG, K., FRANKLIN, S. E., GUO, X., COLLINGWOOD, A., STENHOUSE, G. B. and LOWE, S., 2010, Comparison of Landsat multispectral and IRS panchromatic imagery for landscape pattern analysis of grizzly bear habitat in agricultural areas of western Alberta. *Canadian Journal of Remote Sensing,* 36, pp. 36-47.

WARDLOW, B. D., 2008, Large-area crop mapping using time-series MODIS 250 m NDVI data: An assessment for the U.S. Central Great Plains. *Remote Sensing of Environment,* 112, pp. 1096-1116.

WATTS, J. D., LAWRENCE, R. L., MILLER, P. R. and MONTAGNE, C., 2009, Monitoring of cropland practices for carbon sequestration purposes in north central Montana by Landsat remote sensing. *Remote Sensing of Environment,* 113, pp. 1843-1852.

YAN, G., MAS, MAATHUIS, B., XIANGMIN, Z. and VAN DIJK, P., 2006, Comparison of pixel-based and object-oriented image classification approaches—a case study in a coal fire area, Wuda, Inner Mongolia, China. *International Journal of Remote Sensing,* 27, pp. 4039-4055.

YANG, C., EVERITT, J. H. and BRADFORD, J. M., 2009, Evaluating high resolution SPOT 5 satellite imagery to estimate crop yield. *Precision Agriculture,* 10, pp. 292-303.

YU, Q., GONG, P., CLINTON, N., BIGING, G., KELLY, M. and SCHIROKAUER, D., 2006, Object-based detailed vegetation classification with airborne high spatial resolution remote sensing imagery. *Photogrammetric Engineering and Remote Sensing,* 72, pp. 799-811.

CHAPTER 4 PREFACE

Previous chapters presented background information and detailed rationale for selecting a particular image analysis approach (object-based) and classification algorithm (Random Forests), which were used to create land cover maps over selected sites within a larger study area. In this chapter, the focus shifts towards examining several change detection methods that utilize remotely sensed imagery. These change detection methods are compared to determine which approach achieves the best change detection results, and which is best suited to handling multiple sources of remotely sensed imagery. As in Chapter 2, the results of the comparison are assessed using a variety of statistical and visual assessments.

CHAPTER 4

A HYBRID OBJECT-BASED CHANGE DETECTION METHOD FOR USE WITH MULTI-SENSOR DATASETS IN HISTORICAL LANDSCAPE RECONSTRUCTION[‡]

[‡] Submitted to *Photogrammetric Engineering & Remote Sensing* on November 24, 2011. "Conditionally accepted" on March 3, 2012. Currently in revision at the time of submission to the College of Graduate Studies and Research with the following citation:

DURO, D.C., FRANKLIN, S.E., DUBÉ, M.G. (In revision). A hybrid object-based change detection method for use with multi-sensor datasets in historical landscape reconstruction. *Photogrammetric Engineering & Remote Sensing.*

All work reported in this chapter, including the review of the literature, theoretical and experimental design, analysis and discussion of the results, and writing of the text, was carried out by the Ph.D. candidate. As supervisor, Dr. S.E. Franklin reviewed all parts of the work. Dr. M.G. Dubé was involved in early conceptual design.

4.1 ABSTRACT

A hybrid object-based change detection method utilizing cross-correlation analysis (CCA) and a hierarchical image object segmentation strategy is introduced for the analysis of agricultural land cover change using medium spatial resolution satellite imagery. The performance of the proposed CCA method achieved an overall change detection accuracy of 73.14%, which was marginally less than the accuracy achieved using two non-CCA methods (74.64 and 74.86%). Differences between classification accuracies achieved by non-CCA methods were not statistically significant ($p>0.05$), but were significant between the hybrid object-based CCA method and non-CCA methods examined ($p<0.05$). Despite lower overall accuracy, the hybrid object-based CCA change detection method achieved errors of commission for changed areas that were approximately 10% better than non-CCA methods, and produced results that more effectively reflected the visual appearance of the reference change map.

4.2 INTRODUCTION

The combination of historical maps, aerial photographs, and satellite-based earth observation (EO) imagery has been used recently to map changes in historical land use and land cover (LULC) in a variety of environments. Such historical LULC information is increasingly valuable in agricultural areas as anthropogenic change has been linked to large alterations in global carbon, water, and nitrogen cycles (Houghton 1995; Postel et al. 1996; Vitousek et al. 1997), and is an essential component to understanding how human demographics and socioeconomic decisions relate to local and global environmental impacts (Liverman 1998; Entwisle and Stern 2005; Lambin and Geist 2006). Detailed LULC maps over long time horizons are required to better understand the magnitude and trajectory of LULC change caused by humans on local and global scales (Petit and Lambin 2002). Key to this goal is the ability to readily detect change on the landscape considered significant for a particular application.

Various methods developed to detect land use and land cover (LULC) change have been described (see Singh 1989; Coppin et al. 2004; Lu et al. 2004; Rogan and Chen 2004; Treitz and Rogan 2004), and are typically divided into two general approaches: i) multi-temporal analysis of spectral data, and ii) post-classification analyses. In the former approach, spectral information extracted from two or more dates of imagery is compared in order to identify a change in LULC. In the simplest bi-temporal case of assessing spectral change over time, thresholds are established using manual and/or statistical based methods, to determine the point at which recorded spectral differences represent meaningful LULC change. This change detection strategy generally requires that images undergo some level of radiometric processing to maintain comparability between spectral information, which may exhibit differences due to atmospheric and phenological conditions, as well as differences in sensor calibration and radiance values caused by differing earth-sun-sensor geometry between acquisition dates (Chander et al. 2009). In contrast, post-classification change detection methods rely on summarizing differences in land cover change labels that have been derived from independently classified images from two or more dates. This approach allows for a detailed account of land cover classes and their changed state to be assessed over time, generally avoids the need to perform radiometric processing required by multispectral change detection strategies, and can be readily used to compare classified imagery obtained from sensors with similar characteristics (e.g., Landsat Thematic Mapper and Enhanced Thematic Mapper Plus) when comparable land cover classes are used.

Several examples of multi-temporal analysis of object-based spectral information have emerged in recent years: in one early study, Desclée et al. (2006) utilized a statistical approach ("multivariate iterative trimming") to assess whether spectral differences in between image objects derived from medium resolution SPOT (Système Pour d'Observation de la Terre) imagery of forested environments were statistical outliers, and therefore more likely to represent real land cover change. The obvious appeal of such an approach, as compared to qualitative visual examinations, is that change thresholds are based on probability distributions

which can produce statistically rigorous and comparable results when parametric assumptions are met.

In a similar statistically driven approach, Im et al. (2008) compared image objects segmented from multi-date imagery in order to create and assess correlation, slope, and intercept information in urban and suburban environments with high spatial resolution imagery (Quickbird). Changes in the magnitude and direction of multispectral information contained within image objects (created with and without neighborhood correlation information) were statistically assessed, with significant differences indicating unique change information in the form of a lower correlation coefficient, or varying slope and intercept (Im and Jensen 2005). While they found object-based approaches produced higher overall change detection accuracies than per-pixel based classifications, Im et al. (2008) found few statistical differences between image analysis approaches when conditions were held constant.

Using high spatial resolution imagery in a built environment, Niemeyer et al. (2008) applied the Iteratively Reweighted Multivariate Alteration Detection (IR-MAD) transformation (Nielsen 2007; Canty and Nielsen 2011) as an underlying analytical approach for object-based change detection. Such an approach provides a robust statistical change detection method as MAD components are invariant under affine transformation of the original data, and theoretically can be applied to multi-sensor datasets (Canty 2010). Using bi-temporal pan-sharpened Quickbird imagery segmented at three different scale parameters, a combination of four multispectral bands and shape information (e.g., border index, roundness, compactness, etc.) were subjected to the IR-MAD transformation, followed by an unsupervised cluster analysis using fuzzy maximum likelihood estimation (FMLE) and label relaxation to identify potential areas of change within the MAD components (Niemeyer et al. 2008). Using this approach, the authors were able to detect and classify several types of change related to construction activities underway in a nuclear facility over the course of a year.

Post-classification of EO imagery classified using object-based image analysis has also been used for change detection purposes. Ruelland et al. (2011) compared pixel-based and object-based image analysis using a post-classification change detection strategy for mapping

LULC change in the Sahel region of Africa using multi-sensor datasets over a 50 year time period. Aerial photographs and EO imagery from the Corona "spy-satellite" program, Landsat, and SPOT platforms were independently classified and used to track and quantify historical LULC change in a 100 km^2 watershed (cf. Franklin et al. 2005) using a post-classification analysis strategy. Ruelland et al (2011) found that the manual digitization of landscape features provided the highest overall classification accuracies (over 0.915 Kappa) over three dates of imagery, with pixel-based and object-based image analysis also producing relatively high accuracies (0.841-0.976 Kappa). Overall proportions of land cover between approaches were relative consistent over time, but could vary by as much as 10% for some land cover classes (Ruelland et al. 2011).

In another recent example of object-based change detection using post-classification analysis, Robertson and King (2011) assessed land cover change between two image dates in an agricultural environment using medium resolution Landsat data. They found no statistically significant differences in classification accuracies of land cover between image analysis approaches; however, based on an intensive visual comparison, they found that object-based image analysis produced more accurate representations of landscape change as compared to pixel-based maps.

Hybrid approaches to change detection that integrate elements of both multispectral change detection and post-classification analysis have also been developed. One such approach is based on an initial formulation of “cross-correlation analysis” (CCA) (Koeln and Bissonnette (2000) that uses existing land cover maps to ‘guide’ the process (Note: CCA should not to be confused with canonical correspondence analysis). In this hybrid approach, land cover boundaries delineated based on an existing map are used as the basis for collecting spectral information specific to each land cover class. The CCA is then performed using a multivariate calculation of class-specific information to assess which areas within a given land cover type exhibit change in the updated imagery. As spectral information is drawn from the imagery used to update the map there is less need to perform complex radiometric or atmospheric corrections (Koeln and Bissonnette 2000); however, the accuracy of the initial classification or

GIS-based map is important as these land cover boundaries are used to derive spectral class information used in the CCA calculation.

4.2.1 CHALLENGES TO OBJECT-BASED MAP UPDATING AND CHANGE DETECTION WITH MULTI-SOURCE IMAGERY

The above examples illustrate several promising object-based change detection methods and have helped clarify important issues identified with map updating strategies that incorporate object-based image analysis. For example, McDermid et al. (2008) illustrated the impact of "sliver" objects, which are small and potentially spurious elements of change, created by the inconsistent delineation of boundaries between change objects and image objects within an existing base map. Despite representing a relatively small percentage of the overall changed area, the presence of sliver objects was shown to have significant impacts on the magnitude and trajectory of four common landscape metrics (number of patches, edge density, mean patch size, and mean shape index) when examined over a series of updated thematic maps representing 'annual-change' (Linke et al. 2009). Efforts to mitigate or eliminate issues related to sliver objects led to the formulation of a comprehensive methodological framework whereby a GIS-based system is used to maintain an inventory of disturbance features suitable for producing consistent object-based thematic maps over time (Linke and McDermid 2011). However, the implementation of this change detection framework requires significant effort and is recommended in situations where the overall goals of the mapping process demands that updating strategies minimize such artifacts (e.g., when calculating landscape metrics over time).

Most of the examples of object-based change detection listed here utilize the same or similar sources of imagery between acquisition dates (e.g., Landsat Thematic Mapper and Enhanced Thematic Mapper Plus); however, several issues have been identified when post-classification analysis is conducted on maps derived from sensors with substantially different

characteristics. For example, differing pixel sizes can lead to certain land cover elements being detected by one sensor, but not another. In addition, complications typically arise from misregistration of imagery with different spatial resolutions. And finally, differences in the spectral and radiometric resolutions of the sensors being compared must be managed in the change detection and mapping process (Serra et al. 2003). Such issues are not limited to post-classification analysis of land cover change, but also affect change detection strategies that rely on multi-temporal analysis of spectral change. Resampling procedures have been suggested as a means of minimizing differences between disparate sources of EO imagery by placing imagery into a common (lowest) spatial resolution (Petit and Lambin 2001). In one example, such procedures created mixed results when comparing overall classification accuracies using post-classification analysis of land cover change obtained using several different sources of imagery over time (Ruelland et al. 2011). Change detection methods that utilize multiple sources of EO imagery will become increasingly important to overcome limitations inherent to a single source; therefore, more research focused on integrating GIS and multiple sources of imagery for change detection analysis has been suggested (Lu et al. 2004).

4.2.2 AN OBJECT-BASED HYBRID CHANGE DETECTION APPROACH

In the present study, a method for change detection and map updating is introduced using an object-based hybrid change detection approach suitable for integrating multi-sensor datasets acquired over long time periods. The goal is to enable object-based change detection that allows for disparate sources of EO imagery to be used with few 'map' related problems that would otherwise reduce the effectiveness of the update products. Specifically, two advancements are integrated into the proposed object-based hybrid change detection approach to address the aforementioned challenges:

1) The CCA change detection method described by Koeln and Bissonnette (2000), and subsequently used in later studies (Hurd et al. 2001; Civco et al. 2002), is adapted for use in an object-based image analysis environment. This hybrid change detection

approach allows for disparate sources of imagery to be utilized with a minimum of radiometric processing by using per class spectral information obtained from update imagery using existing land cover boundaries from a base map. Furthermore, unlike many multi-spectral change detection methods, the use of CCA approach contains significant promise because of the ability to fine-tune the degree of change detected on a per land cover class basis, allowing for a higher degree of confidence that the change detected is of significance in the study area under investigation.

2) While previous change detection and LULC mapping over long time periods have utilized object-based image analysis to classify disparate sources of imagery, such studies have relied on post-classification analysis of independently classified imagery (e.g., Ruelland et al. 2011). In the present study, in order to minimize compounding classification errors between entire maps that have been classified independently, only areas labeled as change are updated in the base map. Such an approach has been advocated for operational settings where a consistent time series of LULC is desired (e.g., Feranec et al. 2000; Feranec et al. 2007; McDermid et al. 2008; Linke et al. 2009). In this study, this updating procedure is accomplished through the use of "hierarchical object networks" (Benz et al. 2004), whereby existing object boundaries are used as the basis for subsequent image object segmentation. Such an approach has been used in previous object-based change detection studies (e.g., Willhauck 2000; Walter 2004), as a means of integrating multiple sources of information (e.g., an existing thematic map), while maintaining consistent boundaries for image objects of interest between map updates.

4.2.3 OBJECTIVES OF THIS STUDY

This study implements an object-based hybrid change detection approach based on CCA (Koeln and Bissonnette 2000) in conjunction with a hierarchical image segmentation strategy (Benz et al. 2004) to enforce image object boundaries between map updates derived from multiple sources of EO imagery and an existing base map. The goal is to illustrate the enhanced

change detection capability and map updating versatility of such an approach. In order to accomplish this, we compare the performance of the proposed object-based hybrid change detection method with other object-based methods that have recently been recommended in land cover change applications.

4.3 METHODS

4.3.1 STUDY AREA

The change detection methods considered in this study were tested over an area undergoing intensive agricultural development in southwest Saskatchewan in western Canada; 51.751N, -109.408W). Figure 13 depicts several types of land cover change typical of land undergoing agricultural development. In addition, other forms of anthropogenic landscape change (e.g., oil and gas development) and natural events (e.g., periodic flooding of crop lands) are present. Crop reports coinciding with the acquisition date of the 2005 SPOT-5 multispectral imagery indicate significant rainfall in the area (Saskatchewan Agriculture and Food 2005). This change in the appearance of the imagery is evident in the large areas of inundated crop land (Figure 13).

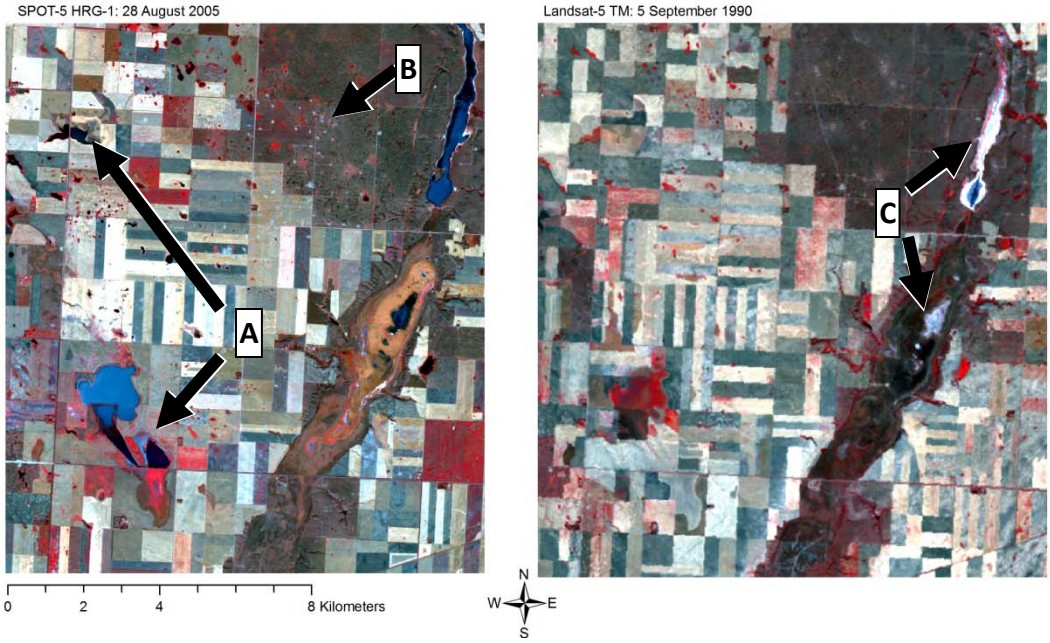

Figure 13: A) areas of crop land inundated in 2005, but either in-filled and/or experiencing dry conditions in 1990; B) well pads and support roads in 2005, but missing in 1990; C) change in water level for two small natural drainage areas. SPOT-5 HRG and Landsat-5 TM imagery presented as a false color composite (Red=XS3, Green=XS2, Blue=XS1, and; Red=Band 4, Green=Band 3, Blue=Band 2, respectively).

4.3.2 SATELLITE-BASED EO IMAGERY AND INITIAL PROCESSING

Two sources of multi-spectral EO imagery were used to perform object-based change detection based on the selected comparison of methods: SPOT-5 10 m High Resolution Geometric (HRG-1) imagery for the base time period (28 August 2005) and Landsat-5 30 m Thematic Mapper (TM) imagery for the retrospective time period (5 September 1990). While not necessary for CCA change detection method (Koeln and Bissonnette 2000), these satellite images were converted to exoatmospheric reflectance to maintain radiometric consistency between data obtained from different sensor types (Chander et al. 2009). Both dates of multispectral EO imagery were georectified to the high spatial resolution air photo (circa 1990) using nearest neighbor resampling, achieving a RMSE of equal to or less than 0.5 pixels for both

TM and SPOT imagery. An inspection of features visible in both the air photo and EO imagery (e.g., road intersections, corners of large agricultural fields, large built up environments, etc.) revealed that an accurate image registration was achieved between all images.

4.3.3 CREATION OF THE CHANGED AREA REFERENCE MAP

To assess the relative performance of each change detection method in this study, a reference map of change occurring over the two time periods was created using independently acquired high spatial resolution imagery. A combination of image segmentation and manual delineation was used to create a reference change map. The reference map for the base time period (circa 2005) was created using SPOT-5 2.5 m panchromatic imagery, while the reference map for the retrospective period (circa 1990) was based on the interpretation of a scanned panchromatic aerial photographs with a spatial resolution of approximately 0.80 m. Both images were georectified to a road network vector layer with a root mean square error (RMSE) equal to or less than 0.5 pixels using nearest neighbor resampling. Image segmentation was performed independently on both images using a multiresolution segmentation algorithm with the following parameter values: scale of 200, 0.5 for shape, and 0.5 for compactness. In order to identify changed areas, image objects in the 2005 base map were intersected with image objects in the 1990 retrospective map. Change objects were assessed by visually examining the high resolution imagery to ascertain whether actual land cover change had occurred between dates. A change mask with two classes, "change" and "no-change", was created and used as the reference to assess all change detection methods examined in this study.

4.3.4 OBJECT-BASED CHANGE DETECTION AND ASSOCIATED IMAGE SEGMENTATION STRATEGIES

As previously explained by Niemeyer et al. (2008), and adapted here, there are several basic potential image segmentation strategies for object-based change detection (Figure 14). The first strategy (Figure 14a) involves segmenting spectral information shared between two images to identify change objects. For example, Linke and McDermid (2011) segmented a differenced EWDI image acquired between two dates to obtain only change objects. This approach can be considered useful when the imagery is reasonably comparable in resolution (e.g., similar spatial and spectral resolution). The second strategy (Figure 14b) involves segmenting one image and retaining those image objects over time. Using this strategy, spectral information obtained from other imagery is used to determine whether an individual object has changed and what its new land cover label should be updated to. This latter approach was recommended by Pape and Franklin (2008), in situations where the spectral or spatial resolution of imagery being compared for change may be quite different. The third strategy (Figure 14c) involves independently segmenting imagery obtained at different times (i.e., using information from both images to create change objects). This approach can involve significant post-processing to reduce or eliminate differences in objects that arise when the segmentation process creates different results for similar features (e.g., Linke et al 2009). A fourth strategy introduced in this study, which can be considered as a hybridized extension of the second and third, involves maintaining land cover boundaries generated from one date of imagery, but allowing for new image objects to be segmented within existing land cover boundaries derived from other imagery in a hierarchical fashion (see Figure 14d). Based on these different image segmentation strategies, three approaches to object-based change detection were considered and compared in the Saskatchewan study area for two time periods (T_0 = 2005; T_{-1} =1990):

i) a differenced pixel-based NDVI image obtained from two dates (one SPOT-5 HRG and Landsat-5 TM image) is segmented and used to identify change objects (e.g., Linke and McDermid 2011);

ii) segmentation of T_0 imagery (SPOT-5 HRG) whereby image objects remain static between both dates and types of imagery. NDVI information from T_{-1} is summarized within image objects derived from T_0 imagery. NDVI information contained within image objects at T_0 and T_{-1} imagery SPOT-5 HRG and Landsat-5 TM imagery are then differenced and a threshold of change is established. Image objects that exhibit spectral change above the analyst determined threshold are labeled as change and undergo land cover class updating (e.g., Pape and Franklin 2008); and,

iii) segmentation and classification of T_0 imagery (SPOT-5 HRG) to establish land cover boundaries for the base map (circa 2005). Cross-correlation analysis (CCA) as originally described in a remote sensing study by Koeln and Bissonnette (2000), but adapted here for object-based image analysis, is used to determine areas of change.

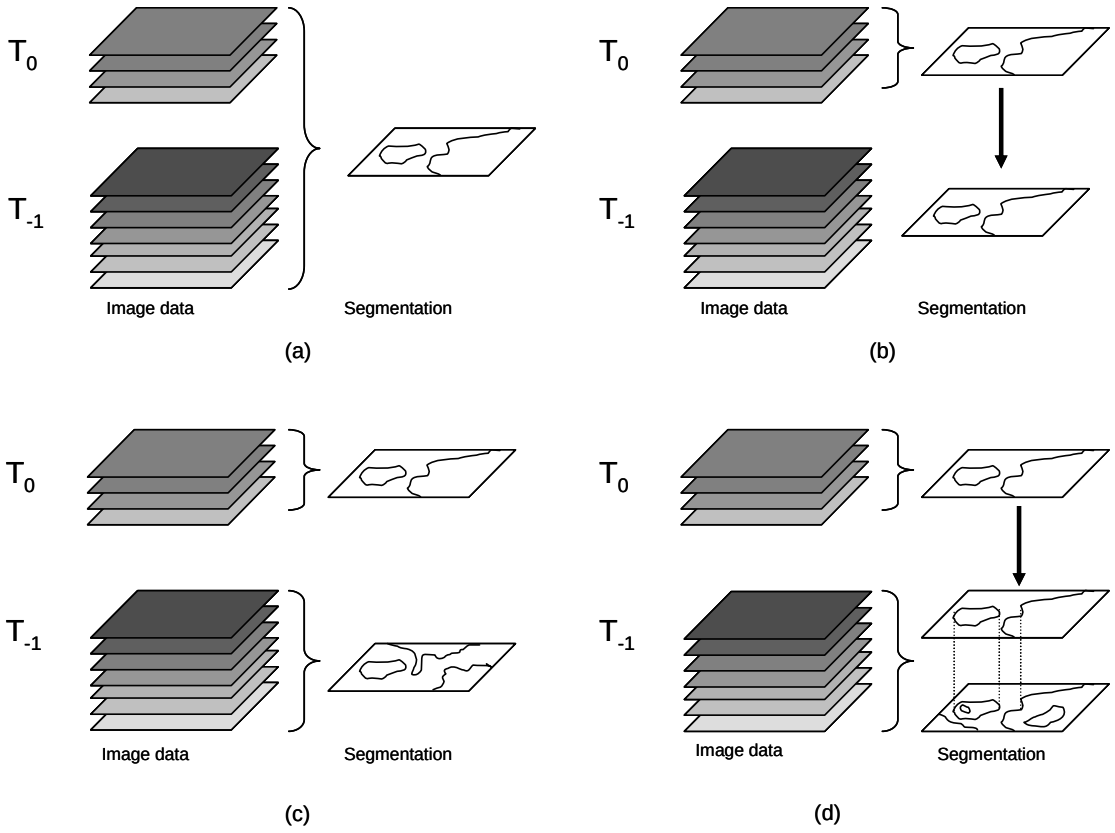

Figure 14: (adapted from Niemeyer et al. 2008) a) Segmentation of combined multispectral information from both T_0 and T_{-1} ("combined object change detection" - COCD); b) static segmentation of T_0, with image objects carried over to T_{-1} ("static object change detection" - SOCD); c) independent segmentations for both T_0 and T_{-1}; d) hierarchical segmentation where land cover boundaries from T_0 are retained, with new image objects segmented based on T_{-1} imagery ("hierarchical object CCA change detection" - HOCD-CCA).

4.3.5 CROSS-CORRELATION ANALYSIS FOR OBJECT-BASED CHANGE DETECTION

When using CCA for change detection, a land cover map of the area under investigation at the base acquisition date (T_0) is used to delineate class boundaries for the bi-temporal change detection process (Figure 14d). In this study, the land cover map used to describe T_0 was derived using object-based image analysis and a Random Forest machine learning algorithm to classify SPOT-5 HRG imagery acquired over the study area (28 August 2005), which achieved an overall classification accuracy above 90%. Seven broad land cover classes were selected (water,

wetland, riparian, crop, mixed grassland, built, and exposed soil/rock) based on the needs of larger studies attempting to assess potential cumulative environmental effects on aquatic ecosystems caused by development (Dube 2003; Squires et al. 2009; Seitz et al. 2011), and to ensure consistency between thematic maps produced using sensors with different characteristics (Petit and Lambin 2001; Petit and Lambin 2002). The land cover boundaries derived from the T_0 map were overlaid on the Landsat-5 TM imagery representing the 1990 retrospective time period (T_{-1}). The mean and standard deviation of multispectral information (from T_{-1}) contained within individual image objects (derived at T_0) were then summarized for each class boundary to derive an expected spectral signature for that land cover class (Koeln and Bissonnette 2000). A multivariate Z-statistic was then calculated to determine how much an individual image object's information deviates from the expected multispectral signature of a given class using the following equation (adapted from Hurd et al. 2001):

$$Z_{jk} = \sum_{i=1}^{n} \left(\frac{r_{ijk} - \mu_{ic_{jk}}}{\sigma_{ic_{jk}}} \right)^2 \qquad (1)$$

where

Z_{jk} is the Z statistic for the image object with indices *j* and *k*,
i is the band number in the multispectral image,
n is the number of bands,
r_{ijk} is the mean reflectance in band *i* of the image object with indices *j* and *k,*
c_{jk} is the corresponding thematic class with indices *j* and *k,*
μ_{ic} is the mean reflectance value in band *i* of all image objects of class *c*, and
σ_{ic} is the standard deviation of the reflectance values in band *i* of all image objects of class *c*

Using such an approach, image objects with high Z-score values potentially represent land cover change, whereas lower Z-score values indicate unchanged areas. Image objects identified as changed based on Z-scores are then extracted and reclassified, and used to update an existing

base map within a GIS environment. Two image segmentation strategies for the hybrid object-based change detection method using CCA are explored:

i) maintaining static image objects derived at T_0 throughout the change detection process (e.g., Pape and Franklin 2008); and,

ii) creating new image objects segmented from imagery from the second acquisition date (T_{-1}) that respect existing land cover boundaries derived at T_0 (e.g., Koeln and Bissonnette 2000; Willhauck 2000) using hierarchical image segmentation approach as formally described by Benz et al. (2004). (see Figure 14d).

Image objects in the former approach used "object primitives" (Castilla and Hay 2008) from an existing object-based classification with the following image segmentation parameter values: scale 10, shape 0.1, and compactness of 0.5. For the latter image segmentation strategy, Landsat-5 imagery from T_{-1} was used to derive new image objects using three image segmentation scales (10, 30, and 60). This was done to assess the effect of the scale parameter on change detection accuracy, while keeping other segmentation parameter values constant (shape 0.1, and compactness of 0.5).

In addition, modified versions of the object-based change detection methods described by Pape and Franklin (2008) and Linke and McDermid (2011) are used for comparison. In the former two studies, a differenced EWDI (Franklin et al. 2001) image was used as the spectral basis of the change detection. In the present study, two disparate sources of sensor data were utilized (SPOT-5 HRG and Landsat-5 TM). The "wetness" parameter derived using the Tasseled Cap transformation (Crist and Kauth 1986), which is used for the calculation of the EWDI, has been recently described for the SPOT-5 HRG sensor; however, the stability of the transformation has been found to be uncertain when applied to imagery with seasonal and geographical differences (Ivits et al. 2008). Therefore, for ease of comparison a differenced Normalized Difference Vegetation Index (NDVI) image based on the SPOT-5 HRG imagery (circa 2005) and the Landsat-5 TM imagery (circa 1990) was used in place of the EWDI.

To maintain comparability with the hybrid object-based change detection method proposed in this study, the modified versions of the object-based change detection method using differenced NDVI imagery used identical image segmentation parameters (scale 10, shape 0.1, and compactness of 0.5). In addition, the overall performance and sensitivity of the above change detection methodologies were all assessed using the same threshold of change, whereby values above two standard deviations were considered as change. Previous work by others (e.g., Franklin et al. 2001; Pape and Franklin 2008), has recommended a threshold of two standard deviations; the experience in those studies and others provided a reasonable first approximation of change/no-change areas that could be applied within the present study area. The following assumptions regarding this approach were made: 1) a normal distribution in change values exists; 2) the amount of changed area considered is small relative to the total area, or class area, under investigation, and; 3) areas of actual change are represented by high absolute values generated by the change detection methods.

4.3.6 CHANGE DETECTION ACCURACY ASSESSMENT

Change detection accuracy was assessed using a point-based random sample, and an area based comparison of changed areas. To obtain a point-based sample that was not biased by the large amount of no-change area, a stratified random sample of equal proportions was conducted in change/no-change areas delineated in the reference change map. Using this method, 700 change and 700 no-change points were selected. These 1400 points, representing change/no-change areas across the study area, were then intersected with the change and no-change areas generated by the different object-based change detection methods. For the area-based change detection accuracy assessment, areas detected as change were intersected with areas verified as change in the reference map, with the percentage of overlap reported. Confusion matrices with producer's and user's accuracy are reported (Congalton and Green 1998). While a modified method for comparing Kappa coefficients based on related samples has been developed for testing dichotomous outcomes (Donner et al. 2000) suitable for change/no-change studies, the use of the Kappa statistic has been found to be problematic due

to a violation of statistical independence when comparing paired samples (Foody 2002; 2004). The McNemar's test for paired-sample nominal scale data (Agresti 2002; Zar 2009) was used without Yates' continuity correction, to assess whether statistically significant differences between change detection methods exist. Particular attention in this study is paid to user's accuracy, which refers to the amount of change detected in relation to the change actually verified on the change reference map.

4.4 RESULTS

Figure 15 depicts a change and no-change masks using: a) manually delineated high spatial resolution panchromatic imagery (hereafter "change reference map" – CRM – Figure 15a); b) segmentation of NDVI imagery differenced from T_0 and T_{-1} (hereafter "combined object change detection" – COCD – Figure 15b); c) image objects derived at T_0 and carried over to T_{-1}, using differenced NDVI imagery (hereafter "static object change detection" – SOCD – Figure 15c), and; d) CCA of multispectral imagery utilizing land cover boundaries derived from T_0 (hereafter "hierarchical object CCA change detection" - HOCD – Figure 15d).

Figures 15b and 15c show the results of the COCD and SOCD methods, respectively. Overall, both COCD and SOCD show considerably more change than was detected in the CRM (Figure 15a) and by the HOCD-CCA method (Figure 15d). An overall visual assessment reveals that the CRM and the HOCD-CCA method showed the highest degree of agreement. Generally, the large areas of cropland in the southeast and northwest which were detected as change by COCD and SOCD, are missing from the CRM and HOCD-CCA. In the HOCD-CCA approach (Figure 15d), there is a notable absence of inundated crop land/wetland in the southwest portion of the study area which is present in all other change detection methods (Figures 15a-c). A network of roads and well pads present in the northern section of the CRM, but are absent in change masks produced by all change detection methods (Figures 15b-d).

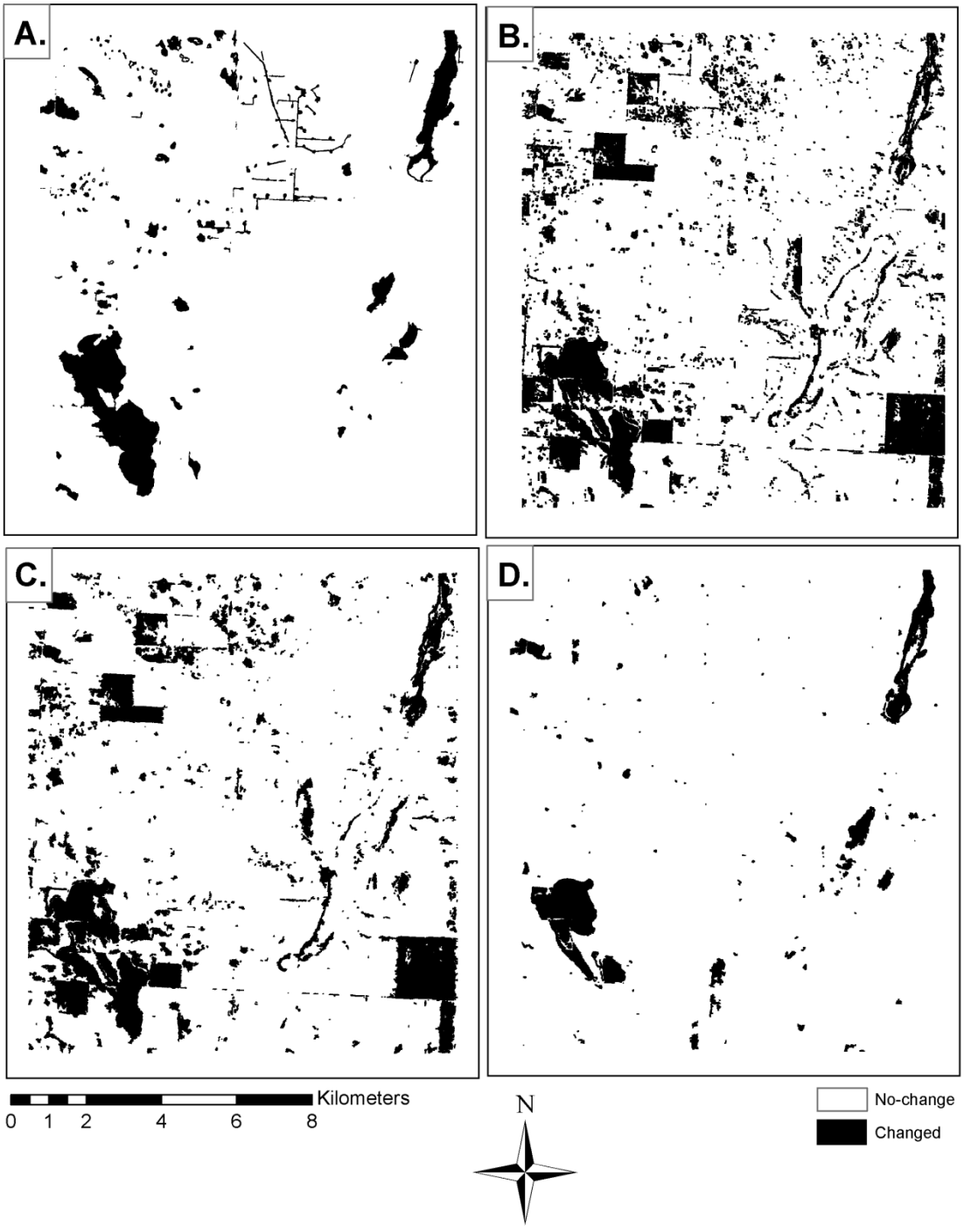

Figure 15: a) Reference change map derived from high spatial resolution imagery (CRM); b) combined object change detection (COCD); c) static object change detection (SOCD); d) hierarchical object CCA change detection (HOCD-CCA) using static objects from T_0 imagery.

Figure 16 summarizes the overall accuracy of the object-based change detection methods and the percentage of area detected as change with the area of change verified in the CRM (Figure 16a). Static object change detection (SOCD) which maintains image objects between dates (Figure 15b) and is driven by establishing a threshold of change using differenced NDVI information between dates (e.g., Pape and Franklin 2008), provided the highest overall change detection accuracy (74.9%). Areas detected as change using this method also achieved the highest level of overlap with areas verified as change in the CRM (56.66%). Combined object change detection (COCD) (e.g., Linke and McDermid 2011) using difference NDVI information achieved an overall accuracy and percentage of detected changed area that overlapped with the CRM that were nearly identical to the previous method (74.6% and 56.59%, respectively). Hierarchical object CCA change detection (HOCD-CCA) using static objects from T_0 imagery performed marginally less well in overall change detection accuracy than the two previous methods (73.1%); however, there was a marked decrease in the amount of detected changed area that overlapped with the changed area delineated in the CRM (44.27%). The overall classification accuracy dropped to 69.9%, and the percentage of changed area in agreement with the CRM dropped to 41.51% when using HOCD-CCA with image objects derived from T_{-1} imagery with a scale parameter value of 10. HOCD-CCA using a scale parameter value of 30, a size that coincides with the underlying 30 m spatial resolution of the imagery (Landsat-5 TM) used to segment new image objects at T_{-1}, improved the overall change detection accuracy slightly to 71.0%, with a slight drop in the percentage of changed area in agreement with the CRM (39.7%). Using HOCD-CCA with a scale parameter value of 60 slightly decreased the overall change detection accuracy to 70.8%, with a slight drop in the percentage of changed area in agreement with the reference map (39.55%).

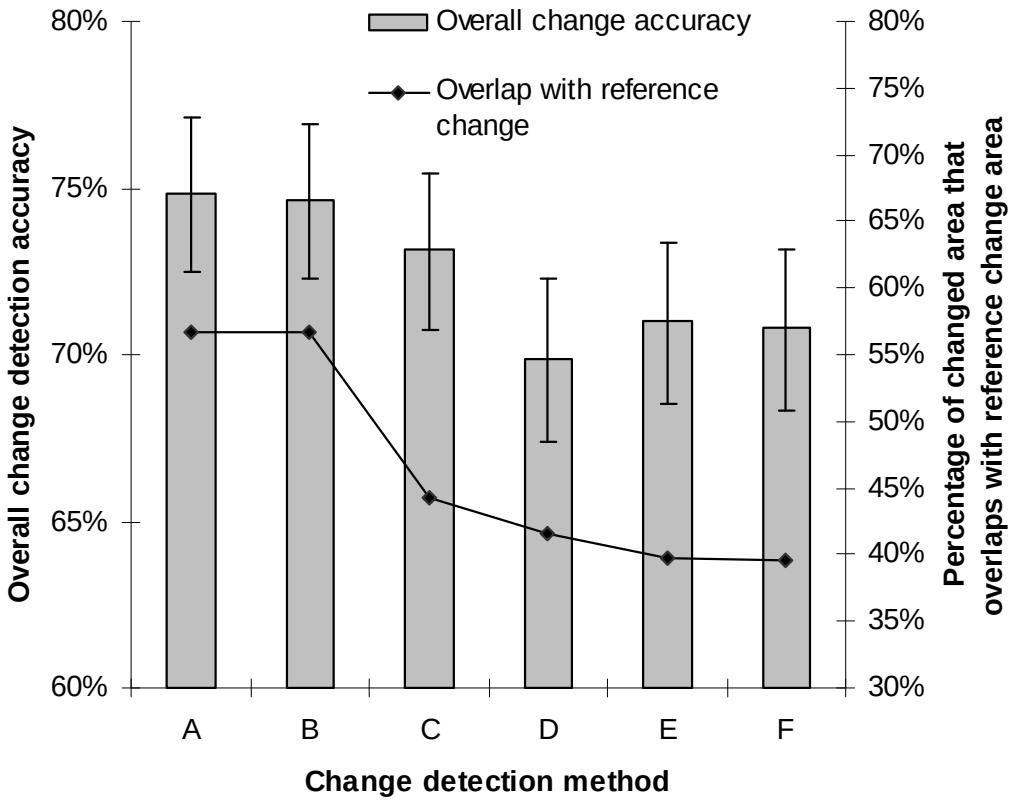

Figure 16: Overall change detection accuracy using: A) static object change detection (SOCD); B) combined object change detection (COCD); C) hierarchical object CCA change detection (HOCD-CCA) using static objects from T0 imagery; D) HOCD-CCA using image objects derived from T-1 imagery (scale 10); E) HOCD-CCA using image objects derived from T-1 imagery (scale 30); F) HOCD-CCA using image objects derived from T-1 imagery (scale 60).

Table 9 provides detailed matrices of user's and producer's accuracy (Congalton and Green 1998) for the top three performing object-based change detection methods as reported by overall accuracy in Figure 16. For the SOCD and COCD approaches, there was near identical agreement in overall classification accuracy, and in user's and producer's accuracy (Tables 9a and 9b). User's accuracy for non-CCA methods detected between 87.83 and 87.91% of the change areas verified in the CRM, whereas the HOCD-CCA change detection method using static objects from T_0 was capable of detecting 97.65% of the change verified in the CRM.

Table 9: Change detection accuracy reported for three object-based change detection methods: A) static object change detection; B) combined object change detection; and, C) static object CCA change detection. Ua=user's accuracy; Pa=producer's accuracy.

a) static object change detection (SOCD)								
	Reference							
Class	No-change	Change	**Total**					
Prediction				Ua				
No-Change	**644**	296	940	68.51%				
Change	56	**404**	460	87.83%				
Total	700	700	**1400**					
Pa	92.00%	57.71%						
Overall accuracy: 74.86% (95% lower and upper confidence limits: 72.50-77.11%)								
b) combined object change detection (COCD)								
	Reference							
Class	No-change	Change	**Total**					
Prediction				Ua				
No-Change	**645**	300	945	68.25%				
Change	55	**400**	455	87.91%				
Total	700	700	**1400**					
Pa	92.14%	57.14%						
Overall accuracy: 74.64% (95% lower and upper confidence limits: 72.28-76.90%)								
c) hierarchical object CCA change detection (HOCD-CCA) using static objects from T_0								
	Reference							
Class	No-change	Change	**Total**					
Prediction				Ua				
No-Change	**692**	368	1060	65.28%				
Change	8	**332**	340	97.65%				
Total	700	700	**1400**					
Pa	98.86%	47.43%						
Overall accuracy: 73.14% (95% lower and upper confidence limits: 70.74-75.45%)								

Using the McNemar test, differences between change detection accuracies achieved by the SOCD and COCD methods depicted were not significant at the 5 percent level of significance ($p = 0.6692$). The difference in change detection accuracy between the static object change detection method SOCD and the COCD method were statistically significant at the 5 percent level of significance when compared to HOCD-CCA change detection method using static objects from T_0 ($p<0.001$). Figure 17a illustrates how change objects created by HOCD-CCA (image segmentation scale 30) respects existing land cover boundaries derived from T_0 imagery. In contrast, Figure 17b illustrates how COCD creates change objects that are generally localized to the same area of change (e.g., inundated area), but that do not conform to land cover boundaries derived from T_0 imagery. There are notable differences in the amount of area detected as change between methods, as well as the size and shape of the individual change objects due to differences in image segmentation strategies used.

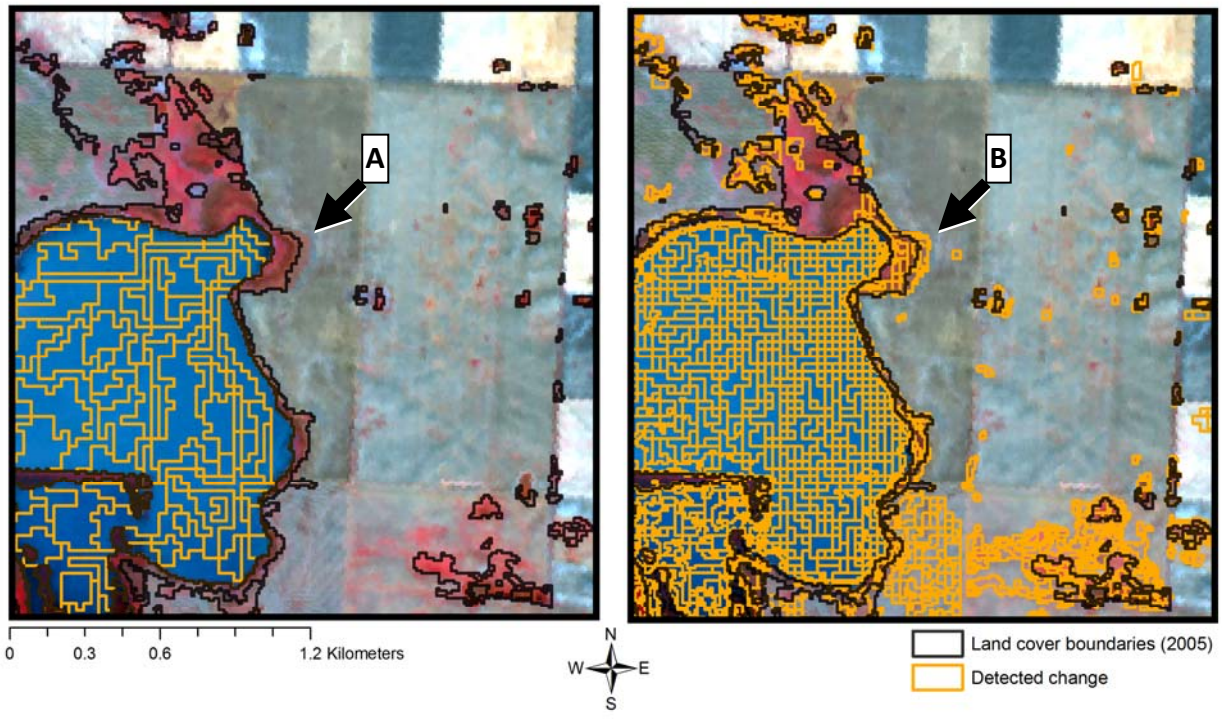

Figure 17: Comparison of change detected by various methods: a) Change objects derived from HOCD-CCA change detection methods conform to pre-existing land cover boundaries derived from T0 imagery using image object derived from T-1 imagery (scale 30); b) COCD change detection introduces change objects that have a pixelated appearance and do not conform to pre-existing land cover boundaries. Background imagery: SPOT-5 HRG (28 August 2005) shown in false color composite (XS3=Red, XS2=Green, XS1=Blue).

4.5 DISCUSSION

In general, all three object-based change detection methods tested in this paper achieved similar overall classification accuracies; however, there was considerable difference in the amount and types of change detected by each method using a threshold of two standard deviations. Most notably, the HOCD-CCA based change detection method introduced in this study (Figure 15d) showed considerably less change at a threshold of two standard deviations relative to the other methods compared in this study (Figures 15b and 15c). The most obvious explanation for the high degree of change detected by the non-CCA methods relative to the CRM (Figure 15a), is that these methods are based on differenced spectral information that provides information that is not discernible in a visual interpretation of high spatial resolution panchromatic imagery used to produce the CRM. For example, variations in crop vigor between years would not necessarily be readily apparent in the panchromatic imagery, but may in fact be readily discernible in multispectral imagery in the near-infrared portion of the spectrum.

A visual examination of Figure 13 reveals that the crop areas detected by the non-CCA approaches in the southeast and northwest portion of the study area (Figures 15b and 15c) show up as red areas in the circa 2005 SPOT-5 imagery, but as grey or light-green areas in the circa 1990 Landsat-5 imagery, indicating differences in phenology or vegetation type. Visual inspection of high spatial resolution imagery used to derive the CRM reveal no discernable change in land cover type (i.e., a crop land cover type is visible in circa 2005 and 1990 imagery). In contrast, the HOCD-CCA approach does not detect this subtle spectral difference (Figure 15d). This effect is likely due to the way thresholds for the CCA calculation is derived. Using CCA, thresholds are determined on a per-class basis, rather than for the entire study area as is the case with the non-CCA methods. A cursory examination of change objects representing the areas of crop land detected by the non-CCA approaches (Figures 15b and 15c) that appear bright red in the southwest and northeast portions of the study area (Figure 13), reveal a mean Z-score of 8.07, which is well below the two standard deviation threshold determined for crop

land cover types (Z-score value of 25.88) using the CCA method. In this case, the use of per-class thresholds with the CCA method, as determined by a pre-existing land cover map (derived at T_0), has effectively eliminated an element of subtle spectral change. To achieve a similar result using non-CCA methods presented here, the analyst would have to manually adjust the threshold of change to eliminate unwanted change area, an activity that can consume a major portion of the analyst's time (Desclée et al. 2006; Pape and Franklin 2008). As the non-CCA change detection approaches examined here operate on a per-scene basis, manual adjustment of the threshold for these approaches may not be capable of producing the same less-noisy change mask depicted by the CCA method. However, since all methods examined in this study were conducted within an object-based environment (i.e., GIS), it should be possible to adapt the per land cover class threshold strategy used in the CCA approach to other methods, while implementing more statistically rigorous means of establishing change thresholds (e.g., Desclée et al. 2006).

Despite similar overall change detection accuracies between the object-based methods examine in this study, the amount of area detected as change that overlapped with areas of change verified in the reference change map neared 60% with the two non-CCA change detection methods, and between 40-44% using variations of CCA method. The high levels of overlap reported by non-CCA change detection methods could potentially be explained by the high amount of subtle spectral change present in the non-CCA change detection methods. In other words, the cumulative addition of small areas of change detected by the non-CCA methods may have increased the amount of changed area detected. While the detection of subtle change likely represents real elements of change in the land cover map (e.g., differences in phenology and/or moisture content of crop fields), it represents change that is not of interest in this study. Another potential explanation for the higher amount of changed area in common with the CRM is the omission of a large amount of wetland/inundated crop land area in the southwest (Figure 15a) not detected by the CCA method (Figure 15d), but largely detected by the non-CCA methods (Figures 15b and 15c). In this case, the per-class threshold established by the CCA method may have performed sub-optimally. A visual examination of this area reveals a

wetland-like environment, with a bright-red tip extending from the southern portion of the inundated cropland area (Figure 13a). A cursory examination of image objects in this area reveal a mean Z-score of 3.2 for the wetland land cover type, which is under the two standard deviation threshold (Z-score of 24.43), therefore indicating that these image objects are considered unchanged by the CCA change detection method. While adjusting the threshold may improve the results in this case, it is possible that the map used to establish land cover boundaries and image objects used in the CCA approach was incorrect (i.e., the area should be considered as crop land cover type instead of a wetland land cover type). As the CCA approach is entirely based on the accuracy of the underlying base map, which is consequently used to establish land cover boundaries and related change thresholds, any error in this map may potentially result in errors of omission or commission in the change detection process. Such a situation highlights the potential pitfalls of applying the CCA change detection method when using inaccurate base maps.

Differences in overall change detection accuracy between CCA and non-CCA methods were statistically different ($p<0.05$); however, the large degree of overlap in 95 percent confidence intervals (Figure 16) suggests that determining which approach actually achieved better change detection performance is problematic. A closer examination of detailed confusion matrices presented in Table 9 provides some insight into this matter: While non-CCA change detection methods achieved higher classification accuracies overall, user's accuracy for the CCA change detection method was approximately 10% higher than non-CCA change detection methods. The low amount of commission error indicated by this result indicates that the CCA change detection method was better able to detect change as indicated in the CRM. This finding supports the visual correspondence between the CRM (Figure 15a) and the HOCD-CCA change detection method (Figure 15d). The higher producer's accuracy for changed areas achieved by non-CCA change detection methods is likely due to the large amounts of subtle spectral change detected. In other words, the large amounts of subtle spectral change detected by the non-CCA change detection methods may confer an advantage in avoiding errors of omission that can occur when applied to other mapping situations (i.e., the producer's accuracy

for detecting changed areas would be higher). This finding is also logically consistent with the results presented in the study.

Previous research examining object-based change detection and map updating highlighted the need to address the issue of respecting boundary delineations of an existing map when undergoing map updating procedures (McDermid et al. 2008). The CCA method as demonstrated in this study utilized a hierarchical image segmentation strategy (Benz et al. 2004), whereby existing object boundaries are used as the basis for subsequent image object segmentation, which has been used in previous object-based change detection studies (e.g., Willhauck 2000; Walter 2004). When hierarchical image segmentation is not implemented, the resulting image objects that are created do not have to conform to the land cover boundaries of an existing base map (Figure 17b). Such a situation may contribute to change objects not aligning correctly when overlaid on an existing land cover map (Linke et al. 2009).

In the comparison outlined in Figure 17, the CCA method retains land cover boundaries and creates new image objects which correspond to the (coarser) underlying imagery from T_{-1}, using a scale parameter value of 30, resulting in larger change objects. However, when performing image segmentation on the differenced pixel-based NDVI imagery from T_0 and T_{-1}, the resulting image objects become pixelated due to the coarser spatial resolution (30m) of the Landsat-5 TM imagery, and relatively finer scale parameter scale used (10). The over-segmented appearance of the non-CCA approach depicted in Figure 17b may contribute to spurious change being detected as the underlying image objects effectively become pixel-like, which may result in a salt-and-pepper effect in the change detection process. Segmentation scale has been found to directly effect the overall accuracy of object-based land cover classifications (Kim et al. 2011; Smith 2010; Myint et al. 2011), and has been shown in this study to degrade overall change detection accuracy when not commensurate with the underlying imagery (Figure 16).

4.6 CONCLUSION

A hybrid object-based change detection method based on CCA utilizing a hierarchical image segmentation strategy was introduced and compared to two object-based change detection methods. While the CCA change detection method performed slightly less well than the two non-CCA change detection methods compared in this study, the visual depiction of areas detected as change using CCA was superior to the non-CCA change detection methods. Furthermore, the underlying flexibility of the method remains promising, especially if disparate sources of EO imagery are to be used. The hierarchical image segmentation strategy utilized in this study has been confirmed to be a viable solution for respecting existing land cover boundaries when conducting map updating procedures, which could potentially reduce or eliminate the number of spurious change objects introduced. The use of per-class thresholds used by the object-based CCA change detection method outlined in this study show potential promise over using a singular threshold typically used in bi-temporal multispectral change detection. Adapting per-class thresholds to non-CCA object-based change detection methods along with more statistically rigorous threshold selection processes should prove useful to reducing or eliminating unwanted change from being detected. Overall the hybrid object-based CCA change detection method introduced in this study was capable of utilizing multiple sources of EO imagery for the purposes of detecting land cover change with a high degree of accuracy.

4.7 REFERENCES

BENZ, U. C., P. HOFMANN, GREGOR WILLHAUCK, I. LINGENFELDER, AND M. HEYNEN. 2004. Multi-resolution, object-oriented fuzzy analysis of remote sensing data for GIS-ready information. *ISPRS Journal of Photogrammetry and Remote Sensing* 58 (3-4): 239-258.

CANTY, M. J. 2010. *Image Analysis, Classification, and Change Detection in Remote Sensing: With Algorithms for ENVI/IDL*. Taylor and Francis.

CANTY, M. J., AND ALLAN A. NIELSEN. 2011. Linear and kernel methods for multivariate change detection. *Computers and Geosciences* (0).

CASTILLA, G., AND G. J. HAY. 2008. Image objects and geographic objects. In *Object-Based Image Analysis*, ed. T. Blaschke, S. Lang, and Geoffrey J. Hay, 91-110. Berlin, Heidelberg: Springer Berlin Heidelberg.

CHANDER, G., B. L. MARKHAM, AND D. L. HELDER. 2009. Summary of current radiometric calibration coefficients for Landsat MSS, TM, ETM+, and EO-1 ALI sensors. *Remote Sensing of Environment* 113 (5): 893-903.

CIVCO, D. L., J. D. HURD, E. H. WILSON, M. SONG, AND Z. ZHANG. 2002. A comparison of land use and land cover change detection methods. In *American Society for Photogrammetry and Remote Sensing/ American Congress on Surveying and Mapping*, 12.

CONGALTON, R. G., AND K. GREEN. 1998. *Assessing the Accuracy of Remotely Sensed Data: Principles and Practices*. 1st ed. CRC Press.

COPPIN, I. JONCKHEERE, K. NACKAERTS, B. MUYS, AND E. LAMBIN. 2004. Digital change detection methods in ecosystem monitoring: a review. *International Journal of Remote Sensing* 25 (9): 1565-1596.

CRIST, E. P., AND R. J. KAUTH. 1986. The Tasseled Cap de-mystified (transformations of MSS and TM data). *Photogrammetric Engineering and Remote Sensing* 52: 81-86.

DESCLÉE, B., P. BOGAERT, AND P. DEFOURNy. 2006. Forest change detection by statistical object-based method. *Remote Sensing of Environment* 102 (1-2): 1-11.

DINGLE ROBERTSON, L., AND D. J. KING. 2011. Comparison of pixel- and object-based classification in land cover change mapping. *International Journal of Remote Sensing* 32 (6): 1505-1529.

DONNER, A., M. M. SHOUKRI, N. KLAR, AND E. BARTFAY. 2000. Testing the equality of two dependent kappa statistics. *Statistics in Medicine* 19 (3): 373-387.

DUBE, M. G. 2003. Cumulative effect assessment in Canada: a regional framework for aquatic ecosystems. *Environmental Impact Assessment Review* 23 (6): 723-745.

DURO, D.C., FRANKLIN, S.E., DUBE, M.G., 2012. A comparison of pixel-based and object-based image analysis with selected machine learning algorithms for the classification of agricultural landscapes using SPOT-5HRG imagery. Remote Sensing of Environment 118, 259-272.

ENTWISLE, BARBARA, AND PAUL C. STERN, eds. 2005. *Population, land use, and environment*. National Academies Press.

FERANEC, JAN, G. HAZEU, S. CHRISTENSEN, AND G. JAFFRAIN. 2007. Corine land cover change detection in Europe (case studies of the Netherlands and Slovakia). *Land Use Policy* 24 (1): 234-247.

FERANEC, JÁN, M. SÚRI, J. OT'AHEL', T. CEBECAUER, J. KOLÁR, T. SOUKUP, D. ZDENKOVÁ, ET AL. 2000. Inventory of major landscape changes in the Czech Republic, Hungary, Romania and Slovak Republic 1970s - 1990s. *International Journal of Applied Earth Observation and Geoinformation* 2 (2): 129-139.

FOODY, G. 2004. Thematic Map Comparison: Evaluating the Statistical Significance of Differences in Classification Accuracy. *Photogrammetric Engineering and Remote Sensing* 70 (5): 627-634.

FOODY, G. M. 2002. Status of land cover classification accuracy assessment. *Remote Sensing of Environment* 80 (1): 185-201.

FRANKLIN, S.E., P. K. MONTGOMERY, AND G. B. STENHOUSE. 2005. Interpretation of land cover changes using aerial photography and satellite imagery in the Foothills Model Forest of Alberta. *Canadian Journal of Remote Sensing* 31 (4): 304-313.

FRANKLIN, S.E., M. B. LAVIGNE, L. M. MOSKAL, M. A. WULDER, AND T. M. MCCAFFREY. 2001. Interpretation of forest harvest conditions in New Brunswick using Landsat TM enhanced wetness difference imagery (EWDI). *Canadian Journal of Remote Sensing* 27 (2): 118-128.

HOUGHTON, R. A. 1995. Land‐use change and the carbon cycle. *Global Change Biology* 1 (4): 275-287.

HURD, J. D., E. H. WILSON, S. G. LAMMEY, AND D. L. CIVCO. 2001. Characterization of Forest Fragmentation and Urban Sprawl Using Time Sequential Landsat Imagery. In *American*

Society for Photogrammetry and Remote Sensing/ American Congress on Surveying and Mapping, 12.

IM, J., J. R. JENSEN, AND J. A. TULLIS. 2008. Object-based change detection using correlation image analysis and image segmentation. *International Journal of Remote Sensing* 29 (2): 399.

IM, JUNGHO, AND JOHN R. JENSEN. 2005. A change detection model based on neighborhood correlation image analysis and decision tree classification. *Remote Sensing of Environment* 99 (3): 326-340.

IVITS, E., A. LAMB, F. LANGAR, S. HEMPHILL, AND B. KOCH. 2008. Orthogonal transformation of segmented SPOT5 images: seasonal and geographical dependence of the tasselled cap parameters. *Photogrammetric Engineering and Remote Sensing* 74 (11): 1351-1364.

KIM, M., T. WARNER, M. MADDEN, AND D. ATKINSON. 2011. Multi-scale GEOBIA with very high spatial resolution digital aerial imagery: scale, texture and image objects. *International Journal of Remote Sensing* 32 (10): 2825-2850.

KOELN, G., AND J. BISSONNETTE. 2000. Cross-correlation analysis: mapping landcover changes with a historic landcover database and a recent, single-date, multispectral image. In *American Society for Photogrammetry and Remote Sensing/ American Congress on Surveying and Mapping*, 12.

LAMBIN, ERIC F., AND H. GEIST. 2006. *Land-Use and Land-Cover Change: Local Processes and Global Impacts*.

LINKE, J., G. J. MCDERMID, D. N. LASKLN, A. J. MCLANE, A. PAPE, J. CRANSTON, M. HALL-BEYER, AND S.E. FRANKLIN. 2009. A disturbance-inventory framework for flexible and reliable landscape monitoring. *Photogrammetric Engineering and Remote Sensing* 75 (8): 981-995.

LINKE, J. AND G. J. MCDERMID. 2011. A Conceptual Model for Multi-Temporal Landscape Monitoring in an Object-Based Environment. *Selected Topics in Applied Earth Observations and Remote Sensing, IEEE Journal of* 4 (2): 265-271.

LINKE, J., G.J. MCDERMID, A. PAPE, A. MCLANE, D. LASKIN, M. HALL-BEYER, AND S E. FRANKLIN. 2009. The influence of patch-delineation mismatches on multi-temporal landscape pattern analysis. *Landscape Ecology* 24 (2): 157-170.

LIVERMAN, D. M. 1998. *People and Pixels Linking Remote Sensing and Social Science*. Washington, D.C.: National Academy Press.

LU, D., P. MAUSEL, E. BRONDÍZIO, AND E. MORAN. 2004. Change detection techniques. *International Journal of Remote Sensing* 25 (12): 2365.

MCDERMID, G. J., J. LINKE, A. PAPE, D. N. LASKLN, A. J. MCLANE, AND S. E. FRANKLIN. 2008. Object-based approaches to change analysis and thematic map update: challenges and limitations. *Canadian Journal of Remote Sensing* 34 (5).

MYINT, S. W., P. GOBER, A. BRAZEL, S. GROSSMAN-CLARKE, AND Q. WENG. 2011. Per-pixel vs. object-based classification of urban land cover extraction using high spatial resolution imagery. *Remote Sensing of Environment* 115 (5): 1145-1161.

NIELSEN, A. A. 2007. The Regularized Iteratively Reweighted MAD Method for Change Detection in Multi- and Hyperspectral Data. *IEEE Transactions on Image Processing* 16 (2): 463-478.

NIEMEYER, I., P. R. MARPU, AND S. NUSSBAUM. 2008. Change detection using object features. In *Object-Based Image Analysis*, ed. T. Blaschke, S. Lang, and Geoffrey J. Hay, 185-201. Lecture Notes in Geoinformation and Cartography. Springer Berlin Heidelberg.

PAPE, A., AND S.E. FRANKLIN. 2008. MODIS-based Change Detection for Grizzly Bear Habitat Mapping in Alberta. *Photogrammetric Engineering and Remote Sensing* 74. Photogrammetric engineering and remote sensing.

PETIT, C. C., AND E. F. LAMBIN. 2001. Integration of multi-source remote sensing data for land cover change detection. *International Journal of Geographical Information Science* 15 (8): 785.

PETIT, C. C., AND E.F. LAMBIN. 2002. Impact of data integration technique on historical land-use/land-cover change: Comparing historical maps with remote sensing data in the Belgian Ardennes. *Landscape Ecology* 17 (2): 117-132.

POSTEL, S. L., G. C. DAILY, AND P. R. EHRLICH. 1996. Human appropriation of renewable fresh water. *Science* 271 (5250): 785-788.

ROGAN, J., AND D. CHEN. 2004. Remote sensing technology for mapping and monitoring land-cover and land-use change. *Progress in Planning* 61 (4): 301-325.

RUELLAND, D., A. TRIBOTTE, C. PUECH, AND C. DIEULIN. 2011. Comparison of methods for LUCC monitoring over 50 years from aerial photographs and satellite images in a Sahelian catchment. *International Journal of Remote Sensing* 32 (6): 1747-1777.

SASKATCHEWAN AGRICULTURE AND FOOD. 2005. *Crop Report*. Saskatchewan Agriculture and Food.

SEITZ, N. E., C. J. WESTBROOK, AND B. F. NOBLE. 2011. Bringing science into river systems cumulative effects assessment practice. *Environmental Impact Assessment Review* 31 (3): 172-179.

SERRA, P., X. PONS, AND D. SAURÍ. 2003. Post-classification change detection with data from different sensors: Some accuracy considerations. *International Journal of Remote Sensing* 24: 3311-3340.

SINGH, A. 1989. Review Article Digital change detection techniques using remotely-sensed data. *International Journal of Remote Sensing* 10: 989-1003.

SMITH, A. 2010. Image segmentation scale parameter optimization and land cover classification using the Random Forest algorithm. *Journal of Spatial Science* 55 (1): 69.

SQUIRES, A. J., C. J. WESTBROOK, AND M. G. DUBÉ. 2009. An Approach for Assessing Cumulative Effects in a Model River, the Athabasca River Basin. *Integrated Environmental Assessment and Management*: 1.

TREITZ, P., AND J. ROGAN. 2004. Remote sensing for mapping and monitoring land-cover and land-use change--an introduction. *Progress in Planning* 61 (4): 269-279.

VITOUSEK, P. M., J. D. ABER, R. W. HOWARTH, G. E. LIKENS, P. A. MATSON, D. W. SCHINDLER, W. H. SCHLESINGER, AND D. G. TILMAN. 1997. Human alteration of the global nitrogen cycle: sources and conseqences. *Ecological Applications* 7 (3): 737-750.

WALTER, V. 2004. Object-based classification of remote sensing data for change detection. *ISPRS Journal of Photogrammetry and Remote Sensing* 58 (3-4): 225-238.

WILLHAUCK, G. 2000. Comparison of object oriented classification techniques and standard image analysis for the use of change detection between SPOT multispectral satellite images and aerial photos. In *International Society for Photogrammetry and Remote Sensing*. Vol. XXXIII. Amsterdam, Netherlands: Organising Committee of the XIX International Congress for Photogrammetry and Remote Sensing.

CHAPTER 5 PREFACE

In this concluding chapter, the cumulative knowledge gained from research efforts outlined in previous chapters is combined and applied over a large agricultural area in southwest Saskatchewan. The application demonstrates how land cover information derived from disparate sources of remotely sensed imagery spanning three decades can be used to spatially disaggregate land use information over the same time period. Using this approach, selected land use information can be depicted at local landscape scales, allowing for spatial and temporal trends in land use to be examined. The results of the spatial disaggregation procedure are compared against traditional choropleth mapping techniques.

CHAPTER 5

INTERPRETATION OF CHANGE IN LAND COVER AND AGRICULTURAL LAND USE INTENSITY OVER A LARGE WATERSHED IN SOUTHWEST SASKATCHEWAN, CANADA (1976-2005) USING REMOTE SENSING OBSERVATIONS AND SPATIAL DISAGGREGATION[4]

[4] In review at the time of submission to the College of Graduate Studies and Research. Submitted to the *International Journal of Applied Earth Observation and Geoinformation* on January 6, 2012. using the following citation:

DURO, D.C., FRANKLIN, S.E., DUBÉ, M.G. (In review). Interpretation of change in land cover and agricultural land use intensity over a large watershed in southwest Saskatchewan, Canada (1976-2005) using remote sensing observations and spatial disaggregation.

All work reported in this chapter, including the review of the literature, theoretical and experimental design, analysis and discussion of the results, and writing of the text, was carried out by the Ph.D. candidate. As supervisor, Dr. S.E. Franklin reviewed all parts of the work. Dr. M.G. Dubé was involved in early conceptual design.

5.1 ABSTRACT

In the application outlined in this study, land use intensity information derived from agricultural census data were spatially disaggregated using land cover information derived from earth observation (EO) imagery. While cropland area estimated by census data and EO imagery were different, correlations between these datasets were high and statistically significant (n = 19; 1976: Adjusted R^2 = 0.93, p<0.001; 1991: Adjusted R^2 = 0.96, p<0.001; 2005: Adjusted R^2 = 0.91, p <0.001). Medium spatial resolution EO imagery (10-60 m pixels) was used to spatially disaggregate coarse agricultural land use information gathered over large census boundaries. The result of the spatial disaggregation procedure was a spatially explicit representation of land use intensity. While the spatial disaggregation procedure outlined could benefit from refinement, the application as illustrated shows considerable promise as a means of obtaining local spatial and temporal trends on land use intensity in agricultural environments.

5.2 INTRODUCTION

Earth observation (EO) imagery acquired at medium spatial resolutions (10-60 m pixels), provides a valuable synoptic and historic record of detailed global land cover at local landscape scales. In contrast to EO imagery, detailed information on socioeconomic aspects of agricultural land use, often gathered by national censuses over bi-decadal (or longer) time frames, is typically made available to the public in aggregated form. These data are often summarized over spatially coarse administrative units that tend not to be ecologically relevant, and are less suited to conducting analysis at local scales (Comber et al., 2008) where human induced disturbances to ecosystems and potential socioeconomic linkages are more readily apparent (see Liverman 1998; Entwisle and Stern 2005). Most socioeconomic information covered in such censuses will likely remain difficult or impossible to directly infer from remotely sensed data alone, yet such information remains essential to obtaining a complete understanding of

human induced landscape change over historical time periods (Drigo, 2004; Lesschen et al., 2005).

To better leverage the distinct information available from EO imagery and census data, researchers have explored methods of combining aspects of both using a variety of techniques. For example, Kerr and Cihlar (2003) used land cover information derived from the SPOT-4/VEGETATION (VGT) sensor (1 km pixels) to construct a "spatially refined" version of agricultural census data summarized over 336 watersheds across Canada. Cardille and Clayton (2007) related land cover of the Amazon Rainforest derived from Advanced Very High Resolution Radiometer (AVHRR) imagery (1 km pixels) with agricultural census data to produce a "scaled-down" land use map produced at an intermediate resolution (9 km pixels). Comber et al. (2008) applied dasymetric and volume preservation (“pycnophylactic”) techniques to relate coarse spatial resolution agricultural census data with a gridded raster product (1 km pixels) derived from several vector layers depicting land cover. More recently, in an approach paralleling the one described in this study, Mehaffey et al. (2011) linked census data (e.g., crop yields, fertilizer and pesticide application rates, tillage practises, etc.) with a variety of other sources of land use and crop yield data, using the Landsat-based (30 m pixels) National Land Cover Database (NLCD) product for a dozen states in the US Midwest. In contrast to previous examples given, this latter approach utilized relatively fine spatial resolution land cover maps to "spatially constrain" several datasets together, resulting in a spatially explicit database suitable for modeling ecological responses at local scales, which in turn, could be used to drive econometric models capable of assessing tradeoffs between potential cropping scenarios and impacts to ecosystem services in an agricultural environment undergoing intensive development Mehaffey et al. (2011).

5.2.1 OBJECTIVES OF THIS STUDY

In the application outlined here, selected land use information obtained from agricultural census data is combined with medium spatial resolution imagery (10-30 m pixels) using a

spatial disaggregation process. Previous studies utilizing similar spatial disaggregation methods have tended to rely on spatially coarse resolution EO imagery (e.g., 1 km pixels), whereas comparatively few such applications have demonstrated the process using EO imagery with relatively finer spatial resolutions (e.g., 10-60 m pixels). The application demonstrated here shows how spatially disaggregated land use intensity information can provide enhanced insights into local landscape scale agricultural development over traditional choropleth mapping. Land use intensity is defined here to represent the amount of chemical fertilizer applied to field crops. Other information may also be used to define land use intensity, such as field practices employed (e.g., zero-tillage), but such information is not considered here due to lack of suitable information over the time periods examined.

5.3 METHODS

5.3.1 STUDY AREA

The study area is located in the southwest part of the province of Saskatchewan (Canada), and is centered over a large drainage area which represents the downstream confluence of three major river systems in Canada's Western Prairie Provinces: the Oldman, Bow, and Red Deer Rivers (Figure 18). These rivers and their associated drainage areas represent the upper portion of the larger South Saskatchewan River Basin (SSRB), which is facing increasing cumulative environmental impacts from a variety of development activities and climate change scenarios (Schindler, 2001; Schindler and Donahue, 2006).

Figure 18: The study area is centered on a large drainage basin (designated as "Happyland" by the Water Survey of Canada) located in southwest Saskatchewan, Canada.

5.3.2 IMAGE PRE-PROCESSING, SEGMENTATION, AND CHANGE DETECTION

EO imagery from different satellite platforms were used to create land cover maps of the study area at medium spatial resolutions (Table 10). Circa 2005 land cover mapping utilized nine multispectral scenes from the Satellite Pour l'Observation de la Terre (SPOT-5) obtained using the High Resolution Geometric (HRG) sensor (10 m pixels). Land cover for the 1990 period was produced using imagery from Landsat-5's Thematic Mapper (TM) sensor (30 m pixels), while the 1976 land cover map used Landsat-2's Multispectral Scanner (MSS) (60 m pixels). Calibrated digital numbers were processed to exoatmospheric reflectance (Chander et al., 2009), which were then radiometrically normalized to enhance the comparability of spectral information between scenes within each time period using manually collected pseudo invariant features (Schott et al., 1988).

Table 10: Specifications of disparate earth observation imagery used in this study.

Satellite	Acquistion Date	Sensor	Radiometric resolution	Spatial resolution (m)	Spectral resolution (nm)*						
					"Blue"	"Green"	"Red"	"Near-infrared"	"Shortwave-infrared	"Mid-infrared"	"Thermal"
SPOT-5	2005-Aug-06	HRG-1	8-bits	10							
SPOT-5	2005-Aug-06	HRG-1	8-bits	10							
SPOT-5	2005-Aug-27	HRG-2	8-bits	10							
SPOT-5	2005-Aug-27	HRG-2	8-bits	10							
SPOT-5	2005-Aug-28	HRG-1	8-bits	10	NA	500-590	610-680	780-890	1,580-1,750	NA	NA
SPOT-5	2005-Aug-28	HRG-1	8-bits	10							
SPOT-5	2008-Jul-03	HRG-2	8-bits	10							
SPOT-5	2008-Sep-30	HRG-2	8-bits	10							
SPOT-5	2008-Sep-30	HRG-2	8-bits	10							
Landsat-5	1990-Sep-05	TM	8-bits	30	450-520	520-600	630-690	760-900	1550-1750	2080-2350	10400-12500
Landsat-5	1990-Sep-05	TM	8-bits	30							
Landsat-2	1976-Aug-14	MSS	6-bits	57	NA	500-600	600-700	700-800; 800-1100	NA	NA	NA
Landsat-2	1976-Aug-14	MSS	6-bits	57							

* - band name designations are approximations

All images were resampled to a common pixel size corresponding to the finest spatial resolution imagery (i.e., SPOT-5; 10 m pixels). Resampling to the coarsest spatial resolution when comparing disparate image sources has been suggested (Petit and Lambin, 2001), although others have recently found that such an approach generally degrades overall classification accuracy compared to using inherent spatial resolutions of the underlying imagery (Ruelland et al., 2011). In this study, pixels were resampled to the finest spatial resolution of the

available imagery (10 m pixels), but image segmentation parameters were selected based on the coarsest spatial resolution (i.e., 60 m pixels). All imagery and subsequent spatial ancillary data were projected into an Albers Equal Area Conic (NAD 1983).

The selection of appropriate segmentation parameters and classification algorithm for object-based image analysis was based on previous work within the study area, and is described elsewhere (Duro et al., 2012). Image layers and parameter values used in the image segmentation process are listed in Table 11. Change detection was accomplished using Cross-Correlation Analysis (CCA) whereby an existing land cover map is used to guide the change detection process. The CCA is performed using a multivariate calculation of class-specific spectral information contained in the imagery used for updating; class-specific spectral information is, in turn, derived from the class boundaries within the existing land cover map (Koeln and Bissonnette, 2000; Hurd et al., 2001; Civco et al., 2002). Using this approach using object-based image analysis, image objects were segmented within existing land cover boundaries based on the underlying imagery used for the updating procedure (Duro et al., in review).

Table 11: Segmentation parameter values used for object-based image analysis.

Year of image acquistion	Satellite	Input layer	Scale	Color / Shape	Smoothness / Compactness	# of Objects	Median area of objects (sq. m)
1976	Landsat-2	NDVI	60	0.5/0.1	0.5/0.5	406,012	28,800
1990	Landsat-5	NDVI	60	0.5/0.1	0.5/0.5	470,367	16,200
2005 & 2008	SPOT-5	NDVI	60	0.5/0.1	0.5/0.5	536,509	16,700

5.3.3 ANCILLARY DATA

5.3.3.1 BASE MAP (CIRCA 2000)

An existing land cover product (the "Land Cover for Agricultural Regions of Canada, circa 2000), developed by Agriculture and Agri-Food Canada (AAFC) using 30 m Landsat imagery (AAFC 2008) was selected to demonstrate the change detection and map updating procedures outlined in Section 5.3.2. The land cover classes used in the AAFC mapping product are as

follows: Water, Exposed rock/soil, Built-up, Shrubland, Wetland, Grassland, Annual Crops, Perennial Crops and Pasture, Coniferous, Deciduous and Mixed Forest. A thematic accuracy report for this mapping product claims an overall accuracy of 82% (AAFC 2008). Comparisons with agricultural census information suggests that the AAFC land cover map slightly overestimates the amount of area in "Annual Cropland" (3%) and underestimates the amount of area in "Unimproved Pasture"/ "Grassland" (23.2%) land cover classes (AAFC 2008).

For the purposes of this study, and to maintain comparability among disparate image sources, land cover classes were further generalized and modified according to Table 12. Areas identified as "Coniferous" and "Deciduous" in the AAFC land cover map within the southern half of the study area were found to primarily correspond to areas of wetland vegetation types visible in EO imagery at all three time periods, and were relabelled accordingly. Patches of vegetation found within the main river along sand bars or river banks mistakenly classified as "Wetland" in the AAFC map were reclassified as "Riparian", along with "Coniferous" or "Deciduous" land cover types located alongside or within narrow stream banks or the main river. In addition, areas classified as "Perennial Crops and Pasture", "Shrubland", and "Grassland" were generalized into a "Mixed Grassland" land cover type as the limited amount of available imagery made reliably discerning between these land cover types problematic. Furthermore, the acquisition dates of the EO imagery that could be acquired were not optimal for discriminating between grassland species located within the study area (see Price et al., 1997).

Table 12: Generalization and modification of original AAFC land cover classes in circa 2000 base map.

Original land cover class	*Modified land cover classes*
Water	Water
Exposed	Exposed rock/soil
Built-up	Built-up
Shrubland	Mixed Grassland
Grassland	Mixed Grassland
Perennial Crops and Pasture	Mixed Grassland
Wetland	Wetland
Coniferous	Wetland
Deciduous	Wetland
Annual Crops	Cropland
Mixed Forest	Not present in study area
	Riparian

5.3.3.2 CENSUS DATA

Agricultural census data were obtained from Statistics Canada (www.statcan.gc.ca) and/or from the University of Saskatchewan's Data Library (library.usask.ca/murray/data-and-gis). While this data has been made available in aggregate form over several watershed scales (AAFC 2008b), the finest watershed scale available was still too spatially coarse, covering an area approximately 9,000 km^2 in size. In an effort to obtain agricultural census data summarized at finer spatial scales, data from individual census consolidated subdivisions (CCS), which represent agglomerations of incorporated towns, rural municipalities, cities, etc., were gathered and compiled for the study area. As the CCS boundaries are administrative in nature, they do not conform to the drainage area located within the study area (see Figure 19).

The Census of Agriculture (CoA), collected every 5 years since 1896 in the Prairie Provinces of Canada, contains a wide range of information on various aspects of agricultural activity, ranging from socioeconomic to land use practices (Statistics Canada, 2011a). Of the many dozen variables available in the CoA, this study focused on one related to fertilizer use – the amount of fertilizer purchased in dollars ("FERTPD") – in order to assess the relative level of land use intensity within the study area. Data from the CoA was acquired for census years 2006, 1991, and 1976. In contrast to most of the information gathered in the CoA, data on the FERTPD is actually recorded for the previous year (i.e., the CoA survey in 1976 will ask for

information on FERTPD for 1975). EO imagery gathered for this study corresponded to non-CoA years where FERTPD information would have been recorded (i.e., 2005 and 1990), except for in 1976 where imagery was collected in the same year as the CoA (see Table 10), and therefore would not be commensurate with FERTPD information reported for 1975.

Figure 19: Census consolidated subdivisions (CCS) in relation to the drainage basin, and associated effective drainage area, located within the study area.

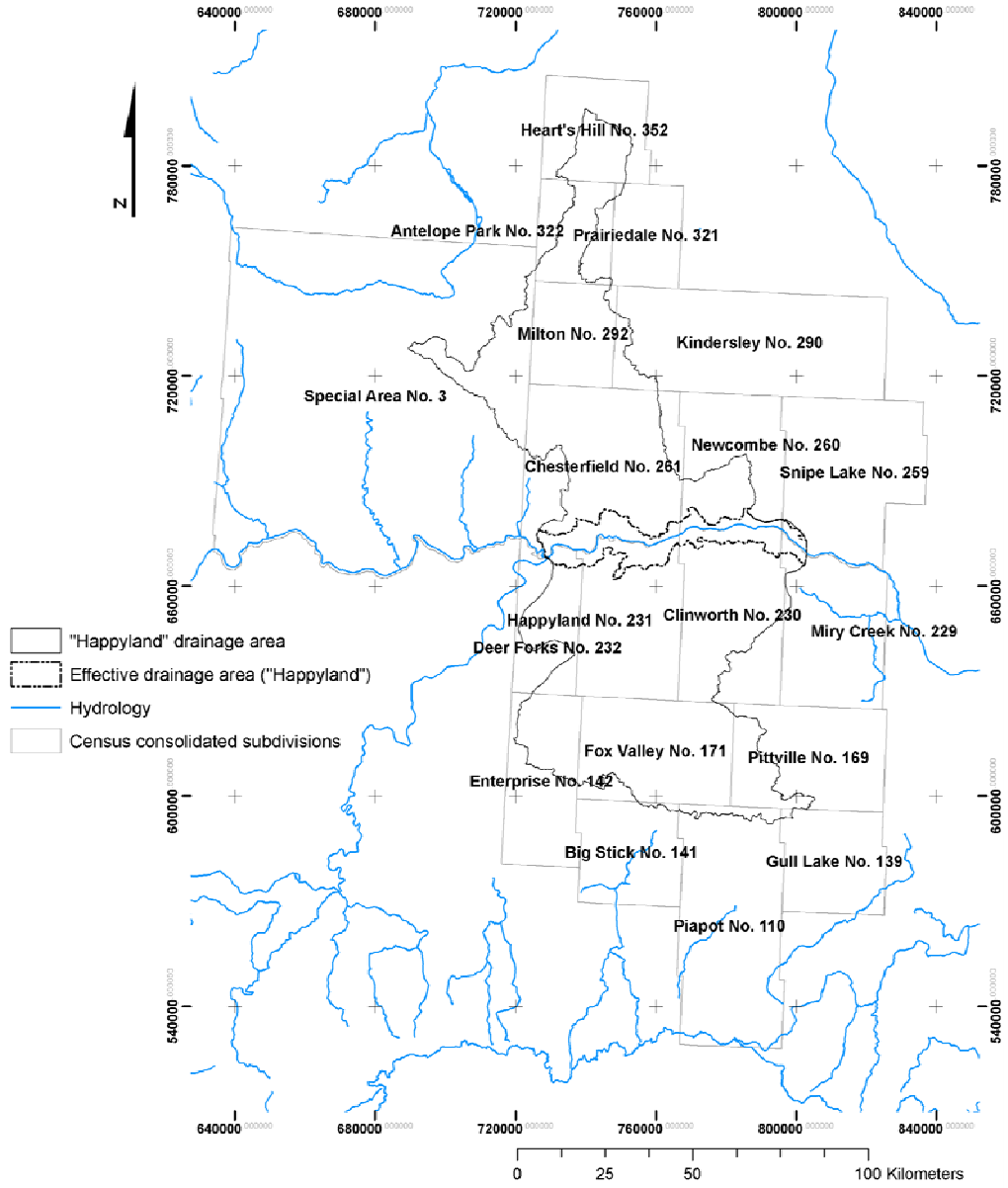

Information on FERTPD was not collected in the 1976 CoA, but was available for previous and following CoAs (i.e., 1971, 1981 and beyond). The data gap for the 1976 CoA (1975 for FERTPD information) was interpolated using a simple arithmetic mean based on the available previous and following values of the FERTPD variable for all 19 CCS examined in this study. Prior to interpolation, all dollar values were normalized to constant 2002 dollars based on the latest Consumer Price Index information (Statistics Canada, 1998, 2011b). Based on the linear increase in fertilizer purchases between 1971 and 1986, the interpolated values generated for each CCS were considered adequate for the purposes of this study. In addition to FERTPD, the amount of area used by cropland (i.e., hectares devoted to field crops) reported by the CoA was also used to compare with estimates of cropland area made by EO imagery. The variable “ECRPLND” includes land in crops, and does not include areas used that are not defined as field crops (e.g., fruits, vegetables, summer fallow, woodland, etc.).

5.3.4 SPATIAL DISAGGREGATION

The method for spatially disaggregating agricultural census data followed an "intelligent areal interpolation" method (Eicher and Brewer 2001), whereby ancillary data were used to reassign information from a given zonal unit into another. In this study, remotely sensed estimates of cropland area were used to reassign land use information derived from the CoA (see Figure 20). Using this approach, selected land use information from the CoA was assigned to areas identified as cropland from EO imagery. In this way, the spatial homogeneity of information assumed in the choropleth maps is spatially disaggregated to correspond to the actual spatial distribution of the information under investigation. In other words, instead of agricultural land use information being reported over an entire CCS area, which may contain large amounts of non-agricultural land cover types, only areas identified as having agricultural uses within each CCS area are assigned appropriate information from the CoA.

Such methods are valuable because they combine the advantages of the relatively higher spatial resolution of EO imagery with typical spatially coarse census information (Comber et al., 2008). Similar methods have been used by others to "spatially refine" agricultural census

information with land cover data derived from EO imagery (e.g., Kerr and Cihlar, 2003; Cardille and Clayton, 2007; Mehaffey et al., 2011), but have been tended to use coarse spatial resolution imagery (i.e., 1 km pixels). In this study, relatively fine spatial resolution EO imagery (10-60 m pixels) was used to spatially disaggregate CoA information, allowing for a better indication of development at the local landscape scale. Such spatially explicit information can then be used to assess the relative impact that spatial configuration and composition of land cover and land use has on various environmental concerns (e.g., anthropogenic eutrophication).

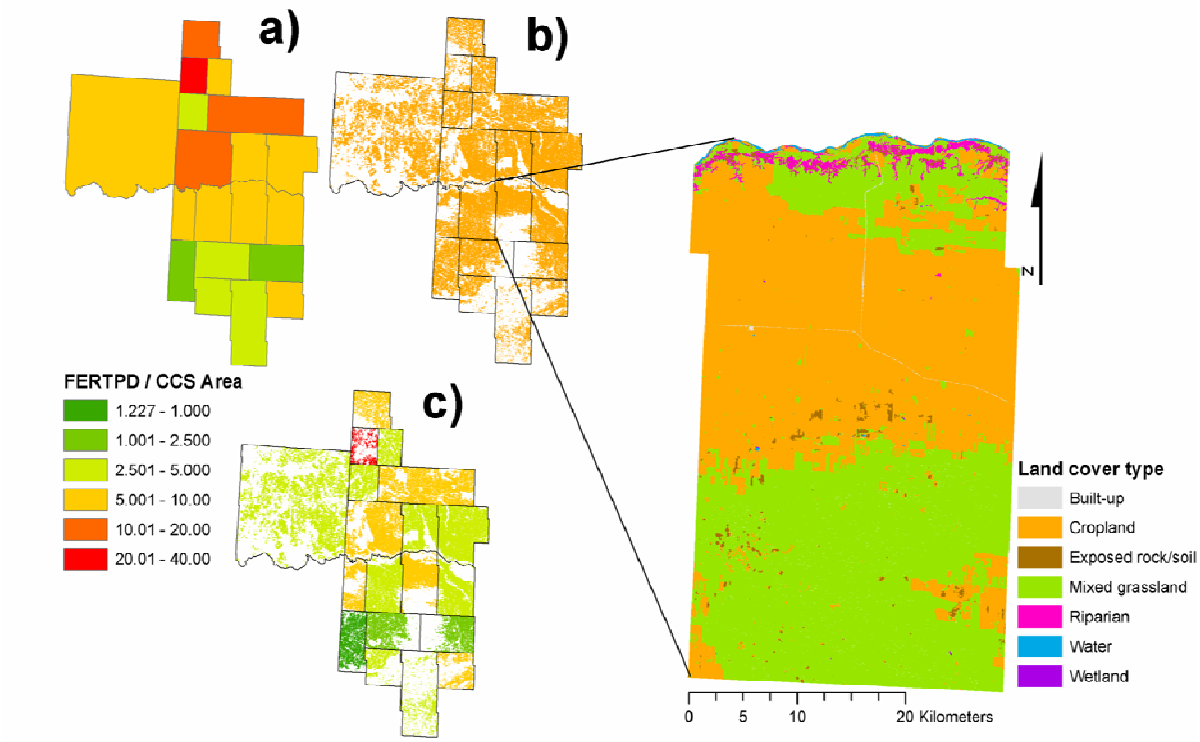

Figure 20: Conceptual diagram of the spatial disaggregation process used in this study: a) Fertilizer purchases per CCS; b) Estimate of cropland area per CCS using EO imagery (example of full land cover map shown in inset); c) Spatially disaggregated fertilizer purchases per CCS area for cropland areas estimated by EO imagery.

While many variables exist within the CoA that could benefit from spatial disaggregation, only a few were amenable to this method in light of the land cover classes that could be reliably mapped with the available EO imagery. For example, while there is information within the CoA on the extent of improved and unimproved pasture areas within each CCS, it would be relatively difficult to reliably discern this particular land use from its underlying land cover type (i.e., grassland species) based on the EO imagery available (see Section 5.3.2). This study illustrates the spatial disaggregation process using information on the amount of fertilizer purchased ("FERTPD") per CCS, as cropland areas could be readily discerned from other land cover types.

5.3.5 VALIDATION

Comprehensive validation of the land cover classifications over the entire watershed was not possible due to the lack of suitable ground reference data (e.g., aerial photographs) for the 1990 and 1976 time periods, and the large size of the study area (almost 30,000 km^2). Acquiring suitable ground reference information for such large areas over historical time periods is problematic; instead, three sample sites within the study area were assessed using similar classification and change detection methods to those employed here. The results from these sample sites revealed overall classification accuracies greater than 90% for the general land cover types used in this study (Duro et al., 2012), and a change detection accuracy of approximately 73% (Duro et al., in review). Comparisons between the amount of cropland area estimated by the CoA and the amount of cropland area derived from EO imagery were used to assess the level of agreement between these independently derived datasets.

5.4 RESULTS

5.4.1 AGREEMENT BETWEEN ESTIMATES OF CROPLAND AREA USING COA DATA AND EO IMAGERY

Figure 21 represents the relationship between the area of cropland estimated by the CoA per CCS (ECRPLND), and the area of cropland per CCS estimated by EO imagery for each CoA year examined in this study. Modelled agreements between CoA years (1976, 1991, and 2006) showed linear relationships between EO imagery (1976, 1990, and 2005/2008) that were statistically significant ($n=19$; $p<0.001$). While all models indicate the presence of large deviations, the overall relationships between estimates of cropland area derived from the CoA and EO imagery were consistently linear over all three time periods examined.

If CoA estimates of cropland area per CCS are used as reference of actual on-the-ground conditions, cropland area estimates derived from EO imagery show varying degrees of overestimation, and to a lesser extent, underestimation. On average, there was 46.77% more cropland area per CCS estimated using 2005/2008 EO imagery as compared to estimates in the 2006 CoA. Based on this comparison, the Root-Mean-Square-Error (RMSE) was approximately 32,986 ha, or approximately 330 km^2 per CCS. When comparing 1990 EO imagery with the 1991 CoA, the average percent difference in the amount of area estimated per CCS was 54.37% higher for estimates made using EO imagery, with a corresponding RMSE of 36,671 ha, or approximately 367 km^2. In the only instance where CoA and EO imagery were acquired contemporaneously, the amount of area in cropland estimated per CCS by 1976 EO imagery was 16.55% higher, on average, than that estimated by the 1976 CoA. The corresponding RMSE for this latter comparison was 13,021 ha, or approximately 130 km^2.

Figure 21: Relationships between cropland area estimated from EO imagery (hectares) per CCS vs. Census of Agriculture estimates of cropland area per CCS (hectares) using ECRPLND variable. There are statistically significant agreements between these independent estimates of cropland area (n = 19; 1976: Adjusted r^2 = 0.93, p<0.001; 1991: Adjusted r^2 = 0.96, p<0.001; 2005: Adjusted r^2 = 0.91, p<0.001).

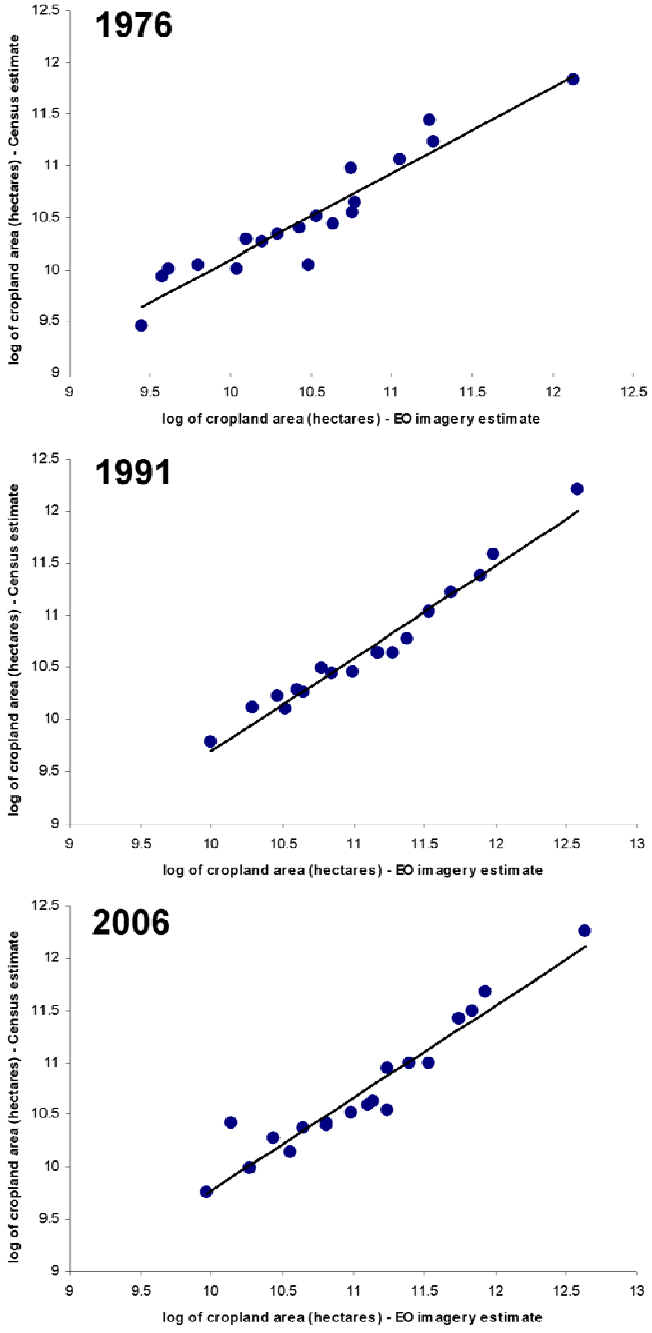

The differences between estimates of cropland area for each CCS area, either derived from the CoA (ECRPLND) or EO imagery, two completely independent sources of information, show similar patterns (Figure 22). As mentioned, the main difference between both sources of information is that EO imagery appears to overestimate the amount of cropland area in later years (1991 and 2005) as compared to CoA estimates. For the 1976 period, estimates of cropland area made by EO imagery reported lower values for several CCS areas. Another notable difference between both sources of information is the degree at which cropland areas increase between years: for CoA based estimates of cropland area, the increase appears to be relatively consistent and small between years, with the exception of CCS area "Special Area No.3" (see Figure 19 for reference), where the increase between 1976 and 1991 is large. For estimates of cropland area derived from EO imagery, there is a notable increase in cropland area between 1976 and 1991 in all CCS areas, and a relatively smaller increase in cropland area between 1991 and 2005. The one exception is in CCS area "Piapot No. 169", where less cropland area was reported in 2005 using EO imagery. Interestingly, the large relative increase in cropland area between 1976 and 1991 in CCS area "Special Area No.3" estimated by the CoA is also present in the estimate derived from EO imagery, although the absolute values in estimated cropland area differ substantially.

Figure 22: Comparison of independently derived estimates of cropland area made by Census of Agriculture (CoA) and earth observation (EO) imagery for all 19 CCS areas for three time periods: a) 1976, b) 1991, and c) 2005.

5.4.2 SPATIAL DISAGGREGATION OF LAND USE INTENSITY

Figure 23 compares the difference in the depiction of the FERTPD variable (dollars spent on fertilizer in constant 2002 dollars) normalized using different areal accounting units for 1975, 1990, and 2005 (i.e., the year in which FERTPD was reported). When the area of each CCS boundary is used to normalize the data (Figure 23a), which includes non-cropland areas where fertilizer would not be applied, the spatial pattern shows relatively lower amounts of fertilizer purchased in the southern and western halves of the study area in 1975 and 1990. In 2005, there was a marked increase in overall fertilizer purchases compared to previous years.

The previous spatial and temporal pattern is evident when the CoA estimate of cropland area per CCS is used to normalize the data, which scales the depiction of fertilizer purchases to areas where cropland is present within the CCS (Figure 23b). When using the CoA estimate of cropland area to normalize the data, the spatial distribution of the amount of fertilizer purchased shows relatively higher concentrations overall across all CCS areas, with notably higher relative purchases depicted in earlier CoA years. This can be seen by the relatively high amounts of fertilizer purchased in the CCS areas of Chesterfield and Antelope Park (see Figure 19 for reference) in 1975 and 1990, as compared to other CCS areas. More notably, by 2005, the amount of fertilizer purchased is relatively equal (and relatively high) among all CCS areas as compared to previous years.

Finally, when using estimates of cropland area derived from EO imagery (Figure 23c), the spatial and temporal distributions of the amount of fertilizer purchased is relatively similar to when using CoA estimates of cropland area (Figure 23b). However, the most notable difference between the latter two products is in the overall intensity and spatial arrangement of the FERTPD information. Where Figure 23b shows relatively higher amounts of fertilizer purchased per CCS area, Figure 23c shows relatively less fertilizer purchased per CCS area. This difference is most notable in northern CCS areas in earlier years (1975 and 1990) as the relative amounts of fertilizer purchased appear to decrease. However, by 2005, the spatial pattern in fertilizer purchases shows the large increase relative to previous years, a pattern confirmed using other areal normalizations (Figures 23a and 23b).

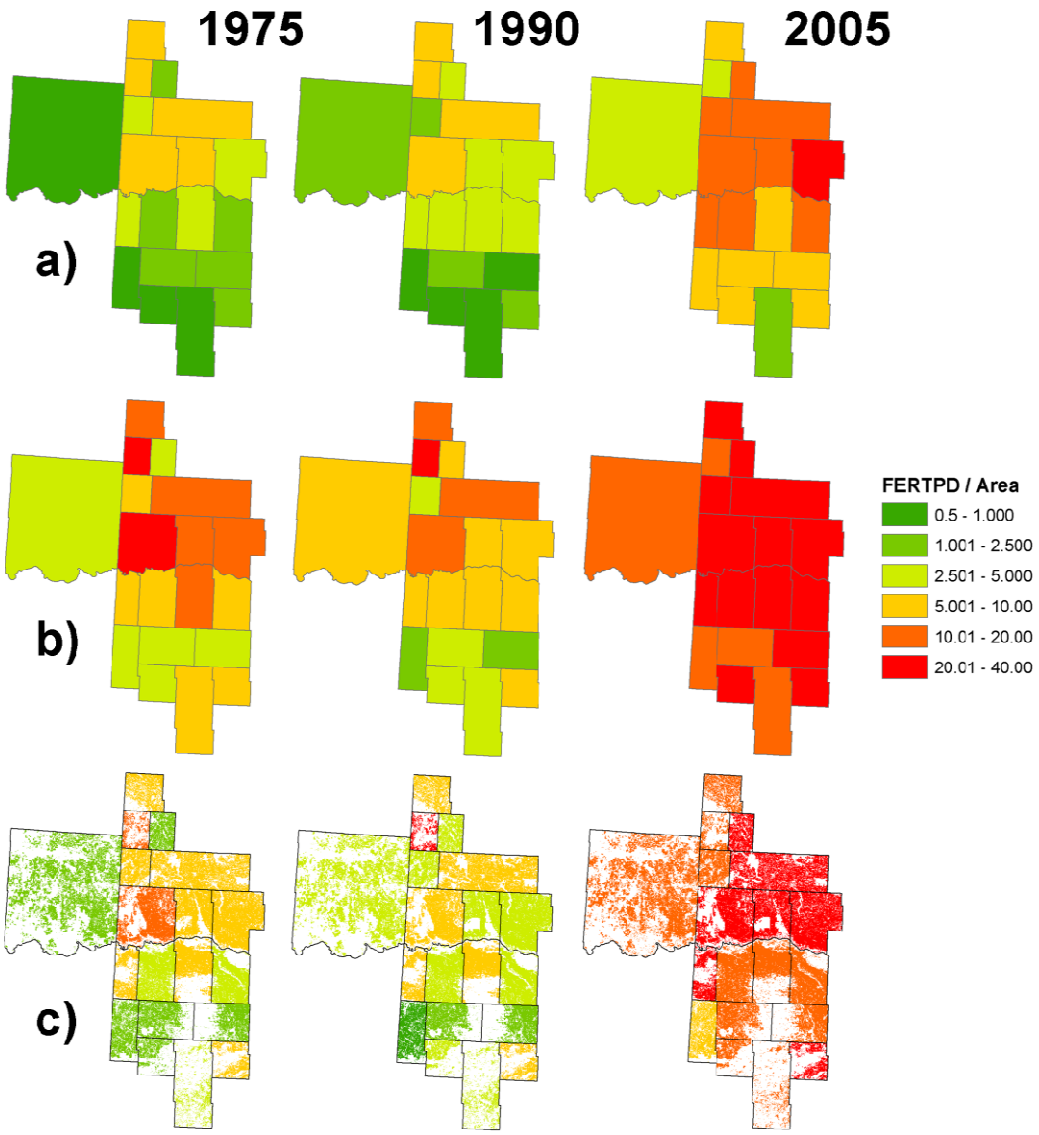

Figure 23: Spatial disaggregation of FERTPD information normalized per area of: a) CCS boundaries; b) CoA estimate of cropland area; c) EO imagery estimate of cropland area.

5.5 DISCUSSION

The relationship between cropland area estimates derived from the CoA and EO imagery were highly correlated and linear in nature (see Section 5.4.1 and Figure 21). When averaged over the three years examined, EO imagery overestimated the amount of cropland area by 39.23% or approximately 27,559 ha (~276 km^2) as compared to CoA estimates. The average size of each CCS is approximately 156,732 ha (1,567 km^2), which corresponds to an average overestimation of approximately 18% per CCS area as compared to CoA estimates. Interestingly, the potential overestimation of cropland area derived from EO imagery in this study has been noted by others: As in this study, Frolking et al. (1999) were able to relate cropland area estimated using EO imagery (1 km pixels) with estimates from comparable agricultural censuses data with a high degree of correlation (r^2 = 0.82); however, they found that estimates of cropland area derived from EO imagery were 50-100% higher than that found in agricultural census data. In another study from a similar region, Liu et al. (2005) found that estimates of cropland area using Landsat TM imagery (30 m pixels), a spatial resolution used in this study, were 50% larger than that estimated by national census data. Using 1 km pixels, Kerr & Cihlar (2003) found that the amount of "agricultural area" reported in CoA data (which included grassland areas) were well correlated and statistically significant when compared with estimates made by EO imagery (r^2=0.78, $p<0.001$). In contrast to the findings here, they found that estimates of agricultural areas were consistently underestimated by EO imagery. The land cover product used as the basis for this work (see Section 5.3.3.1), which also utilized medium spatial resolution imagery (30 m pixels), reported a slight overestimation (3%) of cropland areas (AAFC 2008) when compared to cropland area estimates in the CoA.

Perhaps one of the more compelling results revealed that the estimates of cropland area derived from two completely independent sources showed a great deal of overall correspondence (Figures 21 and 22). The notable exception was that EO imagery showed relatively higher estimates of cropland area in 1991 and 2005 as compared to CoA estimates, whereas estimates for 1976 from both sources were relatively similar, both overall and on a per-CCS basis. A potential explanation for this upward bias in estimated cropland area derived

from EO imagery in 1991 and 2005 might be that the median object size was almost half that found in 1976, with a corresponding smaller number of objects overall. Smaller and more numerous objects derived from 1990 and 2005/2008 imagery may have caused cropland area to be over reported. Despite the difference in the median image object size, the scale parameter value (60), which sets the minimum image object size, ensured that all years consistently utilized a similar minimum mapping unit. In addition, areas of cropland are typical found in a spatially cohesive pattern, therefore differences in image object sizes are relatively meaningless as all objects are effectively summed when determining overall area coverage. However, in situations where there are small, isolated fragments, over reporting of cropland area may result.

In this study, a potentially large source of error is the mismatch between acquisition dates and when CoA data were gathered, causing a discrepancy between the amounts of cropland area estimated in the CoA and that estimated by EO imagery. For EO imagery and the CoA from the same year (1976), the average percent difference between CoA and EO imagery estimates of cropland area dropped to 16.57%. Given that both independent datasets show a remarkable correspondence in the general temporal trends in cropland area, it is likely that the overall trends are representative of actual ground conditions. However, the reported difference in magnitude, especially in later years, indicates that the accounting of cropland areas between data sources is different.

Indeed, an explanation for the discrepancy between CoA and EO imagery estimates of cropland area could be related to how data are collected for the CoA. For example, “data suppression” procedures to ensure privacy of respondents may remove data from an analysis; data inconsistencies from rounding error or the effects of sampling may introduce error; and, perhaps the largest potential source of error when using CoA data, is the use of the “headquarters rule”, whereby all data collected for an agricultural operation is assigned to the geographic area where the farm headquarters is located (Statistics Canada, 2008). This latter rule may introduce an overestimation (or underestimation) regarding land use information within a given census boundary (e.g., CCS), as information is effectively removed (or added) within a census reporting boundary. Such practices, while preserving anonymity, hamper multi-

temporal analysis of land use data, as information is deliberately obfuscated. Ultimately, estimates of cropland area made by either data source likely contain errors, raising the possibility that CoA estimates may actually underestimate the amount of cropland area (Kerr and Cihlar, 2003).

The spatial disaggregation outlined and conducted in this study used data on fertilizer purchases, a measure of land use intensity, and land cover information derived from EO imagery. When compared to standard choropleth mapping (Figures 23a and 6b), the disaggregated agricultural land use information (FERTPD) in Figure 23c was more suited to representing the amount of fertilizer purchased per CCS area in a spatially explicit manner. In other words, the extent and configuration of cropland area was evident in the spatially disaggregated maps, whereas traditional choropleth maps – even after normalization of area – depicted the land use intensity information in a spatially homogenous fashion.

While comparisons between CoA and EO imagery estimates of cropland area were different, they showed nearly identical spatial patterns of land use intensity when displayed normalized to the amount of area identified as cropland (Figures 23b and 23c). Regardless of which estimate of cropland area is more accurate, the main advantage of the disaggregation procedure is that a more spatially representative depiction of cropland area per CCS can be achieved. In this form, the land use variable under investigation can be readily assessed, allowing for spatially explicit analyses to be conducted. For example, the number and area of cropland patches can be assessed, adding enhanced insight into the spatial configuration of individual land cover types. Such local landscape level analysis would not be possible using standard choropleth mapping as the spatial distribution of the variable of interest is assumed to be homogenous throughout the selected boundary (e.g., CCS areas depicted in Figures 23a and 23b).

Future work to extend the methods outlined here could focus on obtaining ancillary information and/or EO imagery capable of providing detailed land cover classes that allow the spatial disaggregation to be carried out in more detail, or by using other CoA information that

can benefit from the spatial disaggregation process. With more detailed land cover classes (i.e., specific crop types), information on the amount of fertilizer applied per crop type could be estimated, as different crop types require varying amounts of fertilizer. Such an application could be adopted within the study area to assess the relative trade-offs between increasing agricultural land use intensity and various ecosystem services, which is an approach being pursued by others in similar intensively developed agricultural regions (Mehaffey et al., 2011). Another example might involve using appropriate EO imagery and ancillary data to locate areas and extents of improved and unimproved pastures, feedlots, and other livestock operations, which could provide greater insights into the spatial distribution of livestock related land use intensity information in the study area.

5.6 CONCLUSIONS

While both independent agricultural census data and EO imagery estimates of cropland area were different, the overall relationship between both sources was found to be highly significant, and the overall temporal trend in cropland area per census boundary showed considerable similarity. Using medium spatial resolution EO imagery (10-60 m pixels) to spatially disaggregate land use information contained in agricultural census data provided a spatially explicit representation of land use intensity, which when compared to traditional choropleth mapping, would be better suited to understanding the effects of local landscape scale development. While further work is needed to select more refined datasets used by the spatial disaggregation procedure outlined here, the application as illustrated shows considerable promise as a means of gathering enhanced insight into spatial and temporal trends in local landscape land use intensity in agricultural environments.

5.7 REFERENCES

AGRICULTURE AND AGRI-FOOD CANADA, 2008A. Land Cover for Agricultural Regions of Canada, circa 2000 [WWW Document]. URL http://geodiscover.cgdi.ca/gdp/search?action=entrySummary&entryType=productCollection&entryId=34485&entryLang=en [Accessed March 23, 2012]

AGRICULTURE AND AGRI-FOOD CANADA, 2008B. Interpolated Census of Agriculture to Soil Landscapes, Ecological Frameworks and Drainage Areas of Canada [WWW Document]. URL http://geodiscover.cgdi.ca/gdp/search?action=fullMetadata&entryType=productCollection&entryId=35045&entryLang=en [Accessed March 23, 2012]

CARDILLE, J.A., CLAYTON, M.K., 2007. A regression tree-based method for integrating land-cover and land-use data collected at multiple scales. Environ Ecol Stat 14, 161-179.

CHANDER, G., MARKHAM, B.L., HELDER, D.L., 2009. Summary of current radiometric calibration coefficients for Landsat MSS, TM, ETM+, and EO-1 ALI sensors. Remote Sensing of Environment 113, 893-903.

CIVCO, D.L., HURD, J.D., WILSON, E.H., SONG, M., ZHANG, Z., 2002. A comparison of land use and land cover change detection methods, in: American Society for Photogrammetry and Remote Sensing/ American Congress on Surveying and Mapping. p. 12.

COMBER, A., PROCTOR, C., ANTHONY, S., 2008. The Creation of a National Agricultural Land Use Dataset: Combining Pycnophylactic Interpolation with Dasymetric Mapping Techniques. Transactions in GIS 12, 775-791.

DRIGO, R., 2004. Trends and patterns of tropical land use change, in: Forests, Water and People in the Humid Tropics: Past, Present and Future Hydrological Research for Integrated Land and Water Management. Cambridge University Press.

DURO, D.C., FRANKLIN, S.E., DUBE, M.G., 2012. A comparison of pixel-based and object-based image analysis with selected machine learning algorithms for the classification of agricultural landscapes using SPOT-5HRG imagery. Remote Sensing of Environment 118, 259-272.

EICHER, C.L., BREWER, C.A., 2001. Dasymetric Mapping and Areal Interpolation: Implementation and Evaluation. Cartography and Geographic Information Science 28, 125-138.

ENTWISLE, B., STERN, P.C. (EDS.), 2005. Population, land use, and environment. National Academies Press.

FROLKING, S., XIAO, X., ZHUANG, Y., SALAS, W., LI, C., 1999. Agricultural land-use in China: a comparison of area estimates from ground-based census and satellite-borne remote sensing. Global Ecology and Biogeography 8, 407-416.

HALL, R.I., LEAVITT, P.R., QUINLAN, R., DIXIT, A.S., SMOL, J.P., 1999. Effects of Agriculture, Urbanization, and Climate on Water Quality in the Northern Great Plains. Limnology and Oceanography 44, 739-756.

HAMMER, U.T., 1968. Toxic blue-green algae in Saskatchewan. Can Vet J. 9, 221–229.
`

HURD, J.D., WILSON, E.H., LAMMEY, S.G., CIVCO, D.L., 2001. Characterization of Forest Fragmentation and Urban Sprawl Using Time Sequential Landsat Imagery, in: American Society for Photogrammetry and Remote Sensing/ American Congress on Surveying and Mapping. p. 12.

KERR, J.T., CIHLAR, J., 2003. Land use and cover with intensity of agriculture for Canada from satellite and census data. Glob. Ecol. Biogeogr. 12, 161-172.

KOELN, G., BISSONNETTE, J., 2000. Cross-correlation analysis: mapping landcover changes with a historic landcover database and a recent, single-date, multispectral image, in: American Society for Photogrammetry and Remote Sensing/ American Congress on Surveying and Mapping. p. 12.

LESSCHEN, J.P., VERBURG, P.H., STAAL, S.J., 2005. Statistical Methods for Analysing the Spatial Dimension of Changes in Land Use and Farming Systems. International Livestock Research Institute; Wageningen University, LUCC Focus 3 Office.

LIU, J., TIAN, H., LIU, M., ZHUANG, D., MELILLO, J.M., ZHANG, Z., 2005. China's changing landscape during the 1990s: Large-scale land transformations estimated with satellite data. Geophys. Res. Lett. 32, 5 PP.

LIVERMAN, D.M., 1998. People and Pixels Linking Remote Sensing and Social Science. National Academy Press, Washington, D.C.

MEHAFFEY, M., VAN REMORTEL, R., SMITH, E., BRUINS, R., 2011. Developing a dataset to assess ecosystem services in the Midwest United States. International Journal of Geographical Information Science 25, 681-695.

PETIT, C.C., LAMBIN, E.F., 2001. Integration of multi-source remote sensing data for land cover change detection. International Journal of Geographical Information Science 15, 785.

PRICE, K.P., EGBERT, S.L., NELLIS, M.D., LEE, R.-Y., BOYCE, R., 1997. Mapping Land Cover in a High Plains Agro-Ecosystem Using a Multidate Landsat Thematic Mapper Modeling Approach. Transactions of the Kansas Academy of Science (1903-) 100, 21-33.

RUELLAND, D., TRIBOTTE, A., PUECH, C., DIEULIN, C., 2011. Comparison of methods for LUCC monitoring over 50 years from aerial photographs and satellite images in a Sahelian catchment. International Journal of Remote Sensing 32, 1747-1777.

SCHINDLER, D.W., 2001. The cumulative effects of climate warming and other human stresses on Canadian freshwaters in the new millennium. Can. J. Fish. Aquat. Sci. 58, 18-29.

SCHINDLER, D.W., DONAHUE, W.F., 2006. An impending water crisis in Canada's western prairie provinces. Proc. Natl. Acad. Sci. U. S. A. 103, 7210-7216.

SCHOTT, J.R., SALVAGGIO, C., VOLCHOK, W.J., 1988. Radiometric scene normalization using pseudoinvariant features. Remote Sensing of Environment 26, 1-14, IN1, 15-16.

STATISTICS CANADA, 1998. Your Guide to the Consumer Price Index [WWW Document]. URL http://www.statcan.gc.ca/bsolc/olc-cel/olc-cel?catno=62-557-X&lang=eng [Accessed March 23, 2012].

STATISTICS CANADA, 2008. General notes - Agriculture–Population Linkage Data for the 2006 Census [WWW Document]. URL http://www.statcan.gc.ca/pub/95-633-x/2007000/6500078-eng.htm [Accessed March 23, 2012].

STATISTICS CANADA, 2011a. About the Census of Agriculture [WWW Document]. URL http://www.statcan.gc.ca/ca-ra2011/110002-eng.htm [Accessed March 23, 2012].

STATISTICS CANADA, 2011b. Consumer Price Index (CPI) [WWW Document]. URL http://www.statcan.gc.ca/cgi-bin/imdb/p2SV.pl?Function=getSurvey&SDDS=2301&lang=en&db=imdb&adm=8&dis=2 [Accessed March 23, 2012].

CONCLUSION

As established in the introduction of this thesis, many regional environmental assessments (e.g., the Saskatchewan Watershed Authority's State of the Watershed report) currently utilize information that has been aggregated over large watershed boundaries. While such approaches utilize ecologically relevant units of analysis, the use of aggregated information confounds understanding how the spatial configuration and composition of land cover and land use related to agricultural development at local scales may impinge upon ecosystem functions over time. As a result, several objectives were established to address this deficiency by introducing and implementing developments in the image analysis and spatial analysis.

Chapter 2 investigated whether pixel-based or object-based approaches to image analysis, along with several machine learning algorithms, provided adequate depictions of land cover in agricultural environments. The results from this chapter established that there was no statistically significant difference in overall classification accuracy between pixel-based and object-based image analysis approaches. However, object-based image analysis allowed for the mapped results to be easily integrated with land use information within a Geographical Information System (GIS). Furthermore, the Random Forest (RF) classification algorithm exhibited advantageous qualities, which singled out its use in research explored in subsequent chapters.

In Chapter 3, object-based image analysis and the RF classifier was explored in more detail and used to combine disparate sources of earth observation imagery for mapping broad agricultural land cover types. In addition, a feature selection algorithm was used to reduce the size of the underlying dataset without affecting overall classification accuracy. The large amount of predictor variables available due to using various sources of earth observation imagery and object-based image analysis was reduced using the feature selection algorithm by up to 60% without unduly impacting overall classification accuracy. In conjunction with the feature importance scores generated by the RF classifier, it was possible to gain greater insight

into which image segmentation scale and sensor specific bands provided relatively more useful information for classifying broad agricultural land cover types.

Chapter 4 adapted an existing change detection method for use within an object-based image analysis environment. The object-based image analysis approach allowed for a more robust means of updating existing land cover maps, as image segmentation procedures could be configured to respect existing land cover boundaries delineated in previous maps. Furthermore, the change detection procedure allowed for multiple sources of imagery with different spatial and spectral characteristics to be utilized in the map updating procedure. The flexibility of the introduced change detection method and associated map updating procedure provides a standardized approach of integrating multi-scale, multi-source, and multi-date imagery.

Building upon image processing, change detection, and map updating methods outlined in previous chapters, a spatial disaggregation procedure was described and implemented in Chapter 5. Selected agricultural land use data information was spatially disaggregated over a modest sized watershed in southwest Saskatchewan for three time periods. The disaggregated land use data showed similar spatial and temporal patterns to independently gathered agricultural census data, but with the advantage of depicting this information in a spatially explicit manner within individual watersheds.

The combination of methods developed in this thesis allow for the creation of maps depicting land cover and land use at local landscape scales in a spatially explicit manner over time periods where remotely sensed information is available. The image processing methods investigated and implemented allow for multiple scales of investigation through the use of object-based image analysis, an RF classifier, and associated feature selection algorithm. The introduced change detection method and map updating procedures described and employed in this thesis allows for multiple sources and dates of imagery to be used within a flexible GIS processing environment. This thesis introduced several developments in image processing and spatial analysis allowing for the multi-scale, multi-source, and multi-date imagery to be processed in a consistent manner suitable for supporting sustainable agricultural development.

FUTURE RESEARCH DIRECTIONS

Opportunities exist to extend this thesis. Potential avenues include:

A) Spatial disaggregation of livestock related information

Due to the lack of suitable imagery, it was not feasible to conduct a spatial disaggregation of stocking densities within the study area. In this thesis, stocking densities and associated waste manure production could only be summarized over relatively large CCS areas and normalized to CCS areas. Access to higher resolution earth observation imagery and/or appropriate business records might be used to locate feedlot operations across the study area, allowing for the effective spatial disaggregation of such data. Collecting multi-date and multi-source imagery (e.g., VNIR and SAR imagery) could be used to improve the discrimination between improved pastures and natural grasslands so that areas used for grazing can be effectively mapped. Although confusion would still remain as natural grasslands can be used as improved pasture and vice versa. Delineating areas that are deliberately set aside for grazing purposes would provide an opportunity to better quantify stocking densities within the region and associated environmental impacts.

B) Detailed crop type mapping

Broad land cover types were utilized in this study to facilitate the integration of earth observation imagery with varying spatial, spectral, and radiometric characteristics. With appropriate resources, the generalized land cover types used in this thesis could be expanded to better represent the variety of crop types found within the study area. Such an effort would have to balance detailed crop type mapping, which would be possible in later years, with what is actually achievable using relatively less suitable multispectral imagery in earlier years (e.g., Landsat MSS imagery). This detailed crop type mapping could then be used to determine the

relative amount of resources (e.g., fertilizer, water, pesticides, etc.) required to produce specific crops, or to assess carbon and nutrient cycling. While such an analysis can be conducted using agricultural census data alone, as shown in this thesis, the relative utility of examining additional information in a spatially explicit manner may lead to more compelling opportunities.

C) Detailed riparian mapping and landscape assessment

Since hydrological characteristics within the prairie provinces suggest that only a small portion of an entire watershed actually contributes flow to the main river stem, it would be advantageous to focus on mapping efforts that can provide a high level of detail of such hydrologically (and ecologically) relevant areas. This approach could utilize relatively advanced sources of remotely sensed information, such as that provided by hyper-spectral or LIDAR sensors, to map vegetation characterises of riparian environments. Detailed field data on the abundance of certain sentinel species, used as indicators of overall aquatic ecosystem health, could be related to remotely sensed estimates of habitat cover. In addition, detailed landscape analysis could be conducted to assess whether the composition and configuration of land cover elements can be related to the condition of riparian environments. If so, this can be used to assess large swathes of area. In this thesis, preliminary information related to landscape metrics within the riparian environments was conducted.